

Investigation of Graphene Growth on Different Natural Substrates  
From Aromatic Plastic Wastes and its Systematic Life Cycle  
Assessment

by

Esra YALÇINKAYA

Submitted to the Graduate School of Engineering and Natural Sciences

in partial fulfillment of

the requirements for the degree of

Master of Science

Sabanci University

July 2022

Investigation of Graphene Growth on Different Natural Substrates  
From Aromatic Plastic Wastes and its Systematic Life Cycle  
Assessment

Approved by:

Assoc. Prof. Dr. Burcu SANER OKAN  
(Thesis Supervisor)

Prof. Dr. Yusuf Ziya Mencilođlu

Assoc. Prof. Dr. Bertan BEYLERGİL

Approval Date: July 25, 2022

Esra YALÇINKAYA 2022 ©

All Rights Reserved

## **ABSTRACT**

# Investigation of Graphene Growth on Different Natural Substrates From Aromatic Plastic Wastes and its Systematic Life Cycle Assessment

Esra Yalçinkaya

MATERIAL SCIENCE AND NANOENGINEERING, MASTER THESIS

JULY 2022

Thesis Supervisor: Assoc. Prof. Dr. Burcu SANER OKAN

Keywords: Upcycling, polystyrene, polyethylene terephthalate, talc, organically modified montmorillonite, hybrid additive, thermoplastic composites, life cycle assessment

Plastic pollution has emerged as one of the widespread environmental issues and causes a series landfilling problem and the accumulation of the plastics in the environment and an increase in the GHS emissions. Especially recycling aromatic plastics, such as polyethylene terephthalate (PET) and polystyrene (PS), is complex and strongly sensitive to the process design and conditions due to the presence of polycyclic aromatic hydrocarbons and interunit C–O and/or C–C linkages. Herein, upcycling process becomes crucial to attain high value-added products from aromatic plastics and the conversion of carbon source in wastes into carbon nanomaterials provides prominent advantages over conventional recycling methods. This thesis aims to grow graphene structures on different natural substrates such as talc and organically modified montmorillonite (OMMT) from waste PS and PET sources by applying a sustainable, affordable, and environment-friendly upcycling technique. This promising method is to promote the formation of 2D or 3D graphene structures from waste PS and PET and provides dimension-controlled graphene growth by tailoring the substrate type and size,

surface composition of substrate and the degree of aromaticity in polymer. In addition, the effect of polymer processing techniques, such as twin-screw extrusion and thermokinetic mixing, was investigated on the development of graphene grown hybrid additives by analyzing degree of crystallinity.

Regarding the developed thermal based upcycling technology, talc substrate with a D50 particle size up to 10  $\mu\text{m}$  promoted the growth of two-dimensional (2D) graphene sheets while talc with a size less than 2  $\mu\text{m}$  assisted the production of three-dimensional (3D) graphene spheres by using PS source. Especially talc treated by iron catalyst triggered carbon accumulation on substrate and increased the number of graphene layers. Instead of talc, OMMT used as a substrate was used to enhance the degradation of PS polymer and indicate the effect of substrate type on graphene growing mechanism. It was possible to attain sheet like graphene on OMMT surface without using any catalyst in the presence of PS waste. In addition to waste PS, PET was used as a carbon source to grow graphene on the surface of iron treated micron sized talc and PS showed better performance than PET polymer since the polymer degradation of PET was more complex than PS.

Prior to thermal upcycling, it was observed that the shear rate had a direct effect on the exfoliation of filler. The structural characterization results showed that high shear rate mixer led to the change in crystalline planes of talc whereas conventional twin screw extrusion preserved the structural properties of talc.

Furthermore, a systematic life cycle assessment was conducted to evaluate the CO<sub>2</sub> footprint of upcycled graphenes grown on talc and OMMT substrates compared to graphene produced by conventional techniques. Upcycled graphene structures obtained by direct carbonization and even catalyst impregnated natural substrate-based graphene growth process with PS or PET source have comparably lower CO<sub>2</sub> emission than graphene produced by chemical exfoliation of graphite. To conclude, these newly developed and upcycled hybrid additives offers beneficial insights to preserve graphene dimension by rigid substrate in polymer blending process and keeping the structural integrity of graphene by adopting a circular economy model.

## ÖZET

# Aromatik Plastik Atıklardan Farklı Doğal Substratlar Üzerinde Grafen Büyümesinin Araştırılması ve Sistemik Yaşam Döngüsü Değerlendirmesi

Esra YALÇINKAYA

MALZEME BİLİMİ VE NANOMÜHENDİSLİĞİ, YÜKSEK LİSANS TEZİ,  
TEMMUZ 2022

Tez Danışmanı: Doc. Dr. Burcu SANER OKAN

Anahtar Kelimeler: İleri dönüşüm, polistiren, polietilen tereftalat, talk, modifiye montmorillonite, hibrit katkı, termoplastik kompozitler, yaşam döngüsü değerlendirme

Plastik kirliliği, yaygın çevre sorunlarından biri olarak ortaya çıkmakta ve bir dizi depolama sorununa ve plastiklerin çevrede birikmesine ve GHS emisyonlarının artmasına neden olmaktadır. Özellikle polietilen tereftalat (PET) ve polistiren (PS) gibi aromatik plastiklerin geri dönüştürülmesi karmaşıktır ve polisiklik aromatik hidrokarbonların ve üniteler arası C–O ve/veya C–C bağlantılarının varlığından dolayı proses tasarımına ve koşullarına son derece duyarlıdır. Burada aromatik plastiklerden yüksek katma değerli ürünler elde etmek için ileri dönüşüm süreci çok önemli hale geliyor ve atıklardaki karbon kaynağının karbon nanomalzemelere dönüştürülmesi, geleneksel geri dönüşüm yöntemlerine göre belirgin avantajlar sağlıyor. Bu tez, sürdürülebilir, uygun maliyetli ve çevre dostu bir ileri dönüşüm tekniği uygulayarak atık PS ve PET kaynaklarından talk ve organik olarak modifiye edilmiş montmorillonit (OMMT) gibi farklı doğal substratlar üzerinde grafen yapıları büyütme amaçlamaktadır. Bu umut verici yöntem, atık PS ve PET'ten 2D veya 3D grafen yapılarının oluşumunu teşvik etmektedir ve substrat tipini ve boyutunu, substratın yüzey

bileşimini ve polimerdeki aromatiklik derecesini uyarlayarak boyut kontrollü grafen büyümesi sağlar. Ek olarak, çift vidalı ekstrüzyon ve termokinetik karıştırma gibi polimer işleme tekniklerinin, kristallik derecesi analiz edilerek grafen ile yetiştirilen hibrit katkı maddelerinin geliştirilmesi üzerindeki etkisi araştırıldı.

Geliştirilmiş termal tabanlı ileri dönüşüm teknolojisi ile ilgili olarak, 10 µm'ye kadar D50 partikül boyutuna sahip talk substratı iki boyutlu (2D) grafen levhaların büyümesini desteklerken, 2 µm'den daha küçük boyutlu talk, üç boyutlu (3D) üretimine yardımcı oldu. PS kaynağını kullanarak grafen küreleri. Özellikle demir katalizörü ile muamele edilen talk, substrat üzerinde karbon birikimini tetikledi ve grafen katmanlarının sayısını artırdı. PS polimerinin bozunmasını arttırmak ve substrat tipinin grafen büyüme mekanizması üzerindeki etkisini göstermek için talk yerine substrat olarak kullanılan OMMT kullanıldı. PS atığı varlığında herhangi bir katalizör kullanmadan OMMT yüzeyinde levha benzeri grafen elde etmek mümkün olmuştur. Atık PS'ye ek olarak, demirle işlenmiş mikron boyutlu talk yüzeyinde grafen büyütme için bir karbon kaynağı olarak PET kullanıldı ve PET'in polimer bozunması PS'den daha karmaşık olduğundan PS, PET polimerden daha iyi performans gösterdi.

Termal geri dönüşümden önce, kesme hızının dolgu maddesinin pul pul dökülmesi üzerinde doğrudan bir etkisi olduğu gözlemlendi. Yapısal karakterizasyon sonuçları, yüksek kesme oranlı karıştırıcının talkın kristal düzlemlerinde değişikliğe yol açtığını, oysa geleneksel çift vidalı ekstrüzyonun talkın yapısal özelliklerini koruduğunu gösterdi.

Ayrıca, talk ve OMMT substratlarında büyütülen grafenlerin CO<sub>2</sub> ayak izini geleneksel tekniklerle üretilen grafene kıyasla değerlendirmek için sistematik bir yaşam döngüsü değerlendirmesi yapıldı. Doğrudan karbonizasyon ve hatta PS veya PET kaynağı ile katalizör emdirilmiş doğal substrat bazlı grafen büyüme süreci ile elde edilen ileri dönüşümlü grafen yapıları, grafitin kimyasal pul pul dökülmesiyle üretilen grafene kıyasla nispeten daha düşük CO<sub>2</sub> emisyonuna sahiptir. Sonuç olarak, bu yeni geliştirilen ve geri dönüştürülmüş hibrit katkı maddeleri, polimer harmanlama işleminde katı alt tabaka ile grafen boyutunu korumak ve dairesel bir ekonomi modelini benimseyerek grafenin yapısal bütünlüğünü korumak için faydalı bilgiler sunuyor.

## ACKNOWLEDGEMENTS

I want to express my gratitude to everyone who made it possible for me to finish my thesis.

First and foremost, I want to express my sincere gratitude to my supervisor, Associate Professor Dr. Burcu Saner Okan, for her valuable guidance and counsel during the research.

I want to thank and appreciate Prof. Dr. Yusuf Mencelođlu for his support, insightful criticism, and recommendations and jury member of Assoc. Prof. Dr. Bertan Beylergil.

I would like to express my gratitude to Dr. Havva Başkan Bayrak, who worked with me on the research, for her support and encouragement throughout. I would like to thank my colleague Atakan Kocanalı who worked with me in TUBITAK project for his support. I also give sincere thanks to my friends, Kuray Dericiler, Gülayşe Şahin Dündar and Büşra Çetiner for SEM characterization and Dr. Semih Dođan for XPS analyses. I also especially thank to SUIMC technicians, Sezer Özdemir, Feyyaz Perem and Sinan Ayazlı.

I also want to thank to Sercan Akgün, Orhun Şenol, Göktuđ Kılıç, Nargiz Aliyeva, Gizem Arıtürk, Nihan Birgün, Fethiye Esin Yakın, Mostafa Mehdipour Aghbolagh and especially to Samet Özyiđit for their support, encouragement, motivation, and their friendships.

I also want to express my gratitude to all SU-IMC members for their cooperation and support throughout this process.

My parents have given me so much support and encouragement, and I truly appreciate it. Finally, I would like to express my sincere gratitude to the 1003 program of the Turkish Council for Scientific and Technological Research (TUBITAK) for providing financial support for the project 218M658.

To my beloved family...

## TABLE OF CONTENTS

ABSTRACT.....	iv
ÖZET.....	vi
ACKNOWLEDGEMENTS.....	viii
LIST OF TABLES .....	xiii
LIST OF FIGURES.....	xv
<b>LIST OF ABBREVIATIONS .....</b>	<b>xviii</b>
CHAPTER 1. STATE OF THE ART .....	1
CHAPTER 2. GRAPHENE SYNTHESIS FROM WASTE SOURCES .....	3
CHAPTER 3. GROWING OF 2D/3D UPCYCLED GRAPHENE ON TALC FROM AROMATIC WASTE BY TAILORING RESOURCES AND HEAT TREATMENT TECHNIQUES WITH A COMPARATIVE CO <sub>2</sub> FOOTPRINT ANALYSIS.....	5
3.1. INTRODUCTION .....	5
3.2. EXPERIMENTAL.....	7
3.2.1. Materials .....	7
3.2.2. Surface activation of talc .....	8
3.2.3. The formation of upcycled graphene/talc hybrid additives from polystyrene waste .....	8
3.2.4. Fabrication of hybrid additive reinforced polypropylene (PP) composites 10	
3.2.5. Characterization .....	11
3.3. RESULTS and DISCUSSION.....	11
3.3.1. The effect of talc size and catalyst on the characteristics of PS-derived hybrid additives from the same mixing system .....	11
3.3.2 The effect of polymer mixing techniques on the characteristics of PS-derived hybrid additives .....	20

3.3.3 Dimension characterization of PS-derived hybrid additives by SEM and TEM .....	24
3.3.4. Thermal properties of graphene grown on talc surface .....	30
3.3.5. Comparative life cycle assessment of PS-derived graphene/talc hybrid additives and their separated graphene structures .....	32
3.4. CONCLUSION.....	36
CHAPTER 4. UPCYCLING OF POLYSTYRENE WASTE INTO GRAPHENE GROWN ON ORGANICALLY MODIFIED MONTMORILLONITE AS A SUBSTRATE.....	38
4.1. INTRODUCTION .....	38
4.2. EXPERIMENTAL.....	38
4.2.1 Materials .....	38
4.2.2. The formation of upcycled graphene/OMMT hybrid additive from polystyrene waste .....	39
4.2.3. Characterization.....	39
4.3. RESULTS and DISCUSSION.....	40
4.3.1. Structural characteristics of the upcycled graphene/OMMT hybrid additive, and its separated graphene structure.....	40
4.3.2. Chemical characteristics of the upcycled graphene/OMMT hybrid additive, and its separated graphene structure.....	42
4.3.3. Morphological properties of the upcycled graphene/OMMT hybrid additive, and its separated graphene structure.....	44
4.3.4. Thermal properties of the upcycled graphene/OMMT hybrid additive, and its separated graphene structure .....	44
4.3.5. Life cycle assesment of the upcycled graphene/OMMT hybrid additive, and its separated graphene structure.....	46
4.4. CONCLUSION .....	49
CHAPTER 5. UPCYCLING OF POLYETHYLENE TEREPHTHALATE WASTE INTO GRAPHENE GROWN ON TALC AS SUBSTRATE .....	50

5.1. INTRODUCTION .....	50
5.2 EXPERIMENTAL .....	51
5.2.1. Materials .....	51
5.2.2. Converting of polyethylene terephthalate waste into upcycled graphene on talc surface .....	51
5.2.3. Characterization.....	51
5.3. RESULTS and DISCUSSION .....	52
5.3.1. Structural characteristics of the upcycled graphene/talc hybrid additives, and their separated graphene structures .....	52
5.3.2. Chemical characteristics of the upcycled graphene/talc hybrid additives, and their separated graphene structures .....	56
5.3.3. Morphological characteristics of the upcycled graphene/talc hybrid additives, and their separated graphene structures.....	57
5.3.4. Thermal properties of characteristics of the upcycled graphene/talc hybrid additives, and their separated graphene structures .....	58
5.3.5 Comparative life cycle assessment of PET-derived graphene/talc hybrid additives and their separated graphene structures .....	60
5.4. CONCLUSION .....	64
CHAPTER 6. CONCLUSIONS .....	65

## LIST OF TABLES

<b>Table 1.</b> The summary of the compound sources used for hybrid additive production based on polymer processing and heat treatment types. ....	10
<b>Table 2.</b> The elemental chemical compositions of neat micron talc and fine talc, their hybrid additives obtained from direct and catalytic carbonization processes, and separated graphene structures after acid treatments. ....	18
<b>Table 3.</b> The elemental composition of the micron talc, directly grown graphene/micron talc hybrid additives processed by twin-screw extrusion, and their separated graphene structures after acid treatments. ....	23
<b>Table 4.</b> Weight loss micron talc, Fe-micron talc, fine talc, Fe-fine talc, directly and catalytically grown graphene/micron talc hybrids, and directly and catalytically grown graphene/fine talc hybrids at 500°C, 750°C and 1000°C. ....	32
<b>Table 5.</b> The environmental impacts of directly and catalytically grown graphene/talc hybrid additives and their separated graphene structures. ....	34
<b>Table 6.</b> The impact of production inputs of the hybrid additives and their separated graphene structures on global warming potential. ....	36
<b>Table 7.</b> The elemental composition of the upcycled graphene/OMMT hybrid additive and its separated graphene structure after acid treatments. ....	43
<b>Table 8.</b> The weight loss of neat OMMT, and upcycled graphene/OMMT hybrid at 250°C, 750°C and 1000°C. ....	45
<b>Table 9.</b> The environmental impacts of neat OMMT, graphene/OMMT hybrid additive, and its separated graphene structure. ....	47
<b>Table 10.</b> The impact of production inputs of the upcycled graphene/OMMT hybrid additive and its separated graphene structure on global warming potential. ....	48
<b>Table 11.</b> XPS elemental analysis of neat micron talc, directly and catalytically grown graphene/micron talc hybrid additives, and their separated graphene structures after acid treatments. ....	56
<b>Table 12.</b> The weight loss of micron talc, Fe-micron talc, directly and catalytically grown graphene/ micron talc hybrid at 250°C, 750°C and 1000°C. ....	60
<b>Table 13.</b> The environmental impacts of directly and catalytically grown graphene/talc hybrid additives from waste PET. ....	62
<b>Table 14.</b> The impact of production inputs of the hybrid additives and their separated graphene structures on global warming potential. ....	64

**Table 15.** Summary of graphene growth on the surface of OMMT, micron and fine talc.  
..... 68

## LIST OF FIGURES

<b>Figure 1.</b> The summary of the experimental scheme of the fabrication of graphene/talc hybrids from waste PS by upcycling. ....	9
<b>Figure 2.</b> FTIR spectra of (a) micron talc, directly and catalytically grown graphene/micron talc hybrids, and (b) micron talc, directly and catalytically grown graphene/micron talc hybrids.....	12
<b>Figure 3.</b> Comparison Raman spectra of upcycled graphene grown on (a) micron talc and (b) Fe-micron talc; (c) fine talc and (d) Fe-fine talc surfaces. ....	14
<b>Figure 4.</b> Comparison XRD patterns of upcycled graphene grown on (a) micron talc, (b) Fe-micron talc, (c) fine talc, and (d) Fe-fine talc. ....	16
<b>Figure 5.</b> XPS survey scan of (a) directly grown graphene/micron talc hybrid and its separated graphene structure, (b) catalytically grown graphene /Fe-micron talc hybrid and its separated graphene structure, (c) directly grown graphene/fine talc hybrid and its separated graphene structure, and (d) catalytically grown graphene/Fe-fine talc hybrid and its separated graphene structure. ....	20
<b>Figure 6. (a)</b> Raman spectra, and <b>(b)</b> XRD patterns of micron talc, directly grown graphene/micron talc hybrid processed by twin-screw extrusion and its separated graphene structure after acid treatments. ....	22
<b>Figure 7.</b> XPS survey scan of directly grown extruded graphene/micron talc hybrid and its separated graphene structure. ....	24
<b>Figure 8.</b> SEM images of (a) micron talc, (b) directly and (c) catalytically grown graphene/micron talc hybrid additives.....	25
<b>Figure 9.</b> SEM image of directly grown graphene/micron talc hybrid by extrusion. ....	26
<b>Figure 10.</b> SEM images of (a) Fe-treated micron talc, and (b) Fe-treated fine talc.....	26
<b>Figure 11.</b> SEM images of (a) fine talc, (b) directly and (c) catalytically grown graphene/fine talc hybrid additives.....	27
<b>Figure 12.</b> SEM images of separated graphene structures: (a) directly and (b) catalytically grown graphene /micron talc by thermokinetic mixer, (c) directly and (d) catalytically grown graphene/fine talc by thermokinetic mixer, and (e) directly grown graphene /micron talc by extrusion.....	28
<b>Figure 13.</b> TEM images of separated graphene structures of (a) directly and (b) catalytically grown graphene /micron talc by thermokinetic mixer, (c) directly and (d) directly grown graphene /micron talc by extrusion. ....	30

<b>Figure 14.</b> d-spacing of separated graphene structures of (a) directly and (b) catalytically grown graphene /micron talc, (c) directly and (d) directly grown graphene /micron talc by extrusion. ....	30
<b>Figure 15.</b> TGA thermograms of under (a) nitrogen and (c) oxygen atmosphere micron talc, Fe-micron talc, and directly and catalytically grown graphene/micron talc hybrids, and (b) under nitrogen and (d) oxygen atmosphere fine talc, Fe-fine talc and directly and catalytically grown graphene/fine talc hybrids. ....	32
<b>Figure 16.</b> The comparison of global warming potential of talc, neat waste PS, directly and catalytically grown graphene/talc hybrid additives, their separated graphene structures, and rGO. ....	35
<b>Figure 17.</b> FTIR spectra of neat OMMT, and upcycled graphene/OMMT hybrid. ....	41
<b>Figure 18.</b> (a) Raman spectra, and (b) XRD patterns of OMMT, upcycled graphene grown on OMMT surface and its separated graphene structure after acid treatments. ..	42
<b>Figure 19.</b> XPS survey scan of upcycled graphene/OMMT hybrid and its separated graphene structure after acid treatments. ....	43
<b>Figure 20.</b> SEM images of (a) upcycled graphene/OMMT hybrid, and (b) its separated graphene structure after acid treatments. ....	44
<b>Figure 21.</b> TGA thermogram of neat OMMT and upcycled graphene/OMMT hybrid.	45
<b>Figure 22.</b> The comparison of global warming potential of neat OMMT, graphene/OMMT hybrid additives, its separated graphene structure, and rGO. ....	48
<b>Figure 23.</b> FTIR spectra of micron talc, directly grown graphene/micron talc hybrid, and catalytically grown graphene/Fe-micron talc hybrid. ....	53
<b>Figure 24.</b> Comparison Raman spectra of micron talc, (a) directly, and (b) catalytically grown graphene/micron talc hybrid additives, and their separated graphene structures.	54
<b>Figure 25.</b> Comparison XRD patterns of micron talc, (a) directly, and (b) catalytically grown graphene/micron talc hybrid additives, and their separated graphene structures.	55
<b>Figure 26.</b> SEM images of (a) directly and (b) catalytically grown graphene /micron talc hybrid additives from waste PET. ....	57
<b>Figure 27.</b> SEM images of separated graphene structures of (a) directly and (b) catalytically grown graphene /micron talc hybrid additives from waste PET. ....	58
<b>Figure 28.</b> TGA thermograms of micron talc, Fe-micron talc, directly and catalytically grown graphene /micron talc hybrid additives from waste PET (a) under nitrogen and (b) oxygen. ....	59

<b>Figure 29.</b> The comparison of global warming potential of neat waste PET, directly and catalytically grown graphene/talc hybrid additives, their separated graphene structures, and rGO.....	63
<b>Figure 30.</b> The concept for creating 2D sheet-like graphene structures from aromatic plastic waste on micron talc.....	65
<b>Figure 31.</b> The concept for creating 3D spherical nano-carbon structures from aromatic plastic waste on fine talc.....	66

## LIST OF ABBREVIATIONS

CVD	Chemical Vapor Deposition
CNMs	Carbon-Nano Materials
CNT	Carbon Nanotubes
CO <sub>2</sub>	Carbon dioxide
FTIR	Fourier Transform Infrared Spectroscopy
GNP	Graphene Nanoplatelet
GWP	Global Warming Potential
GO	Graphene Oxide
LCA	Life Cycle Analysis
LCI	Life Cycle Inventory
LCIA	Life Cycle Impact Assessment
LLDPE	Linear Low-density polyethylene
OMMT	Organically modified montmorillonite
PA	Polyamide
PE	Polyethylene
PP	Polypropylene
PS	Polystyrene
PET	Polyethylene Terephthalate
rGO	Reduced Graphene Oxide
MWNT	Multi-walled Carbon Nanotubes
RAMAN	Renishaw inVia Reflex Raman Microscopy System
SEM	Scanning Electron Microscope
TEM	High Resolution Transmission Electron Microscope
TGA	Thermogravimetric Analysis
T <sub>c</sub>	Crystallization Temperature
T <sub>m</sub>	Melting Temperature
XPS	X-ray Photoelectron Spectroscopy
XRD	X-ray Diffraction

## CHAPTER 1. STATE OF THE ART

Plastic manufacturing and usage have increased dramatically as a result of rapid urbanization and economic growth in many countries. The majority of plastics ends up in ocean, landfills, or incineration plants. The recovery rate of plastic trash remains relatively low due to the poor recycling value of plastics and a lack of technological help [1]. Therefore, upcycling has been offered as a sustainable, and cost-effective solution for the plastic waste management and to obtain high value added materials, such as carbon nanotubes (CNTs), and graphene, from waste plastics [2, 3].

Polyolefins (polypropylene (PP) and polyethylene (PE)), polyethylene terephthalate (PET), and polystyrene (PS) constitute most of the total plastic production and concomitant plastic waste disposal. Among these commodity plastics, PS, PET, polycarbonate, and high-performance polymers are some of the examples of synthetic polymers with aromatic rings that are widely used in modern products such as food packaging, electronics, and building materials. The distinctive qualities conferred by planar and rigid aromatic moieties are reflected in the wide range of applications for these polymers [4]. Hence, the conversion of these plastics into graphene by upcycling and focusing on the structural properties of these polymers on the final characteristics of upcycled graphene need to be examined.

Graphene, a two-dimensional (2D) honeycomb lattice, is a fundamental building block of all graphitic materials. Because of its great electrical and thermal conductivity, mechanical strength, and transparency, graphene is a promising material for a wide range of applications [5]. Graphene can be produced from waste PS by thermal treatment such as pyrolysis and carbonization. Since thermal treatment does not utilize harmful chemicals, and is a simple production method, it can be regarded as an environment-friendly technique due to the decreased carbon release compared to the conventional graphene synthesis techniques [6].

The global warming potential, and carbon footprint of a product or a system can be determined by 'Life Cycle Analysis (LCA)'. The term 'LCA' refers to a methodological framework for assessing and analyzing environmental consequences associated with the life cycle of products, or services. A completed LCA would use a "cradle-to-grave" approach, taking into account each stage of the life cycle: product design/development,

raw material procurement, production, distribution, use/maintenance/re-use, and end-of-life activities. Specifying carbon dioxide (CO<sub>2</sub>) emission for possible production methods shows which process is more environment-friendly [7].

In the second chapter of this thesis, a summary of the literature studies on the formation of graphene from waste aromatic sources through upcycling was comprehended by highlighting state-of-the-art technologies.

In the third chapter, the conversion of waste PS into two-dimensional (2D), and three-dimensional (3D) graphene on talc surface by upcycling was discussed. The impact of utilized talc substrate size, polymer blending method prior to carbonization, the presence of iron catalyst on the final characteristics of upcycled graphene was examined in detail. The reinforcement agent performance of the obtained hybrid additive was examined in PP composites. In addition, the global warming potential of the direct and catalytic carbonization processes in case of iron catalyst was dealt by LCA.

In the fourth chapter, the formation of upcycled graphene from waste PS on organically modified montmorillonite (OMMT) rather than talc substrate was introduced. The upcycled graphene structure grown on OMMT was approved by spectroscopic, morphologic, and thermal characterization methods. Furthermore, carbon dioxide emission of the production of upcycled graphene/OMMT hybrid additive was calculated by LCA.

In the fifth chapter, upcycled graphene formation on talc surface from waste PET was mentioned. The influence of surface activation of talc with iron (III) chloride (FeCl<sub>3</sub>) was inspected, and the structural, morphologic, thermal characteristics of the obtained hybrid additives were analyzed. Finally, LCA was conducted to observe the environmental consequences of the upcycled graphene grown on talc substrates from waste PET.

This research ensured the production of graphene from aromatic waste sources on both talc, and OMMT surfaces. The final characteristics of the produced graphene structure could be tuned by changing the talc size, or polymer processing methods. In summary, this simple and useful approach provides a sustainable hybrid formation for several engineering applications by contributing the plastic waste management, and circular economy.

## CHAPTER 2. GRAPHENE SYNTHESIS FROM WASTE SOURCES

Due to its unique features, graphene has been widely used in a variety of industrial applications in recent years [8]. Graphene can be synthesized from several conventional techniques such as mechanical, and chemical exfoliation of graphite, epitaxial growth of graphene on different substrates, deposition of graphene by chemical vapor deposition (CVD), and reduction of graphene oxide (GO) from graphite by Hummers' technique [8–10]. Among these, reduction of graphite oxide or graphene oxide, mechanical exfoliation of graphite, and CVD are the most popular graphene synthesis methods [11, 12]. In the reduction of graphite oxide or graphene oxide, the oxidation of graphite was achieved by treating graphite particles in a concentrated sulfuric acid ( $\text{H}_2\text{SO}_4$ ) solution in a severe and hazardous manner [10]. Although this process results in the finest grade graphene, a fabrication method for synthesizing wafer scale graphene is required for mass production [13]. On the other hand, due to its widespread popularity, CVD method limited success due to the occurrence of prolonged flaws and voids that risk the film's structural integrity [12]. Therefore, an alternative method, upcycling, has been introduced for the production of graphene from waste sources such as foods, animals, or plastics [14–16].

Muramatsu et al. were the first to report the synthesis of graphene from rice husk in the presence of potassium hydroxide (KOH) and carbon black [17]. Akhavan et al. used the chemical exfoliation method to synthesize high-quality GO and rGO sheets from low-cost natural and industrial carbonaceous wastes such as vegetation wastes (wood, leaf, bagasse, and fruit wastes), animal wastes (bone and cow dung), a semiindustrial waste (newspaper), and an industrial waste (soot powders produced in diesel vehicle exhaust) [18]. In one of the studies, Ruan *et al.* suggested a new method for producing high-quality single-layered graphene from waste PS and other carbon-containing wastes. Waste PS, grass blades, dog excrement, insect legs, waste cookie, and chocolate were among the raw wastes [19]. In the other study, by carbonizing PS at 900 °C, Yang and colleagues were able to create porous carbon materials with hierarchical macro-meso-microporous structure, and the resulting materials, when used as high-rate anode electrodes in LIBs, displayed a steady capacity of 410 mA h g<sup>-1</sup> for more than 100 cycles [20]. In addition, hierarchical porous carbon nanosheets that contained micropores/mesopores were prepared from waste PS using the template approach with

high yields, where the mesopores were inherited from a porous magnesium oxide (MgO) template and the micropores are produced by KOH activation [21]. CNTs were created by Hedeyati et al. using black and white polystyrene plastics [22]. By carbonizing PS on MgO at 700 °C using a one-pot technique, porous carbon sheets and hollow carbon shells could be generated [23]. A straightforward and common two-step technique, char formation and chemical activation, was proposed to obtain activated carbon (AC) with outstanding textural qualities from waste PS foam [24]. In a recent experiment, high-impact polystyrene (HIPS) was heated to 950 °C in a reactor, and then pyrolyzed to produce a carbon material [25]. In another study, waste PS cups were carbonized between 600 and 700 °C to produce a carbon material for sodium-ion battery applications [26]. Besides PS, there were also some attempts for the conversion of waste PET into high-value added carbon materials. PET is typically pyrolyzed by chain scission, depolymerization, and deoxygenation to yield pyrolytic gas and aromatic hydrocarbons, which can then be recondensed to form polyaromatic hydrocarbons [27]. Recent developments include the use of techniques that reduce the expense and negative effects of pyrolysis, such as co-pyrolysis with zinc dust to produce graphite from PET. Boron-assisted catalytic graphitization was also preferred to repurpose the high carbon content within waste polymers into carbon-based nanomaterials [28]. In a study, Kamali and Yang achieved to prepare a porous carbon nanosheet from waste PET in the presence of molten salts [29]. Yuan *et al.* also produced porous carbon structure for the adsorption of carbon tetrafluoride (CF<sub>4</sub>), by the carbonization of PET at 600 °C, followed by post-activation using KOH between 600 and 1000 °C [25]. On the other hand, Lessawy et al. obtained functionalized magnetic fullerene nanocomposites (FMFNC) by thermally decomposing PET in a single step at 800 °C in the existence of ferrocene catalyst [30]. It was concluded that the direct carbonization of PET at a high temperature typically resulted in relatively low carbon content nearly 17-22% at 700 °C in a gas environment, and approximately 25 % at 550 °C in a molten salt [32, 33].

Diverse synthesis methods of graphene and carbon nanomaterials from upcycling of waste plastics or biocursors were evidenced based upon this literature review. Upcycling aromatic waste plastics, specifically PS and PET, allowed to obtain mostly porous nanomaterials and AC. The utilization of aromatic waste plastics opens up new possibilities for cost-effective, and environment-friendly method to bulk graphene manufacturing, as well as a solution to the worldwide plastic waste management.

## **CHAPTER 3. GROWING OF 2D/3D UPCYCLED GRAPHENE ON TALC FROM AROMATIC WASTE BY TAILORING RESOURCES AND HEAT TREATMENT TECHNIQUES WITH A COMPARATIVE CO<sub>2</sub> FOOTPRINT ANALYSIS**

In this chapter, waste polystyrene was converted into two-dimensional and three-dimensional graphene structures on talc substrates, which have different particle size, by upcycling, and the impact of aromaticity, coming from the waste PS, on the graphene formation was investigated. In addition, the effect of Fe-catalyst, and polymer processing techniques on the growth of graphene on talc surfaces was examined in detail. The microstructure, phase structure, elemental composition, and morphology of the graphene /talc hybrid additives and their separated graphene forms were systematically investigated by several spectroscopic and microscopic characterization techniques. The extruded graphene/micron talc hybrid was reinforced to polypropylene composites in order to improve the mechanical performance of the resultant material for industrial applications. In the last stage, the global warming potential of the obtained hybrid additives and their separated graphene structures was determined via life cycle assesment.

### **3.1. INTRODUCTION**

Plastics are inevitable daily-life products in modern life due to their low cost, high strength, and suitability for many applications. The most widely utilized plastic products consist of inert plastics, in particular, polypropylene (PP), polyethylene (PE), polyethylene terephthalate (PET), and polystyrene (PS), which comprise more than half of the total plastic production [1-2]. However, the wide usage of plastic products requires proper plastic waste management since waste plastic materials are quite harmful to the ecosystem, soil, water, and thus human health [34]. It is estimated that by the end of 2030, the amount of plastic waste will increase twice more than today. In particular, the plastic waste amount has risen dramatically during coronavirus disease (COVID-19) which has boosted the single-use applications of plastic products such as food packaging in the last two years [35].

Among the commodity plastics, PS is a miscellaneous polymer commonly used in single-use plastic products like food packaging, coffee/tea cups, and cosmetic and computer goods [4]. The increased single-use of PS-based plastic products and their disposal cause significant environmental concern due to their non-degradable nature.

Indeed, the solid and expanded forms of PS can be recycled into the pen, pencils, other office equipment, video cassette, and so on. However, the production of recycled PS material becomes more expensive than the fabrication of products, and in particular, PS foam loses its novel foam features after recycling [36]. Moreover, due to its blend and copolymer forms and aromatic rings with an identical polymer backbone, it is challenging to recycle PS waste using the conventional recycling methods, such as landfilling, incineration, and mechanical recycling [1, -5]. Therefore, upcycling high-volume PS wastes into high-value products has become prominent [1-8].

Upcycling is an innovative transformation technique to convert plastic wastes into high-value-added products. It is also a cost-benefit and sustainable method that proposes to utilize inexpensive sources to produce precious carbon materials such as carbon nanotubes and graphene [9, 10]. Graphene, a versatile two-dimensional material, is of great interest in both the research community and industry due to its high surface area, mechanical strength, and stable chemical properties [40]. Although there are various methods to obtain graphene structures, such as mechanical [41] and chemical exfoliation of graphite [42] to facilitate graphene growth, epitaxial growth of graphene on different substrates [43], deposition of graphene by chemical vapor deposition (CVD) [44] and reduction of graphene oxide (GO) from graphite by Hummers method [45], these methods need an intensive resource, and result in different qualities of graphene structures and are not appropriate for large-scale production. The production of graphene from waste plastics by upcycling is advantageous in this manner and contributes to plastic waste management [46].

There are few attempts to obtain carbonaceous materials from waste aromatic plastics, for instance, PET, polyurethane (PU), and PS. In one of the studies, Li and coworkers processed PU waste to convert it into activated carbon by upcycling for the adsorption of malachite green dye from aqueous solutions. To this end, carbonization between 300-700°C followed by activation offered to obtain PU waste-based activated carbon with a high specific surface area (1034 m<sup>2</sup>/g) for the maximum adsorption capacity (1428 mg/g) [47]. In another work, Yuan *et al.* carbonized PET waste plastic bottles and further activated them by using potassium hydroxide (KOH) to obtain porous carbon structure in a cost-effective and environmental-friendly technique, upcycling, for the adsorption of carbon tetrafluoride (CF<sub>4</sub>). In the study, PET plastic waste was carbonized in the temperature range of 600-1000°C. The textural features of the concomitant

porous carbon were considerably affected by both the carbonization and activation procedures [48]. Ko *et al.* also studied the upcycling of PET waste plastic bottles to generate a crystal carbon structure, synthetic graphite. Heat treatment, followed by graphitization in the presence of boron, was applied to the waste bottles under an inert atmosphere. Then, graphene nanosheets were acquired from the resultant graphite via liquid-phase exfoliation [49]. In addition, Ezzat and Ali offered a 'green way' to convert PET waste plastic bottles into graphene in an autoclave by pyrolysis to remove dyes from the wastewater [50].

On the other hand, the formation of graphene from PS waste via upcycling was attempted by Mensah *et al.* The effect of carbonization temperature on the features and yield of the graphene structure was inspected by applying heat at temperatures between 500-1000 °C for two hours. Applying heat above 700 °C resulted in a spherical graphene structure with low porosity, while the carbonization below 700 °C allowed to obtain mesoporous carbon [51].

To the best of our knowledge, there is a lack of studies on converting waste PS into graphene on a talc surface by controlling the dimension of graphene structures and explaining the effect of aromaticity on graphene formation. Thus, in this study, graphene growth was achieved from waste PS on different sized-talc surfaces by upcycling, and dimension-controlled graphene/talc hybrid additives from waste PS were attained. In addition, the impact of aromaticity of PS polymer and the presence of iron catalyst on the growth of graphene/talc hybrids were examined as well as the influence of polymer processing techniques. Moreover, the selected graphene/micron talc hybrid was used to reinforce the PP composites to improve the mechanical performance of the resultant product for industrial requirements. Finally, the life cycle assessment of the selected graphene /micron talc hybrid was performed to observe the environmental impacts of the produced hybrid. This research highlighted the significant impact of polymer backbone structure on the formation of graphene with the polymer processing and the utilized substrate size by contributing to the circular economy.

## **3.2. EXPERIMENTAL**

### **3.2.1. Materials**

Micron talc with the particle size of  $D_{50} = 12 \mu\text{m}$  and fine talc with the particle size of  $D_{50} = 1.9 \mu\text{m}$  were supplied from Micron'S company (Turkey) and Imerys company

(France), respectively. The carbon sources of polystyrene (PS) and extruded PS/micron talc compound were purchased from Eurotech Company (Turkey) for upcycled graphene /talc hybrid additive fabrication. To activate the talc surface, iron chloride ( $\text{FeCl}_3$  ( $\geq 97\%$ )) was received from Sigma-Aldrich. To obtain separated graphene structures from hybrid additives, hydrofluoric acid ( $\text{HF} \geq 37\%$ ) and nitric acid ( $\text{HNO}_3$ ,  $\geq 65\%$ ) were taken from Sigma-Aldrich. To prepare the hybrid additive reinforced homopolymer and copolymer polypropylene (PP) composites, PP was obtained from Ravago Petrochemical Company (Turkey).

### **3.2.2. Surface activation of talc**

The type of nanoparticles used, their size and shape, concentration, and interactions with the polymer matrix all influence the properties of polymer composites. The fundamental issue with polymer nanocomposites is particle aggregation avoidance. Nanoparticles agglomerate due to their particular surface area and volume effects, making it challenging to generate monodispersed nanoparticles in a polymer matrix. Furthermore, there are no ionic groups in the talc structure. The hydrophobic surface chemistry of completely pure talc makes it difficult to distribute into the polymer matrix. The surface of the inorganic particles can be modified to solve this problem. The modification improves the inorganic particles' interfacial interactions with the polymer matrix. The surface of inorganic particles can be modified in two ways. The first approach involves surface absorption or interaction with tiny molecules such as silane coupling agents, while the second involves grafting polymeric molecules to the particles' hydroxyl groups via covalent bonding [52].

Chemical activation of micron talc/fine talc was performed in a 0.5 M  $\text{FeCl}_3$  aqueous solution (500 ml) through refluxing at  $80^\circ\text{C}$  for 24 h. Then, the reaction temperature was cooled down to room temperature and vacuum filtration was applied to obtain the Fe-treated micron talc/Fe-treated fine talc samples. Finally, the collected Fe-micron talc/Fe-treated fine talc samples were dried at  $80^\circ\text{C}$  for 24 h.

### **3.2.3. The formation of upcycled graphene/talc hybrid additives from polystyrene waste**

In the initial step, the upcycled graphene was grown separately on micron talc and fine talc surface. For this purpose, the carbon source, waste PS, was mixed with the micron talc in the weight ratio of 80:20 via a thermokinetic mixer (Dusatec) at  $180^\circ\text{C}$  with a

high shear rate of 3000 rpm. Then, the waste PS/micron talc compound was subjected to heat treatment in an Argon atmosphere starting from room temperature up to 1000 °C and keeping the compound at 1000 °C for 5 min for the accumulation of graphene structures on micron talc to get a high degree of graphitization on talc substrate. The same protocol was also performed for the formation of a graphene structure on a fine talc surface. The effect of talc size on the formation of upcycled graphene from waste PS was investigated by keeping all parameters the same. In the second step, iron (Fe)-treated micron talc and Fe-treated fine talc were also utilized as substrates to observe the effect of surface activation of talc on graphene formation. Hereby, chemical activation of micron talc/fine talc was performed in a 0.5 M FeCl<sub>3</sub> aqueous solution (500 ml) through refluxing at 80°C for 24 h. Then, the reaction temperature was cooled down to room temperature, and vacuum filtration was applied to obtain the Fe-treated micron talc/Fe-treated fine talc samples. Finally, the collected Fe-micron talc and Fe-treated fine talc samples were dried at 80°C for 24 h [53]. In the last step, extruded PS/micron talc compound was directly carbonized at 1000°C for 5 min under an Argon atmosphere to form a micron talc-based hybrid additive. The summary of the experimental scheme is given in Figure 1, and the compound types for the fabrication of upcycled graphene structures, polymer processing, and carbonization type of the compounds are depicted in Table 1.

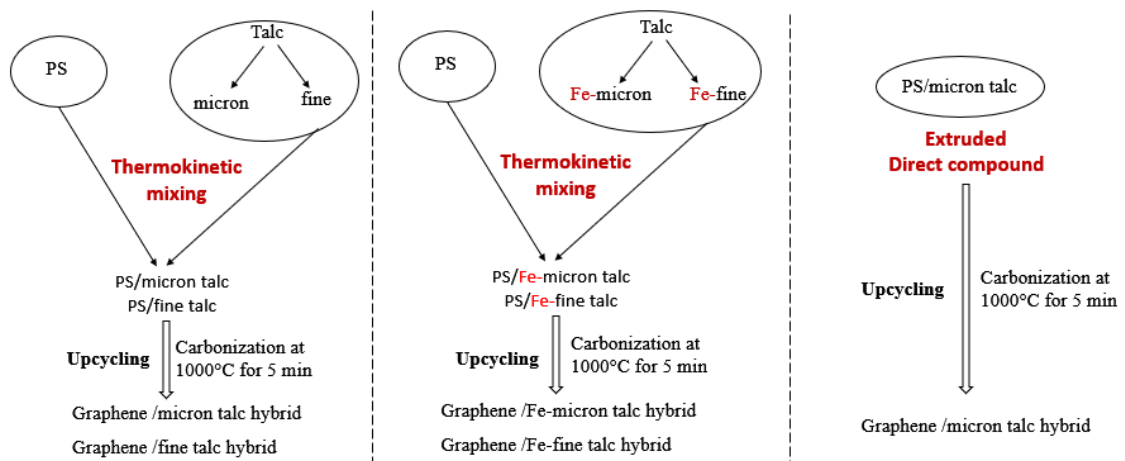


**Figure 1.** The summary of the experimental scheme of the fabrication of graphene/talc hybrids from waste PS by upcycling.

**Table 1.** The summary of the compound sources used for hybrid additive production based on polymer processing and heat treatment types.

<b>Compound type</b>	<b>Polymer processing type</b>	<b>Heat treatment type</b>
PS/micron talc	Thermokinetic mixing	Direct carbonization
PS/fine talc	Thermokinetic mixing	Direct carbonization
PS/Fe-micron talc	Thermokinetic mixing	Catalytic carbonization
PS/Fe-fine talc	Thermokinetic mixing	Catalytic carbonization
PS/micron talc	Twin-screw extrusion	Direct carbonization

Furthermore, graphene growth on treated and non-treated talc surfaces was proved by separating the upcycled graphene from the talc surface via acid treatments to the hybrid additives. For this reason, the hybrid samples were treated with 20 wt % HF acid solution for 48 h at room temperature, followed by vacuum filtration and a subsequent drying process at 50°C for 30 min to collect the treated materials. Then, the dried samples were subjected to HNO<sub>3</sub>: distilled water (1:2, v: v) for three hours at 110°C by refluxing. After three hours, the reaction mixture was cooled down and centrifuged at 7500 rpm for 15 min at room temperature by washing the treated samples with deionized water several times for effective graphene separation. At last, the separated graphene structures were dried at 80°C overnight and obtained in dried black powder forms.

#### **3.2.4. Fabrication of hybrid additive reinforced polypropylene (PP) composites**

The prepared hybrid additive of extruded PS/micron talc was reinforced to the copoPP and homoPP to enhance the mechanical performance of thermoplastic PP polymer for lightweight applications and confirm the newly developed hybrid additive as a reinforcing agent. In composite manufacturing, upcycled graphene/micron talc hybrid additive was reinforced to copoPP and homoPP in the range of 5wt% to 20wt% with four different loading ratios. The polymer mixing was performed by a high shear rate thermokinetic mixer at 3000 rpm at the temperature of 180°C to achieve a high degree of dispersion.

### **3.2.5. Characterization**

Talc samples (micron talc, fine talc, Fe-micron talc, and Fe-fine talc), upcycled graphene /talc hybrid additives, and the separated graphene structures were analyzed in detail via several spectroscopic and microscopic characterization methods. The surface functional groups of the hybrids and separated graphene structures were identified using the Fourier transform infrared spectroscopy (FT-IR, Thermo Scientific, Nicolet iS50 FTIR). Raman spectroscopy was conducted using a Renishaw inVia Reflex Raman Microscope with a 532 nm edge laser to examine the prepared samples' molecular arrangement and vibrational features. X-Ray Diffraction (XRD) characterization technique was applied by a Bruker D2 Phaser diffractometer with a CuK $\alpha$  radiation source to observe the characteristic graphene structure, talc peaks, and crystal structure of the samples. X-Ray Photoelectron Spectroscopy (XPS, Thermo Scientific, Waltham, Massachusetts, USA) characterization was performed for the elemental and chemical analysis of the samples. Surface morphology was investigated by Leo Supra 35VP Field Emission Scanning Electron Microscope (SEM, Carl Zeiss AG, Jena, Germany) and JEM-ARM200CFEG Ultra High-Resolution Transmission Electron Microscopy (TEM, JEOL, Japan). In order to assess thermal degradation rates and weight loss, the thermal characteristics of the samples were examined using a TGA instrument with Mettler Toledo TGA / DSC 3+ under a nitrogen environment between 25°C and 1000°C. In addition, samples were crushed into granules for the investigation of the mechanical properties of the neat and the hybrid additive reinforced composites, and test specimens were obtained using a mini-injection molding machine (Xplore, Sittard, The Netherlands). Afterward, the flexural and tensile properties of the test specimens were inspected via Instron 5982 Static Universal Test Machine (UTM) with 5 kN load cell for ISO 527-2 tensile tests and ISO 178 three-point bending tests. Moreover, the environmental impact of the hybrid additives was analyzed by life cycle assessment (LCA) using SimaPro (release 9.3.0.2) software and ReCiPe 2016 v1.1 midpoint method, Hierarchist version.

## **3.3. RESULTS and DISCUSSION**

### **3.3.1. The effect of talc size and catalyst on the characteristics of PS-derived hybrid additives from the same mixing system**

Talc size used as a substrate triggers carbonization in the presence of catalyst directly

affects the dimension of upcycled graphene. In order to monitor the graphene growing mechanisms, fine talc and micron talc and their iron-treated versions were used to tailor the dimensionality of graphene structures. After the heat treatment processes at 1000°C for 5 min, graphene/talc hybrid additives were characterized systematically to attain an ideal hybrid additive for reinforcing in the PP matrix. Initially, to identify the changes in the spectroscopic features of the obtained materials, FTIR analysis was carried out. Comparison FTIR spectra of micron talc, fine talc, and directly and catalytically grown graphene/micron talc and graphene/fine talc hybrids are given in Figure 2. The presence of talc is clearly seen in the infrared spectra of the first compounds via the very sharp O-H stretching at 3674 cm<sup>-1</sup> and the sharp symmetric Si-O-Si stretching at 667 cm<sup>-1</sup> [54]. The stretching vibration of Si-O was linked to the strong bands at roughly 963–972 cm<sup>-1</sup> [55]. The bending vibration of -OH causes the peak formations at 1645 and 910 cm<sup>-1</sup>, while the stretching vibration of Si-O-Si generates the absorptions at 1041 and 796 cm<sup>-1</sup> [56].

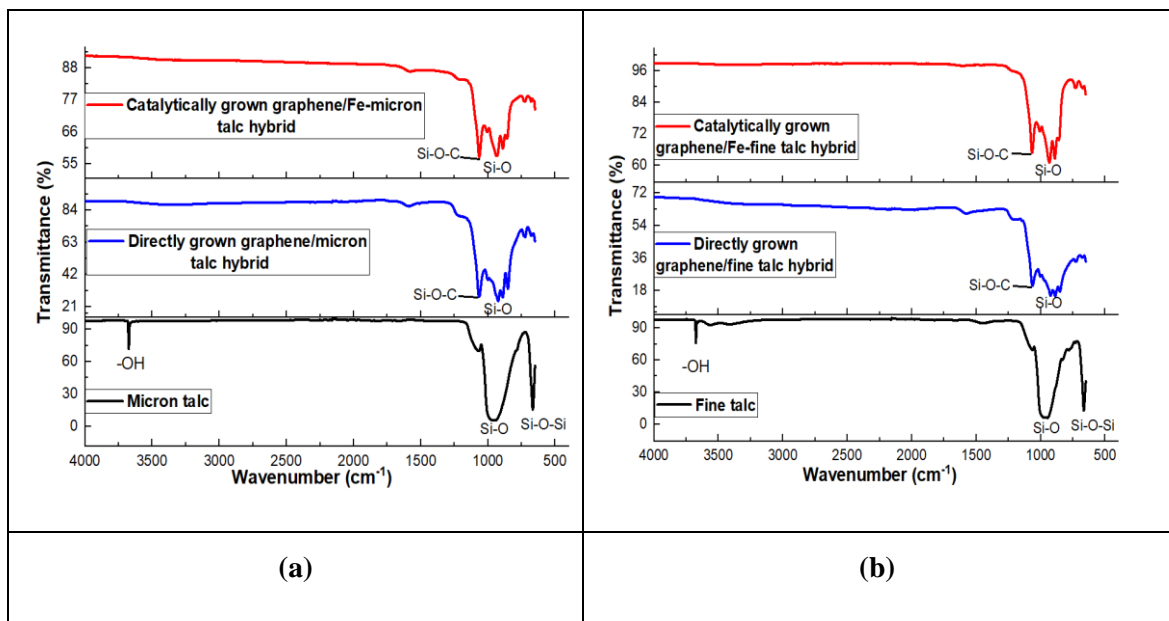


**Figure 2.** FTIR spectra of (a) micron talc, directly and catalytically grown graphene/micron talc hybrids, and (b) micron talc, directly and catalytically grown graphene/micron talc hybrids.

Raman spectroscopy characterization was carried out to confirm the existence of graphene and the number of grown graphene layers [23]. Figure 3 shows the comparison Raman spectra of upcycled graphene structures grown on micron talc and fine talc and Fe-treated talc samples after carbonization and acid treatment steps.

Micron talc has three prominent Raman peaks at  $195\text{ cm}^{-1}$ ,  $363\text{ cm}^{-1}$ , and  $678\text{ cm}^{-1}$  with different intensities, which disappeared after both direct and catalytic carbonization processes, as seen in Figure 3(a). After the carbonization step, the Raman spectrum of each hybrid type has D and G peaks that occurred at  $1344\text{ cm}^{-1}$  and  $1590\text{ cm}^{-1}$ , respectively, due to the stretching of  $\text{sp}^3$  and  $\text{sp}^2$  bonded carbon atoms [24, 25]. However, after the acid treatment processes, D and G peaks shifted to  $1350\text{ cm}^{-1}$  and  $1599\text{ cm}^{-1}$  due to the stress increase on graphene layers [61]. In the Raman spectrum, the D peak belongs to the disorders in the structure, and its peak intensity is directly related to the number of defects in the structure [59]. On the other hand, the G peak is associated with the first-order scattering of the in-plane vibrations of  $\text{sp}^2$  bonded carbon atoms and the degree of graphitization [60]. As the intensity ratio of D and G peaks increases, more  $\text{sp}^3$  bonds and disorders are present in the structure [59]. The  $I_{\text{D}}/I_{\text{G}}$  intensities of the directly grown graphene/micron talc hybrid and catalytically grown graphene/micron talc hybrid were calculated as 0.97 and 0.92, respectively, which were very close. However, the intensities of  $I_{\text{D}}/I_{\text{G}}$  ratios of separated graphene structures after acid treatments of directly grown graphene/micron talc hybrid and catalytically grown graphene/Fe-treated micron talc hybrid were determined as 0.99 and 0.88, respectively, provided in Figures 3(a) and 3(b). This indicated that surface activation of talc triggered the accumulation of graphene structures on Fe-micron talc, and more  $\text{sp}^2$  bonded carbon atoms were constituted via catalytic carbonization. The C–C and C–H bonds initially coordinated to the surface of Fe particles, which then catalyzed the cleavage of these bonds, resulting in many isolated carbon atoms. Isolated carbon atoms were dissolved into Fe particles due to their advantageous carbon solubility and increased carbon diffusion rate. The carbon atom concentration inside Fe particles grew and eventually saturated [62].

In addition, as seen in the Raman spectra (shown in Figures 3(c) and 3(d)) of upcycled graphene grown on fine talc and Fe-fine talc, fine talc showed its characteristic Raman peaks at  $183\text{ cm}^{-1}$ ,  $363\text{ cm}^{-1}$ , and  $677\text{ cm}^{-1}$ , all of which vanished after direct and catalytic carbonization processes. In the Raman spectrum of both directly grown graphene/fine talc hybrid and catalytically grown graphene/Fe-fine talc hybrid, D and G peaks were observed at  $1344\text{ cm}^{-1}$  and  $1590\text{ cm}^{-1}$ , respectively. Furthermore, the intensities of  $I_{\text{D}}/I_{\text{G}}$  ratios of separated graphene structures after acid treatments of directly grown graphene/fine talc hybrid were determined as 1.06, while it was 0.97 for

catalytically grown graphene/fine talc hybrid. This indicated that surface activation of talc contributed to the deposition of graphene structures on Fe-fine talc substrate by generating more  $sp^2$  bonded carbon atoms during catalytic carbonization. Moreover,  $I_G/I_{2D}$  ratios of the hybrid additives show the number of graphene layers. Graphene is considered to have a multi-layer structure if  $I_G/I_{2D}$  ratio is higher than 1, whereas it is single-layer or few-layer if  $I_G/I_{2D}$  ratio is lower than 1 [63]. Since  $I_G/I_{2D}$  ratios of graphene structures were higher than 1, either the graphene structure grown on micron talc, fine talc, Fe-micron talc, and Fe-fine talc or their separated graphene forms have multi-layer structures.

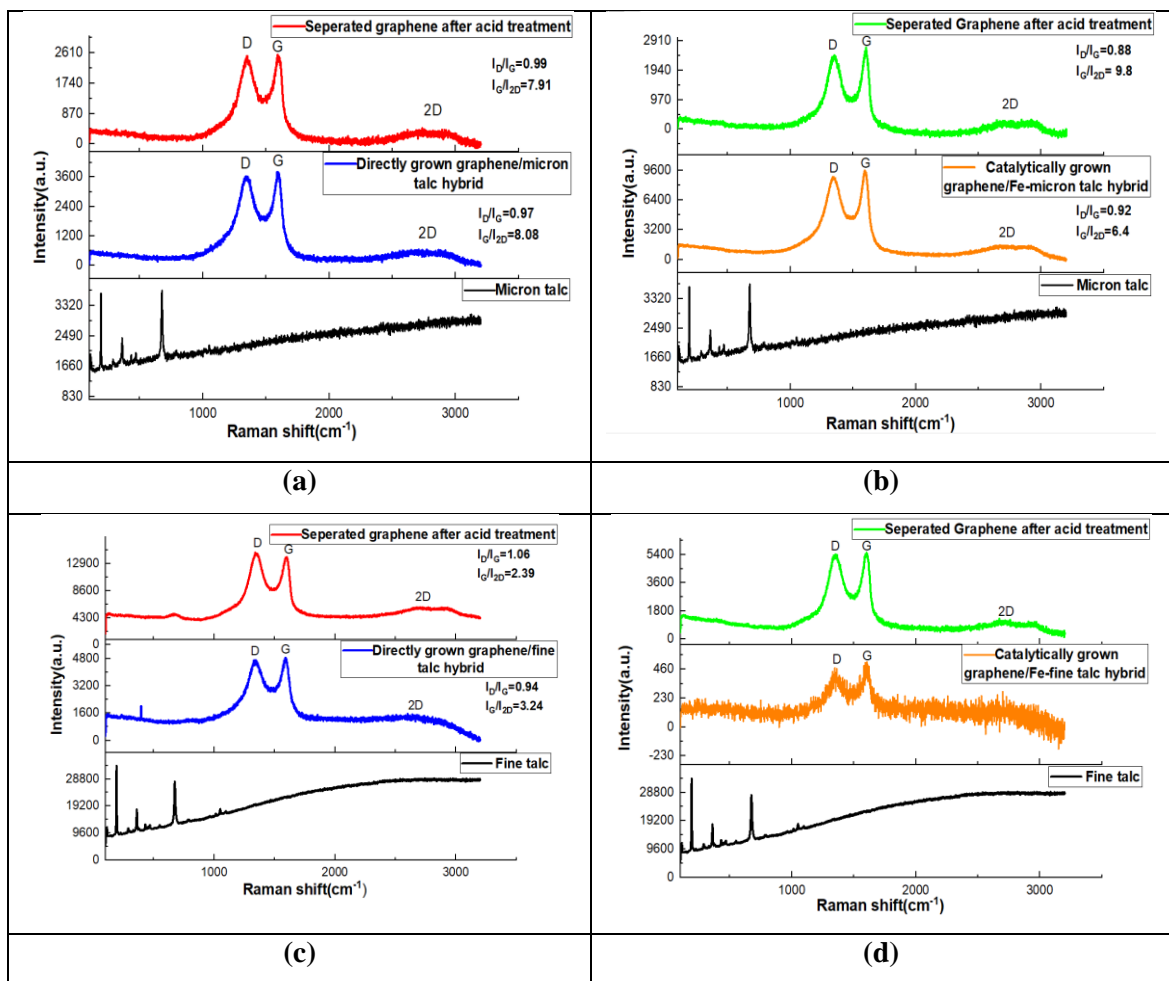


**Figure 3.** Comparison Raman spectra of upcycled graphene grown on (a) micron talc and (b) Fe-micron talc; (c) fine talc and (d) Fe-fine talc surfaces.

XRD characterization is an advantageous technique in order to understand the crystallinity and phase of the materials non-destructively [29]. Comparison XRD patterns of upcycled graphene grown on micron talc, Fe-micron talc, fine talc, and Fe-fine talc are demonstrated in Figure 4. The Micron talc had the characteristic XRD basal

planes, which were (001), (002), (003), (004), and (005) at  $2\theta=9^\circ$ ,  $18^\circ$ ,  $28^\circ$ ,  $37^\circ$ , and  $48^\circ$ , respectively [30, 31]. After direct and catalytic carbonization processes, (002) reflection of graphene structure [32] was seen at  $2\theta=28^\circ$  with intensities of 21.5 and 22.2, respectively. A low-intense peak of the Fe-C bond was observed at  $2\theta=43.8^\circ$  [35]. The same observations were also valid for directly grown graphene/fine talc and catalytically grown graphene/Fe-fine talc hybrid additives shown in Figure 4(c) and Figure 4(d). Moreover, after HF acid treatments of both micron talc-based and fine talc-based hybrid additives, there was a slight shift of (002) graphene peak towards  $24^\circ$ , and the peak intensity of (002) peak in separated graphene structures increased significantly. However, in the graphene structures, there were also some remaining micron talc and fine talc peaks because of the chemical interactions during the carbonization processes between the talc and the accumulated carbon atoms. In summary, carbonization processes changed the diffraction planes of micron talc, fine talc, and their Fe-treated talc forms, resulting in an amorphous graphene structure.

Furthermore, layer numbers of separated graphene structures of hybrid additives were calculated via the Debye-Scherrer equation, in which D corresponds to the average crystallite size,  $\lambda$  belongs to X-ray wavelength, K is Scherrer constant,  $\beta$  shows the Full Width at Half Maximum (FWHM) of XRD peak, and n is related to the number of graphene layers [69].

$$D = \frac{0.89 \lambda}{\beta_{002} \cos\theta_{002}} \quad (1)$$

$$n = \frac{D}{d_{002}} + 1 \quad (2)$$

The graphene structures separated from catalytically and directly grown graphene/micron talc hybrid additives from waste PS had a d-spacing of 0.37 nm at  $2\theta \sim 24.2^\circ$ . Also, the crystalline size of them was 1.25 nm and 1.27 nm, respectively. Related to the crystalline size values, the number of separated graphene layers of micron talc-based hybrid additive from waste PS was calculated as 4, while the number of separated graphene layers of Fe-micron talc-based hybrid additive from waste PS was 5. On the other hand, the graphene structures separated from catalytically grown graphene/Fe-fine talc hybrid from waste PS had a d-spacing of 0.31 nm approximately at  $2\theta = 24.5^\circ$  and

resulted in 7 graphene layers together with spheres. Since the separated graphene from directly grown graphene/fine talc hybrid from waste PS contained only spheres in its structure, the number of graphene layers could not be determined.

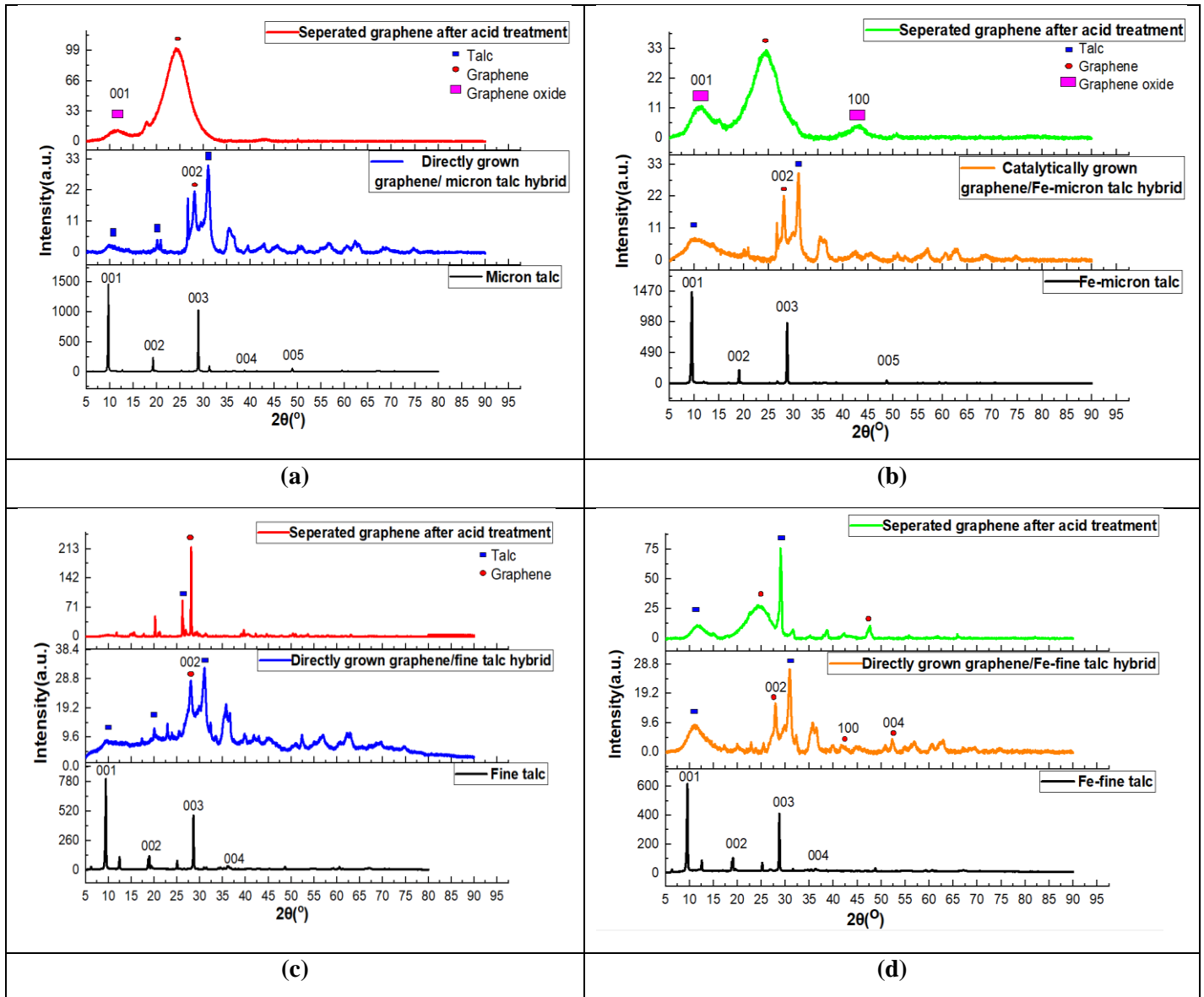


**Figure 4.** Comparison XRD patterns of upcycled graphene grown on (a) micron talc, (b) Fe-micron talc, (c) fine talc, and (d) Fe-fine talc.

XPS survey scan was carried out in order to examine the elemental composition, functional groups, and binding energies of the produced hybrid additives and their separated graphene structures. Table 2 summarizes the elemental chemical compositions of neat micron talc and fine talc, their hybrid additives obtained from direct and catalytic carbonization processes, and separated graphene structures after acid treatments. Micron talc consisted of 52.72 at% of O, 21.66 at% of Si, 18.69 at% of Mg,

and 6.93 at% of Ca in its structure, while fine talc contained 58.98 at% of O, 23.90 at% of Si, and 17.12 at% of Mg. After the direct carbonization process, the carbon content of directly grown graphene/micron talc hybrid and directly grown graphene/fine talc hybrid increased to 35.36 at% and 35.90 at%, respectively, pointing out the carbon accumulation on both micron talc and fine talc substrates. The carbon content of catalytically grown graphene/Fe-micron talc hybrid and catalytically grown graphene/Fe-fine talc hybrid was calculated as 41.98 at% and 20.45 at%, respectively, the amounts of which were higher than the carbon content of their directly grown counterparts. It meant that the deposition of carbon atoms on the micron talc surface was triggered in the presence of iron catalyst, and resulting in a high amount of carbon. In addition, 0.67 of Fe at% was observed in the catalytically grown graphene/Fe-micron hybrid structure due to the functionalization of micron talc and fine talc surfaces with FeCl<sub>3</sub>. The carbon amount of separated graphene from directly grown graphene/micron talc hybrid was determined as 44.43 at% while graphene/Fe-micron talc hybrid from catalytic carbonization had 71.39 of C at%. On the other hand, the separated graphene structures from directly grown graphene/fine talc and catalytically grown graphene/Fe-fine talc hybrids included 38.88 of C at% and 75.70 of C at%, respectively. Especially in some XPS samples produced by catalytic carbonization, the content of elements below 0.1 at% could not be detected, and thus iron element was not detected by the system. For instance, in the catalytically grown graphene /Fe-fine talc hybrid, the at% of the other elements were dominated and thus Fe element was not measured. In summary, the deposition of carbon atoms from waste PS was well-achieved on talc substrates, and the accumulation efficiency of carbon atoms was further developed whether the talc surface was activated by iron [70].

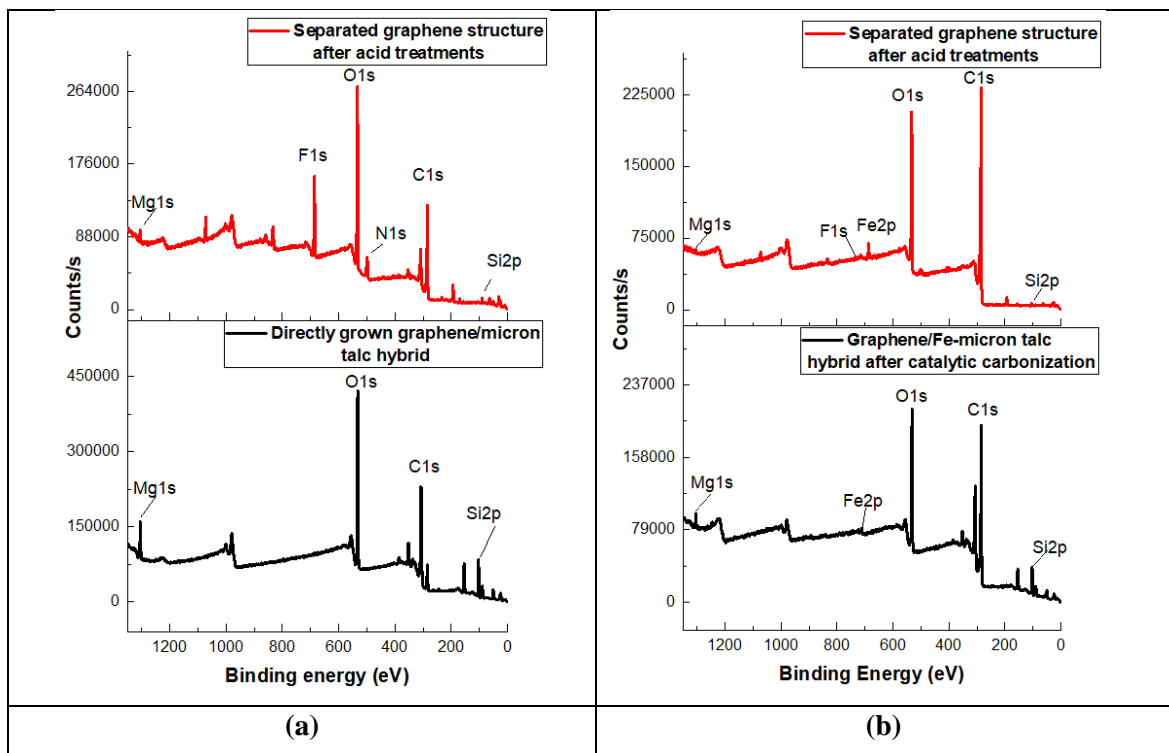
**Table 2.** The elemental chemical compositions of neat micron talc and fine talc, their hybrid additives obtained from direct and catalytic carbonization processes, and separated graphene structures after acid treatments.

<b>Sample</b>	<b>C</b> <b>(at %)</b>	<b>O</b> <b>(at %)</b>	<b>Si</b> <b>(at %)</b>	<b>Fe</b> <b>(at %)</b>	<b>Mg</b> <b>(at %)</b>	<b>Na</b> <b>(at %)</b>	<b>F</b> <b>(at %)</b>	<b>N</b> <b>(at %)</b>	<b>Ca</b> <b>(at %)</b>
Micron talc	-	52.72	21.66	-	18.49	-	-	-	6.93
Fine talc	-	58.97	23.90	-	17.12	-	-	-	-
Directly grown graphene /micron talc hybrid	35.36	44.86	17.05	-	2.73	-	-	-	-
Catalytically grown graphene /Fe-micron talc hybrid	41.98	35.61	14.96	0.67	6.79	-	-	-	-
Directly grown graphene /fine talc hybrid	35.90	34.36	-	-	2.59	2.16	13.90	-	1.44
Catalytically grown graphene /Fe-fine talc hybrid	20.45	53.8	20.78	-	4.97	-	-	-	-
Separated graphene of graphene /micron talc hybrid	44.43	39.55	1.01	-	1.44	-	12.34	1.24	-
Separated graphene of graphene /Fe-micron talc hybrid	71.39	25.19	0.92	0.13	0.22	-	2.15	-	-
Separated graphene of graphene /fine talc hybrid	38.88	37.87	1	-	3.76	-	12.25	-	1.55
Separated graphene of graphene /Fe-fine talc hybrid	75.7	16.15	1.8	-	1.44	-	4.87	-	-

C1s, O1s and Fe2p signals of the graphene/micron talc and graphene/fine talc hybrid additives after direct and catalytic carbonization processes and their separated graphene structures were measured by XPS survey scan analysis. Figure 5 presents the XPS survey scans of graphene /micron talc and graphene/fine talc hybrid additives after direct and catalytic carbonization and their separated graphene structures after acid treatments. The C=C  $sp^2$  bonding was observed at 284.5 eV [38] in the XPS survey scan of all the hybrid additives with the same binding energy (284.5 eV), which underlines the graphene formation from PS waste utilized as a carbon source. After the separation of graphene from micron and fine talc surface, the peak intensity increased drastically. In addition, the O1s signals were seen at 531.5 eV either for all hybrid additives or separated graphene samples, and the intensity decreases after the separation process

because of the removal of talc [39]. In the XPS survey scan of hybrid additives in which carbon atoms were deposited on iron-treated micron talc and its separated graphene, the Fe2p signal was observed at 712 eV, requiring information on the ionic bond [40]. In addition, the graphene growth on micron talc was more effective than the graphene formation on fine talc substrate since the accumulation of carbon atoms, detected in the C1s survey scan, was higher in micron talc based-hybrid additives and their separated graphene structures.

The peak intensity of C1s signals was higher than the peak intensity of O1s signals in the structure of the catalytically grown hybrid additives and their separated graphene structures, which meant that  $sp^2$  bonded carbon deposition was adequately generated via upcycling of PS waste on Fe-micron talc [38], which was not the case for directly grown hybrid additives. In summary, the high carbon content of PS waste could be successfully converted into accumulated carbon atoms on micron talc substrate by catalytic carbonization, where iron acted as a catalyst.



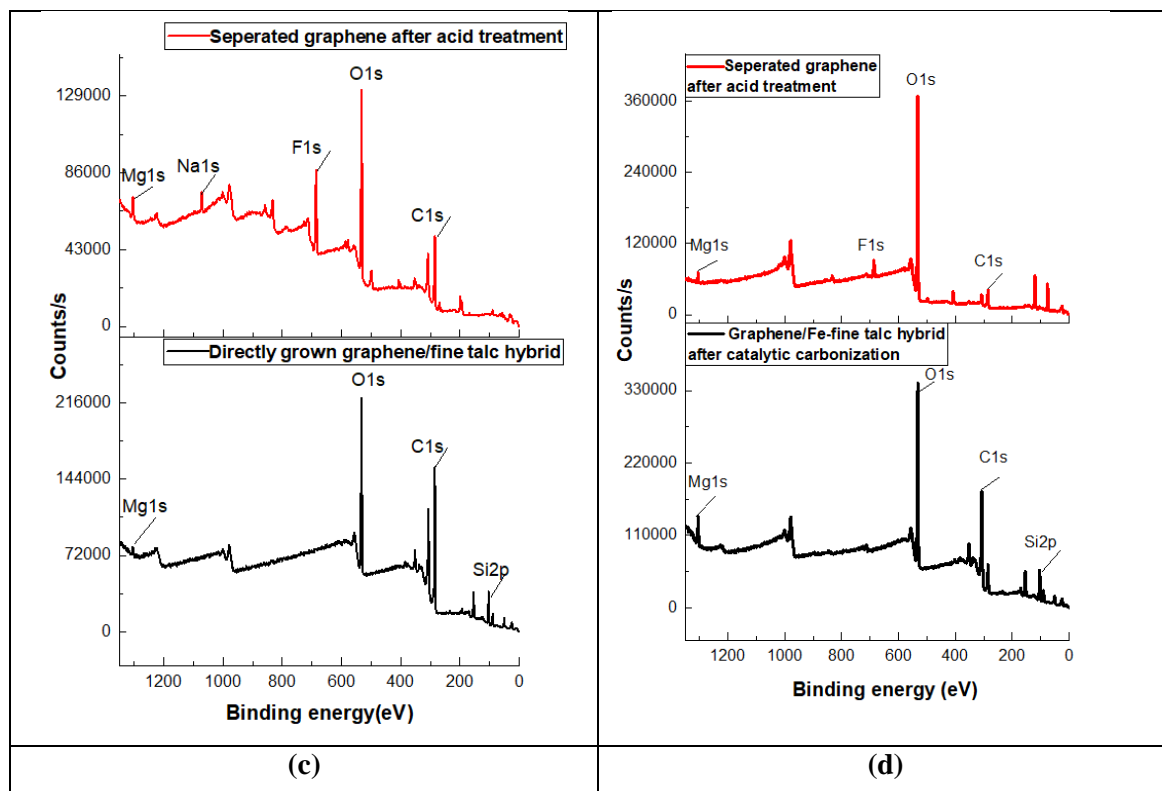


**Figure 5.** XPS survey scan of (a) directly grown graphene/micron talc hybrid and its separated graphene structure, (b) catalytically grown graphene /Fe-micron talc hybrid and its separated graphene structure, (c) directly grown graphene/fine talc hybrid and its separated graphene structure, and (d) catalytically grown graphene/Fe-fine talc hybrid and its separated graphene structure.

### 3.3.2 The effect of polymer mixing techniques on the characteristics of PS-derived hybrid additives

Batch charging and discharging influence productivity, batch-to-batch product consistency, precise melting, and mixing, all the challenges encountered with processing thermokinetic mixers [74]. In order to see the impact of polymer processing techniques on the characteristics of PS-derived hybrid additives, thermokinetic mixing and twin-screw extrusion processes were conducted for mixing the waste PS and micron talc substrate prior to carbonization, and the final features of the obtained hybrid additives were systematically characterized. Comparison Raman spectra of micron talc, directly grown graphene/micron talc hybrid processed by twin-screw extruder, and its separated graphene structure after acid treatments is demonstrated in Figure 6(a). As mentioned in the previous section 3.3.1 in Figure 3, micron talc had three prominent Raman peaks at  $195\text{ cm}^{-1}$ ,  $363\text{ cm}^{-1}$ , and  $678\text{ cm}^{-1}$  with different intensities. Those main talc peaks disappeared after the carbonization process; instead, D and G peaks occurred.

D peak originated at  $1344\text{ cm}^{-1}$  for both approaches, but the G peak occurred at  $1590\text{ cm}^{-1}$  and  $1595\text{ cm}^{-1}$  for twin-screw extrusion and thermokinetic mixing, as shown in the previous section, Figure 3(a). The G band shifted and became narrow due to electron and hole doping in the hybrid processed with thermokinetic mixing [75]. Furthermore, the  $I_D/I_G$  intensities of the directly grown graphene /micron talc hybrid processed by the twin-screw extruder and thermokinetic mixer were determined as 0.99 and 0.97, respectively, which were nearly the same, whereas the intensities of  $I_D/I_G$  ratios of separated graphene structures after acid treatments of directly grown graphene /micron talc hybrid processed by the twin-screw extruder and thermokinetic mixer were calculated as 0.93 and 0.99. Moreover, the hybrid additives and separated graphene structures obtained from either thermokinetic mixing or twin-screw extrusion had multi-layer structures since their  $I_G/I_{2D}$  ratios were higher than 1 [63].

On the other hand, XRD patterns of upcycled graphene grown on micron talc processed by twin-screw extrusion is illustrated in Figure 6(b), whereas XRD patterns of upcycled graphene grown on micron talc processed by thermokinetic mixing is shown in Figure 4(a) in the previous section. After the carbonization, the obtained hybrids processed by either twin-screw extrusion or thermokinetic mixing, (002) peaks belonging to graphene were seen at  $2\theta=26^\circ$  [34] with intensities of 23 and 20. However, in the XRD patterns of the separated graphene structures after acid treatments, there was a slight shift of the (002) graphene peak towards  $2\theta=24^\circ$ , and a significant rise in the peak intensity of the (002) reflection plane was perceived. Moreover, the crystallinity of talc was disturbed by thermokinetic mixing due to the polymorphic transformation in silica [76], which affected the graphene growth and caused defect formation in the nanocarbon structure.

The number of separated graphene layers from graphene/micron talc hybrids processed by twin-screw extrusion and thermokinetic mixing was determined using the Debye-Scherrer equation in section 3.3.1. The separated graphene structures from directly grown graphene/micron talc hybrids processed by twin-screw extrusion and thermokinetic mixing had a d-spacing of 0.37 nm at  $2\theta \sim 24.2^\circ$ . Also, the crystalline size of the graphene separated from directly grown graphene/micron talc hybrid additives by twin-screw extrusion and thermokinetic mixing were 0.95 nm and 1.25 nm, respectively. In conclusion, the usage of twin-screw extrusion or high shear rate thermokinetic mixing prior to thermal treatment did not affect the number of graphene

sheets since the number of separated graphene sheets of extruded graphene/micron talc was obtained as 4.

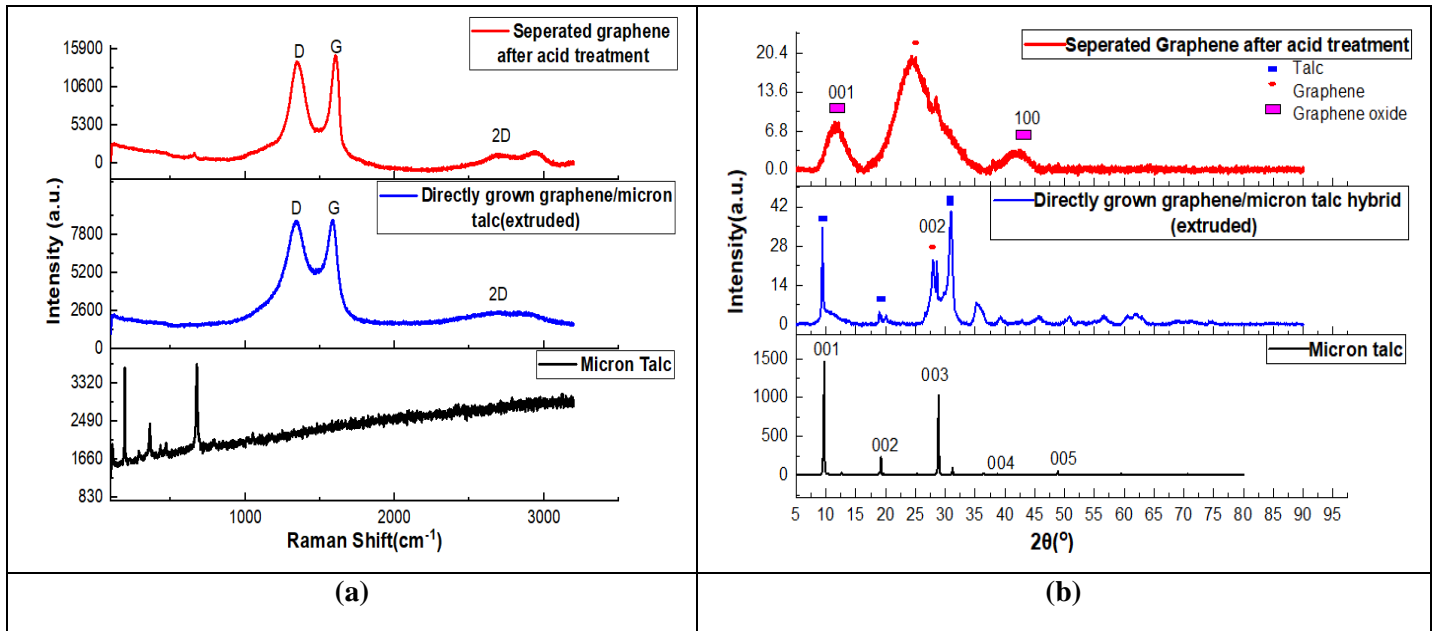


**Figure 6.** (a) Raman spectra, and (b) XRD patterns of micron talc, directly grown graphene/micron talc hybrid processed by twin-screw extrusion and its separated graphene structure after acid treatments.

XPS analysis was also conducted to characterize further the elemental chemical composition of the hybrid additives processed by twin-screw extrusion. Table 3 shows the chemical compositions of upcycled graphene/micron talc hybrid additives processed by extrusion and its separated graphene structure after acid treatments. After direct carbonization processes, the carbon content of directly grown graphene/micron talc hybrids from twin-screw extrusion and thermokinetic mixing reached 17.65 at% and 35.36 at% (given in Table 2), respectively, indicating the carbon deposition on micron talc surface. Moreover, the carbon amount of separated graphene structures from graphene/micron talc hybrid processed by twin-screw increased to 41.82 at% while the carbon amount of separated graphene structures from graphene/micron talc hybrid from thermokinetic mixing reached 44.43 at% (shown in Table 2). The results displayed that the carbon accumulation was higher in the hybrid additives and separated graphene structures when thermokinetic mixing was used to mix the raw materials before carbonization.

**Table 3.** The elemental composition of the micron talc, directly grown graphene/micron talc hybrid additives processed by twin-screw extrusion, and their separated graphene structures after acid treatments.

<b>Sample</b>	<b>C (at %)</b>	<b>O (at %)</b>	<b>Si (at %)</b>	<b>Mg (at %)</b>	<b>F (at %)</b>	<b>N (at %)</b>
Directly grown graphene/micron talc hybrid (from twin-screw extrusion)	17.65	52.35	23.43	6.58	-	-
Separated graphene of directly grown hybrid (from twin-screw extrusion)	41.82	36.42	2.73	4.34	8.52	1.44

Moreover, XPS survey scan of directly grown extruded graphene/micron talc hybrid, and its separated graphene structures after acid treatments are given in Figure 7. After carbonization, The C=C  $sp^2$  bonding was observed at 284.5 eV in the XPS survey scan of the graphene/micron talc hybrid additive processed by extrusion underlining the graphene formation from PS waste. C1s peak intensity of hybrid additives processed by either extrusion (in Figure 7) or thermokinetic mixing (in Figure 5) is almost the same with 73460 counts/s. Also, the O1s signals emerged at 531.5 eV with 421600 counts/s for the hybrid additives regardless of the polymer processing method. After the acid treatments, the intensities of C1s signals at 284.5 eV increased dramatically for the hybrids processed by extrusion and thermokinetic mixing indicating the high amount of carbon existence. Besides, the intensities of O1s signals at 531.5 eV decreased visibly in the XPS survey scan of the separated graphene structures. This showed that talc structure was removed successfully with HF and HNO<sub>3</sub> treatments.

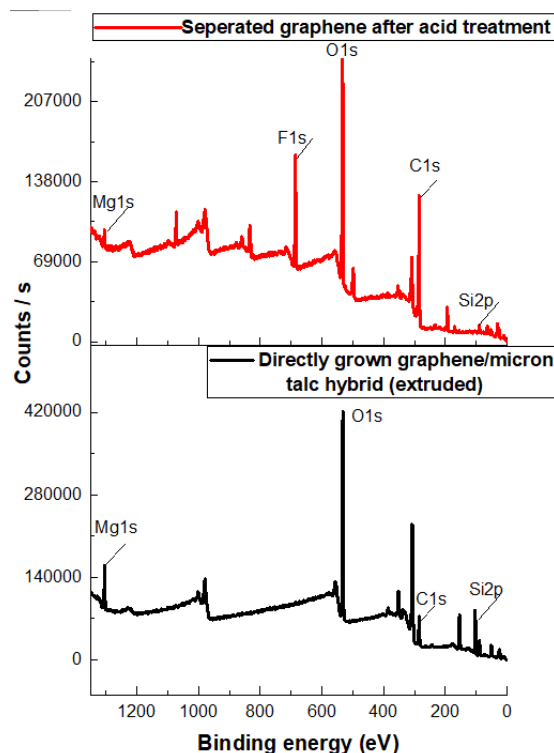


**Figure 7.** XPS survey scan of directly grown extruded graphene/micron talc hybrid and its separated graphene structure.

### 3.3.3 Dimension characterization of PS-derived hybrid additives by SEM and TEM

To examine the surface morphology of untreated and treated micron talc and fine talc, the upcycled graphene/micron talc, and upcycled graphene/fine talc hybrids, SEM characterization was applied to both carbonized and acid-treated samples. SEM images of micron talc, directly and catalytically grown graphene/micron talc hybrids processed by thermokinetic mixing are given in Figure 8, while SEM image of directly grown graphene/micron talc hybrid processed by extrusion is given in Figure 9. The aggregation of talc layers was observed in the SEM images of the neat micron talc particles shown in Figure 8(a). After direct and catalytic carbonization processes, sheet-like and folded upcycled graphene/micron talc hybrids with an average size of 200 nm were obtained, as seen in Figures 8(b) and 8(c). The hybrid additive processed by extrusion also had an approximately 250-300 nm layered nanocarbon structure, as given in Figure 9. On the other hand, Fe particles chemically bonded to the talc substrate after iron treatment of micron talc, as shown in Figure 10(a). Fe particles had a rod-like morphology with a high aspect ratio and rod-like structure was formed because of the relative amount of  $\text{FeCl}_3$  (0.5 M) [77]. In addition, while the size of the Fe particles

varied from 300 to 500 nm, they all had 50 nm thickness. Besides, in the presence of Fe catalyst, layer-like carbon nanostructures were grown on the talc surface with a smaller size than the directly grown hybrid. However, the intensity of the carbon structure layers was higher than that of directly grown graphene/micron talc hybrid additive.

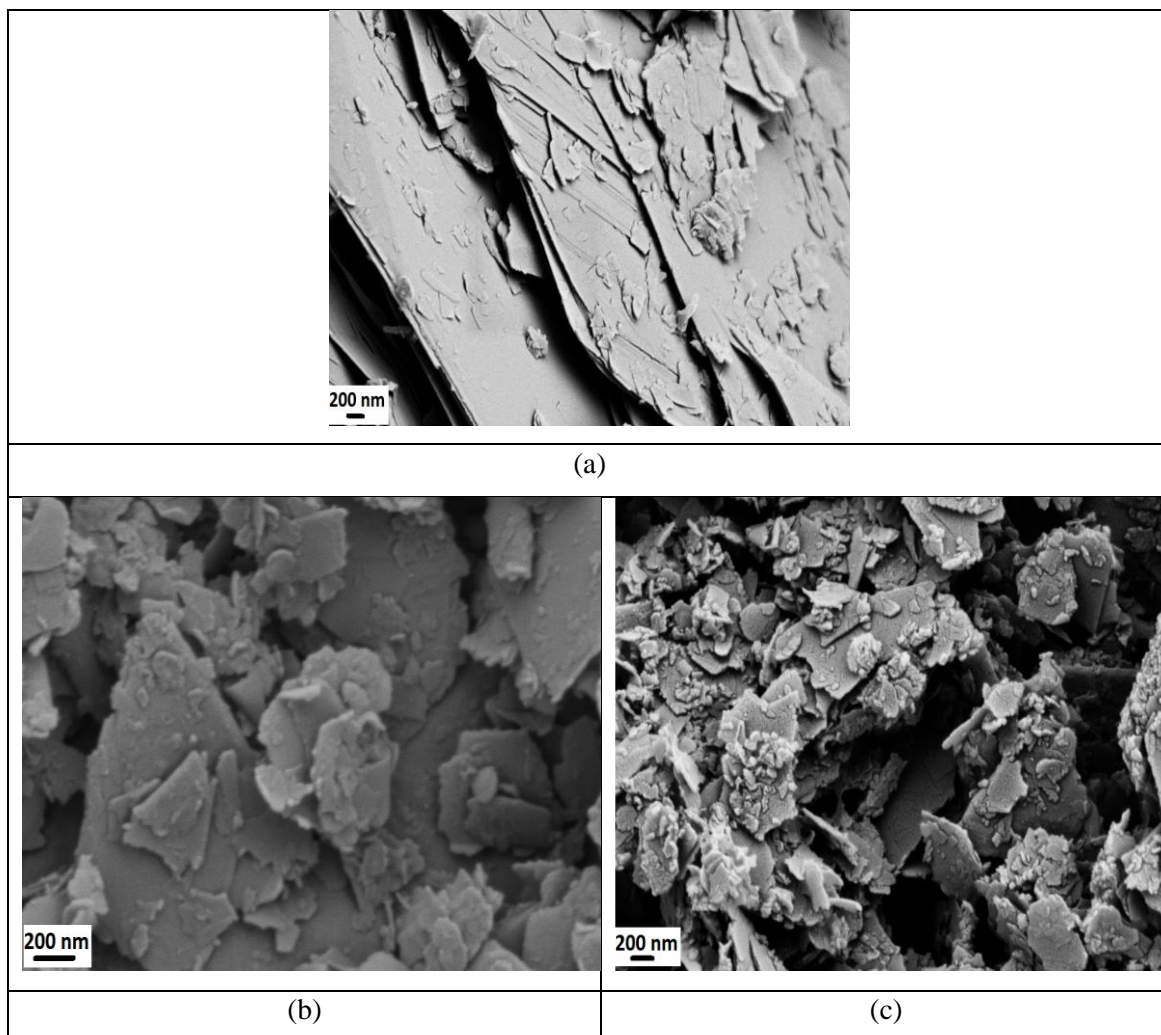


**Figure 8.** SEM images of (a) micron talc, (b) directly and (c) catalytically grown graphene/micron talc hybrid additives.

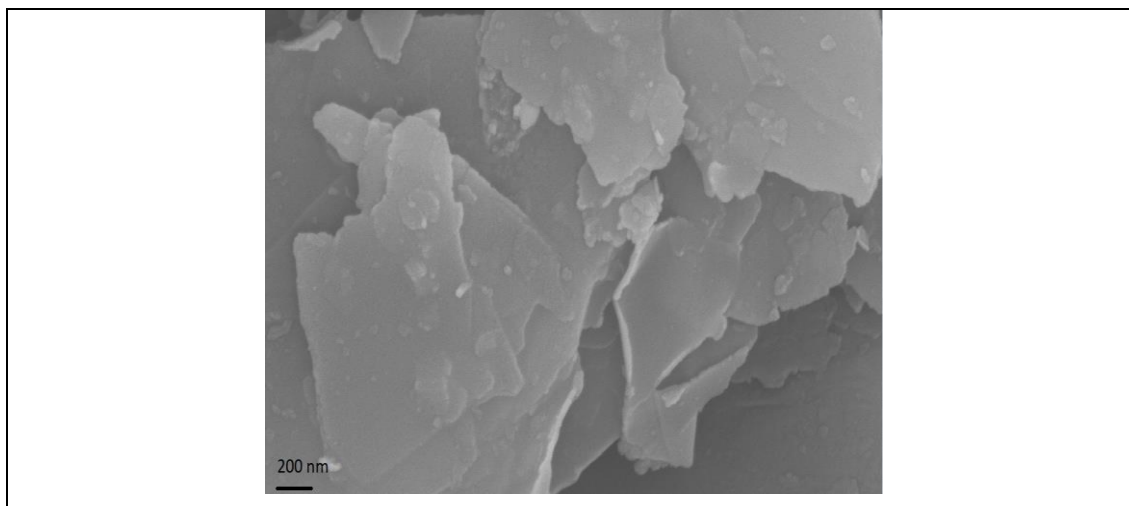


**Figure 9.** SEM image of directly grown graphene/micron talc hybrid by extrusion.

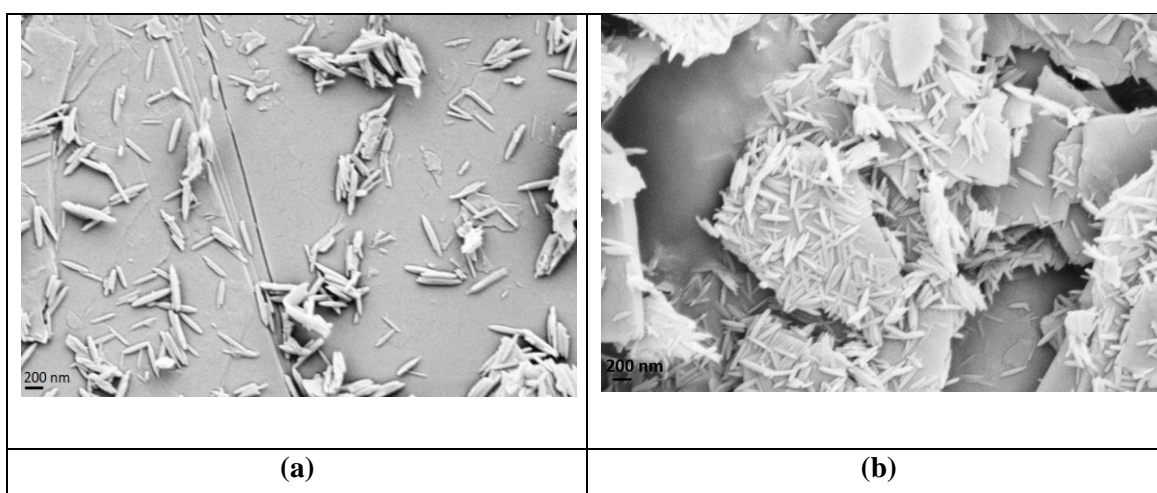


**Figure 10.** SEM images of (a) Fe-treated micron talc, and (b) Fe-treated fine talc.

SEM images of neat fine talc, directly and catalytically grown graphene/fine talc hybrids are demonstrated in Figure 11, while SEM images of separated graphene structures of fine talc-based and micron talc-based hybrids are given in Figure 12. Disordered fine talc plates were observed in Figure 11(a), while both layer-like and approximately 100-150 nm sized spherical nanostructure formations were seen in Figures 11(b) and 11(c). Moreover, layered and spherical structures of upcycled graphene were clearly seen in the SEM images (Figure 12) obtained after acid treatments. Sheet-like nanocarbon structures were obtained after the acid treatments of directly grown graphene/micron talc hybrids processed by thermokinetic mixing and extrusion. The wrinkled structure occurred after extrusion, which was also proved by the Raman spectrum with the formation of the defect-activated band at  $2940\text{ cm}^{-1}$  after acid treatments [78]. In addition, thermokinetic mixing allowed a flat surface with edge-

folding, whereas extrusion gave rise to graphene sheets with many wrinkles on the whole surface [79]. Figure 12(c) shows that the directly and catalytically grown upcycled graphene/fine talc hybrid had a spherical structure.

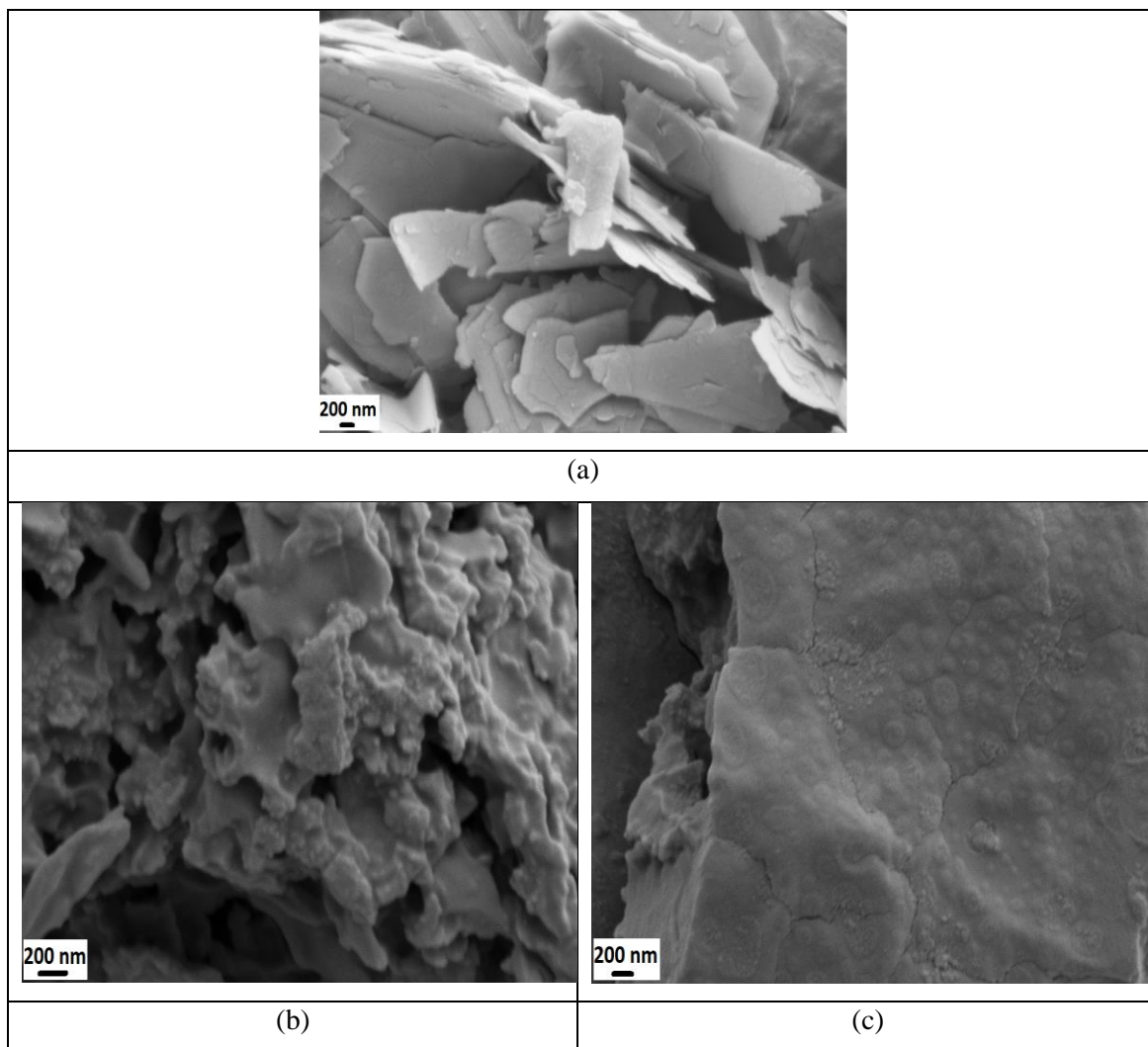


**Figure 11.** SEM images of (a) fine talc, (b) directly and (c) catalytically grown graphene/fine talc hybrid additives.

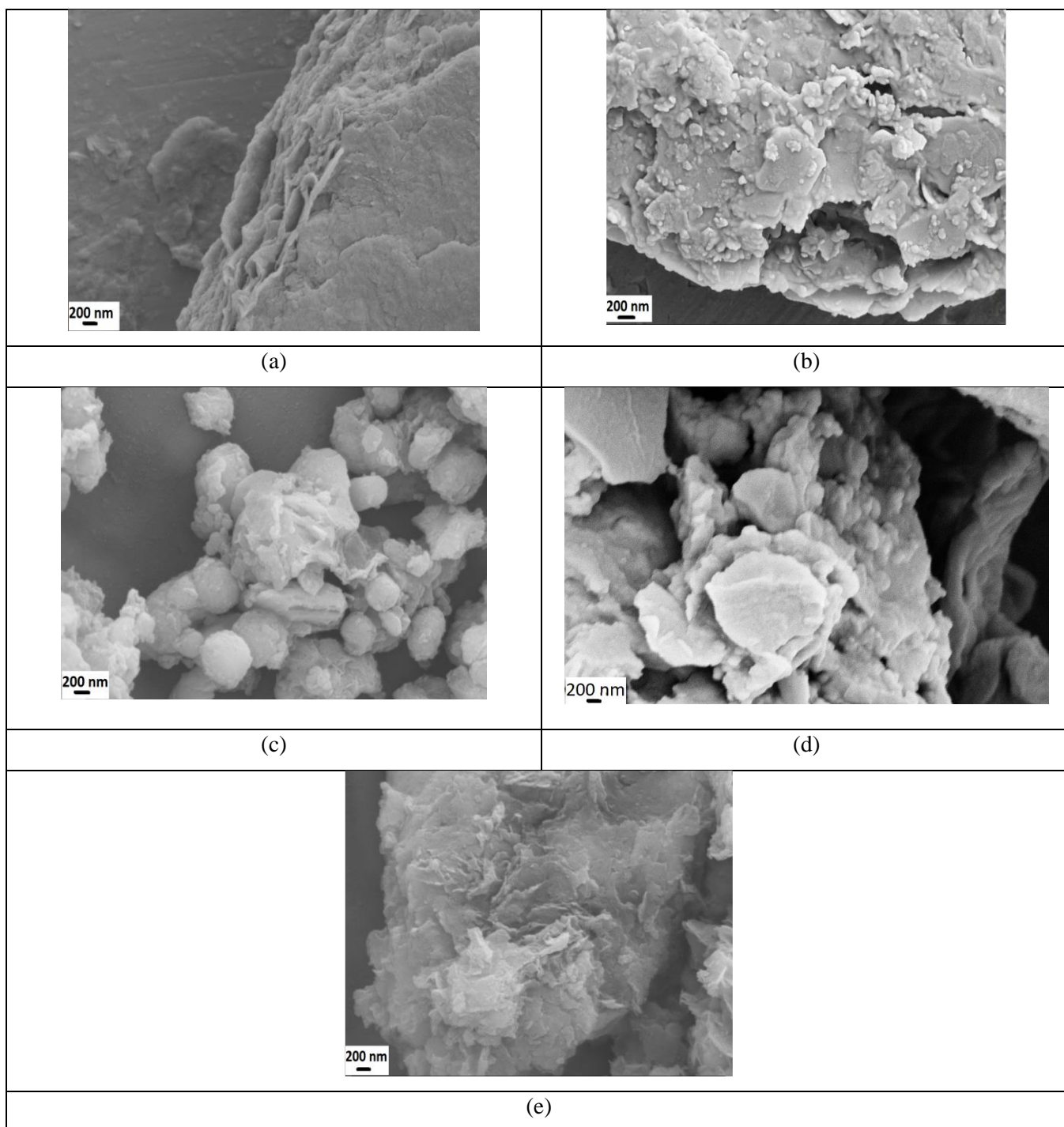


**Figure 12.** SEM images of separated graphene structures: (a) directly and (b) catalytically grown graphene /micron talc by thermokinetic mixer, (c) directly and (d) catalytically grown graphene/fine talc by thermokinetic mixer, and (e) directly grown graphene /micron talc by extrusion.

The morphology of the upcycled separated graphene structures of directly and catalytically grown micron talc-based and fine-talc-based hybrid additives was also examined by TEM analysis. Figure 13 presents the TEM images of separated graphene

structures of directly and catalytically grown graphene /micron talc, directly and catalytically grown graphene /fine talc by thermokinetic mixing, and directly grown graphene /micron talc hybrid processed by extrusion. The separated graphene structures of directly and catalytically grown graphene/micron talc hybrids obtained from thermokinetic mixing and directly grown graphene/micron talc hybrid by extrusion had wrinkled sheet-like nanocarbon structures as seen in Figures 13(a), 13(b), and 13(e). Besides, the separated graphene of upcycled graphene/fine talc hybrid had a spherical and porous structure. In addition, TEM images with d-spacing were given in Figure 14, depicting the  $d_{002}$  graphene lattice fringes, and aiding the visualization of the carbon layer profile. The distance between graphene layers in the dense packing zone was between 0.22 and 0.28 nm, close to the value determined from the XRD measurements, and disordered carbons were also implied.

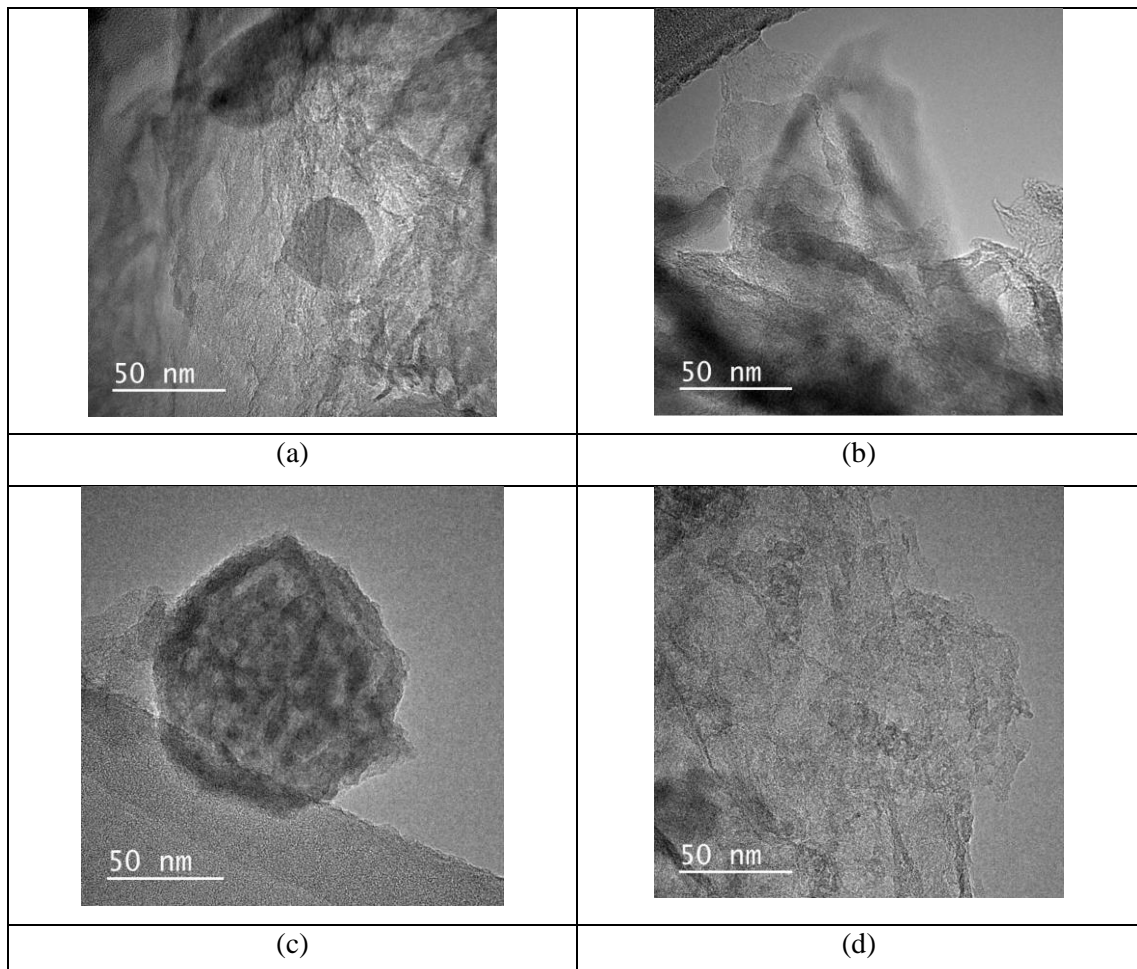


**Figure 13.** TEM images of separated graphene structures of (a) directly and (b) catalytically grown graphene /micron talc by thermokinetic mixer, (c) directly and (d) directly grown graphene /micron talc by extrusion.

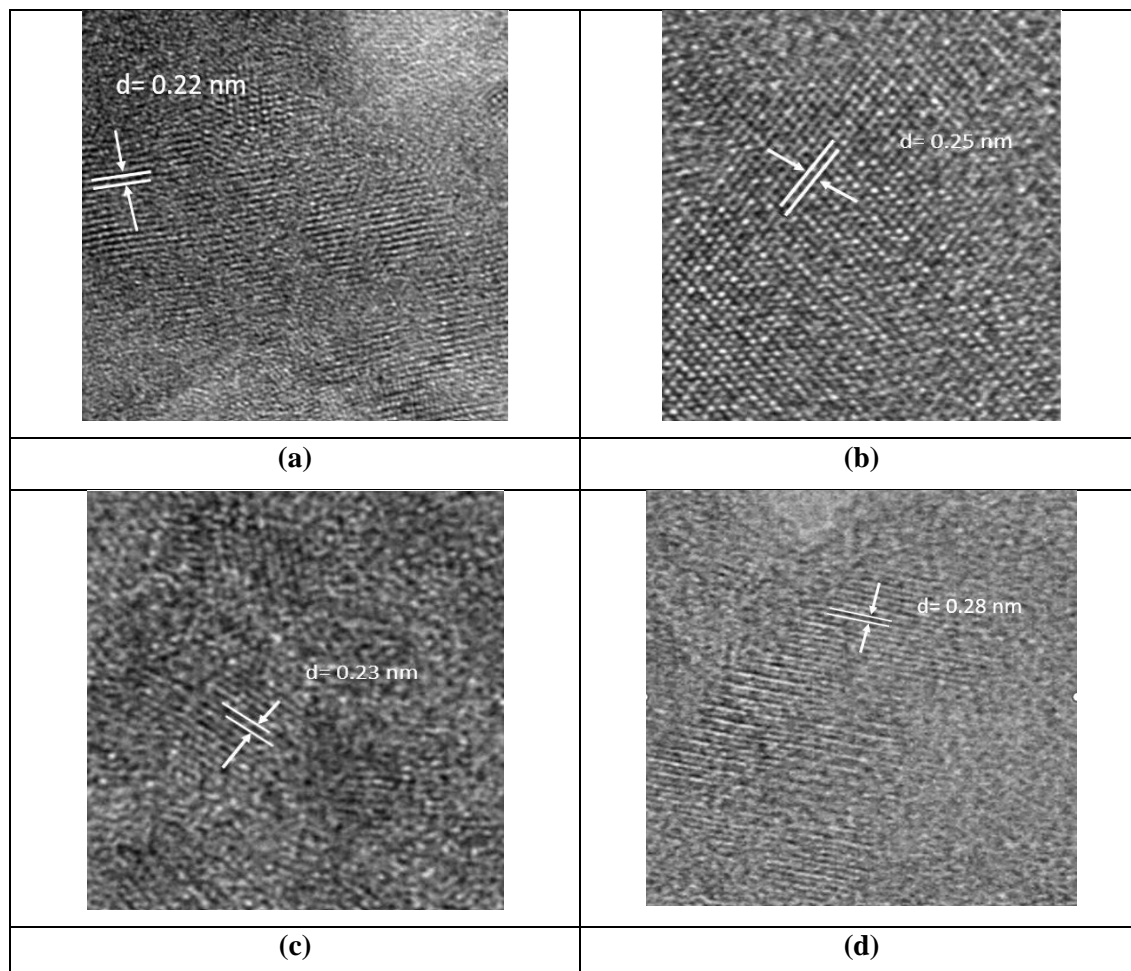


**Figure 14.** d-spacing of separated graphene structures of (a) directly and (b) catalytically grown graphene /micron talc, (c) directly and (d) directly grown graphene /micron talc by extrusion.

### 3.3.4. Thermal properties of graphene grown on talc surface

The thermal features of the neat micron talc, and fine talc, and their graphene/talc hybrid additives were examined by TGA analysis. TGA curves of micron talc, Fe-micron talc, fine talc, Fe-fine talc, and their directly and catalytically grown graphene/talc hybrid additives are given in Figure 15. In addition, the weight loss of micron talc, Fe-micron talc, fine talc, Fe-fine talc, and their directly and catalytically grown graphene/talc hybrid additives at 500°C, 750°C and 1000°C are summarized in Table 4. It was seen that the thermal stability of graphene/talc hybrid additives was

higher than that of their virgin counterparts. Micron talc conserved its weight up to 500°C, but 4.1% weight loss occurred at 1000°C. On the other hand, Fe-micron talc lost 1.8% of its weight at 500°C, and 5.45% at 1000°C. By the surface activation of talc with FeCl<sub>3</sub>, the crystallinity of talc was disturbed thus thermal stability of the talc decreased. The weight loss of talc between 315°C and 525°C dedicated to intercalated ions in the talc layers [80]. Although directly grown graphene/micron talc hybrid lost 4.2% its weight at 1000°C, 3.4 of weight loss occurred for the graphene/Fe-micron talc hybrid after catalytic carbonization. Fine talc lost its %0.1 weight up to 500°C, but 7.2% weight loss occurred at 1000°C, while Fe-fine talc lost 1.8% of its weight at 500°C, and 7.3% at 1000°C. Although directly grown graphene/fine talc hybrid lost 0.9% its weight at 1000°C, 2.5 of weight loss was observed in the graphene/Fe-micron talc hybrid after catalytic carbonization. According to Fig. 15(c) and (d), PS-based hybrids begin to oxidize at temperatures that are roughly 500°C, while the remaining solvents evaporate below 150 C. On the other hand, micron talc as template led to grow more graphitic structure than fine talc.

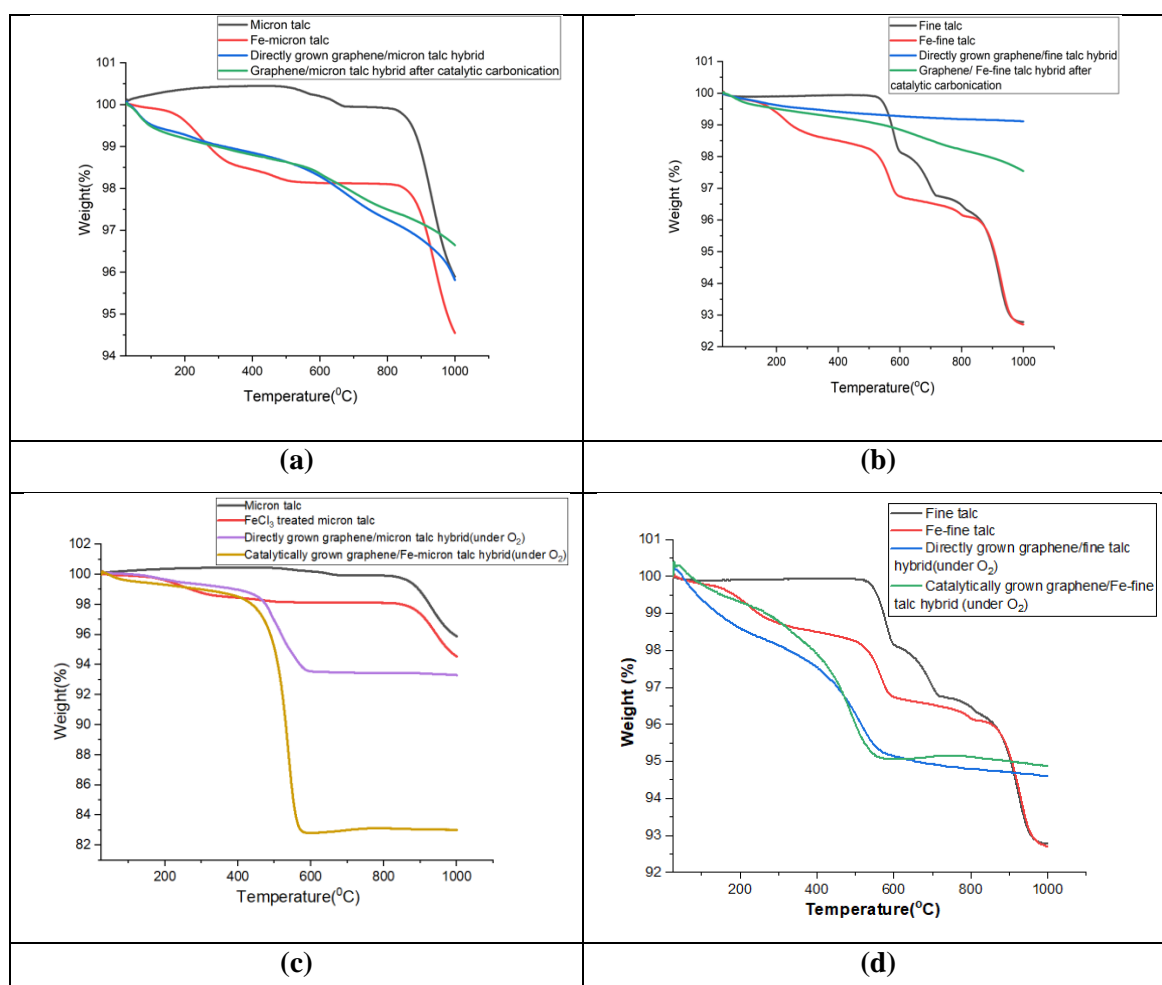


**Figure 15.** TGA thermograms of under (a) nitrogen and (c) oxygen atmosphere micron talc, Fe-micron talc, and directly and catalytically grown graphene/micron talc hybrids, and (b) under nitrogen and (d) oxygen atmosphere fine talc, Fe-fine talc and directly and catalytically grown graphene/fine talc hybrids.

**Table 4.** Weight loss micron talc, Fe-micron talc, fine talc, Fe-fine talc, directly and catalytically grown graphene/micron talc hybrids, and directly and catalytically grown graphene/fine talc hybrids at 500°C, 750°C and 1000°C.

	Weight loss (%)		
	500°C	750°C	1000°C
Micron talc	0	0.1	4.1
Fe-micron talc	1.8	1.9	5.45
Fine talc	0.1	3.3	7.2
Fe-fine talc	1.8	3.6	7.3
Directly grown graphene/micron talc hybrid (under N <sub>2</sub> )	1.4	2.3	4.2
Catalytically grown graphene/Fe-micron talc hybrid(under N <sub>2</sub> )	1.4	2.5	3.4
Directly grown graphene/fine talc hybrid(under N <sub>2</sub> )	0.7	0.8	0.9
Catalytically grown graphene/Fe-fine talc hybrid(under N <sub>2</sub> )	1	1.7	2.5
Directly grown graphene/micron talc hybrid (under O <sub>2</sub> )	3.1	6.6	6.7
Catalytically grown graphene/Fe-micron talc hybrid(under O <sub>2</sub> )	4.8	16.8	17
Directly grown graphene/fine talc hybrid(under O <sub>2</sub> )	1.7	5.2	5.4
Catalytically grown graphene/Fe-fine talc hybrid(under O <sub>2</sub> )	1	4.9	5.2

### 3.3.5. Comparative life cycle assessment of PS-derived graphene/talc hybrid additives and their separated graphene structures

Life assessment (LCA) is a valuable and effective method used to systematically investigate the environmental impacts of a product or a system. The core of this LCA study is the evaluation of the environmental consequences of the PS-derived hybrid additives and their separated graphene structures, and decide and compare the less

hazardous graphene fabrication process. Comparative research on the environmental impacts of directly and catalytically grown graphene/talc hybrid additives and their separated graphene structures was performed using a consequential life cycle assessment, and the results are presented in Table 5, considering only one batch of graphene growth. In addition, during the analysis, Ecoinvent 3- allocation cut off by classification, and Swiss input & output databases were used for the life cycle inventory (LCI). The waste scenario of the input materials was estimated as landfilled municipal solid waste for the rest of the world. The software system, SimaPro release 9.3.0.2, only considers the inputs with mass units in the evaluation of waste disposal scenario. The impact assessment comparison of the inputs was determined by the method, which includes the Intergovernmental Panels on Climate Change (IPCC) equivalence factors. In the scope of this research, global warming potential and health impacts were considered the most crucial parameters. Based on the analyses results given in Table 5, the lowest global warming potential, 0.4 kg CO<sub>2</sub> eq (equivalent), belonged to the neat PS waste, while the highest global warming potential, 5.29 kg CO<sub>2</sub> eq (equivalent), was caused by the separated graphene from graphene/Fe-treated talc hybrid additives. Since the separation of graphene from talc surface was a longer process than the production of graphene/talc hybrid additives, the highest global warming potential of separated graphene from graphene/Fe-treated talc hybrid additives was an expected outcome of the LCA analysis. In addition, due to the iron treatment step for producing graphene/iron-treated talc hybrid additives, the global warming potential of graphene/Fe-treated talc hybrid additives was nearly 3.3 times higher than the global warming potential of graphene/talc hybrid additives. Moreover, the comparison of the global warming potential of neat waste PS, directly and catalytically grown graphene/talc hybrid additives, their separated graphene structures, and reduced graphene oxide (rGO) are given in Figure 16. As ensured in Figure 16, the most influential process on the carbon dioxide release among the upcycled graphene formation was the fabrication of separation graphene structures from graphene/Fe-treated talc hybrid additives. However, the global warming potential of rGO was dramatically higher than that of separation graphene structures of Fe-treated fine talc hybrids, showing that the carbon footprint could be lessened by upcycling compared to the conventional graphene production technique.

**Table 5.** The environmental impacts of directly and catalytically grown graphene/talc hybrid additives and their separated graphene structures.

<b>Impact Category</b>	<b>Unit</b>	<b>PS waste</b>	<b>Graphene/talc hybrid additives</b>	<b>Graphene/Fe-treated talc hybrid additives</b>	<b>Separated graphene from graphene/talc hybrid additives</b>	<b>Separated graphene from graphene/Fe-treated talc hybrid additives</b>
<b>Global warming</b>	kg CO <sub>2</sub> eq	0.4	0.642	2.1	4.86	5.29
<b>Stratospheric ozone depletion</b>	kg CFC11 eq	2.64E <sup>-9</sup>	9.67E <sup>-8</sup>	4.98E <sup>-7</sup>	1.06E <sup>-5</sup>	1.07E <sup>-5</sup>
<b>Ionizing radiation</b>	kBq Co-60 eq	0.00011	-8.38E <sup>-5</sup>	0.0106	0.0373	0.0401
<b>Ozone formation. human health</b>	kg NO <sub>x</sub> eq	0.000598	0.00115	0.00383	0.00995	0.0107
<b>Ozone formation. terrestrial ecosystems</b>	kg NO <sub>x</sub> eq	0.000633	0.00118	0.00389	0.01	0.0108
<b>Terrestrial acidification</b>	kg SO <sub>2</sub> eq	0.000931	0.00208	0.00734	0.0203	0.0218
<b>Freshwater eutrophication</b>	kg P eq	4.2E <sup>-6</sup>	0.000311	0.00151	0.00412	0.00447
<b>Marine eutrophication</b>	kg N eq	5.88E <sup>-5</sup>	8.24E <sup>-5</sup>	0.000394	0.000485	0.000575
<b>Terrestrial ecotoxicity</b>	kg 1,4-DCB	0.0773	0.125	0.662	2.68	2.83
<b>Freshwater ecotoxicity</b>	kg 1,4-DCB	0.0198	0.035	0.206	0.284	0.333
<b>Marine ecotoxicity</b>	kg 1,4-DCB	0.0275	0.0474	0.272	0.376	0.442
<b>Human carcinogenic ecotoxicity</b>	kg 1,4-DCB	0.00622	0.0247	0.111	0.285	0.31
<b>Human non-carcinogenic ecotoxicity</b>	kg 1,4-DCB	0.638	1.04	5.12	7.63	8.81

<b>Land use</b>	m <sup>2</sup> a crop eq	0.000317	0.00165	0.0101	0.0272	0.0297
<b>Mineral resource scarcity</b>	kg Cu eq	5.61E <sup>-5</sup>	0.00553	0.00518	0.00505	0.00495
<b>Fossil resource scarcity</b>	kg oil eq	0.185	0.229	0.556	1.2	1.29
<b>Water consumption</b>	m <sup>3</sup>	0.00526	0.00743	0.0171	0.0373	0.0401

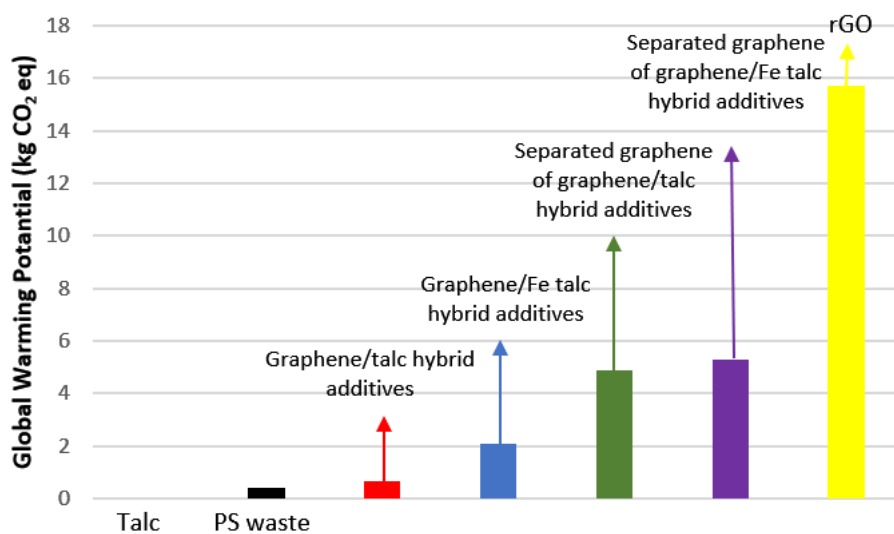


**Figure 16.** The comparison of global warming potential of talc, neat waste PS, directly and catalytically grown graphene/talc hybrid additives, their separated graphene structures, and rGO.

Furthermore, the impact of production inputs of the hybrid additives and their separated graphene structures on global warming potential was summarized in Table 6. As shown in Table 6, electricity was the most critical parameter for tuning the global warming potential for producing hybrid additives and graphene. Due to the additional experimental steps compared to the other hybrid and separated graphene formation processes, the separated graphene from graphene/Fe-treated talc hybrid additives process had the maximum value of electric consumption. Since the upcycled graphene was attempted to be removed from the talc substrate in the graphene separation processes, talc had the minimum effect on global warming during the production of separated graphene structures. During graphene separation, hydrogen fluoride and nitric acid were utilized; that's why they had a global warming effect during the graphene

separation process. On the other hand, the carbon source waste PS had the maximum global warming potential when it was regarded as a single polymer rather than being used in hybrid structures. Related to Table 6, electricity consumption is the hotspot to decrease the global warming potential. Using more energy-efficient devices or shortening the experimental steps can lead to lower greenhouse gas emissions, significantly contributing to sustainability and a circular economy.

**Table 6.** The impact of production inputs of the hybrid additives and their separated graphene structures on global warming potential.

Process	Unit	PS waste	Graphene/talc hybrid additives	Graphene/Fe-treated talc hybrid additives	Separated graphene from graphene/talc hybrid additives	Separated graphene from graphene/Fe-treated talc hybrid additives
<b>Total of all processes</b>	kg CO <sub>2</sub> eq	0.4	0.642	2.1	4.86	5.29
<b>Electricity</b>	kg CO <sub>2</sub> eq	-	0.324	1.54	4.2	4.56
<b>Hydrogen fluoride</b>	kg CO <sub>2</sub> eq	-	-	-	0.0553	0.0553
<b>Iron (III) chloride</b>	kg CO <sub>2</sub> eq	-	-	0.0178	-	0.00517
<b>Nitric acid</b>	kg CO <sub>2</sub> eq	-	-	-	0.32	0.32
<b>PS</b>	kg CO <sub>2</sub> eq	0.385	0.308	0.308	0.0892	0.0892
<b>Talc</b>	kg CO <sub>2</sub> eq	-	0.00696	0.00564	0.00202	0.00163

### 3.4. CONCLUSION

In this study, the effect of aromaticity of polystyrene waste, utilized talc substrate size, the presence of iron catalyst, and polymer mixing method on the formation of upcycled graphene structures was examined and explained via several spectroscopic and microscopic analyses detailly. Two-dimensional graphene sheets were produced on micron talc, and iron-treated micron talc surface while three-dimensional spherical graphene structure was obtained on fine talc, and iron-treated fine talc substrate from PS waste by upcycling. Moreover, the existence of iron catalyst triggered more carbon atom deposition on talc surface, and contributed to the upcycled graphene formation. On the other hand, blending the raw materials using thermokinetic mixing rather than extrusion deteriorated the crystalline structure of talc due to the high shear rate of the mixer. On the other hand, the extruded upcycled graphene/micron talc hybrid additive

was reinforced to the copoPP and homoPP composites to enhance the mechanical features of the resultant products for engineering applications. While the flexural and tensile modulus of the homoPP composites increased in case of the hybrid reinforcement, only flexural modulus of copoPP composites enhanced to some extent by the addition of hybrid additive. This was attributed to the better interaction of homoPP and hybrid additive due to the molecular structure, and chain orders of homoPP. Furthermore, the global warming potential of produced hybrid additives and separated graphene structures of directly and catalytically grown hybrid additives was assessed and compared to the conventional graphene formation technique by life cycle analysis. It was seen that due to the longer production duration, utilized chemicals and energy, separated graphene structure of upcycled graphene/Fe-talc hybrid had the highest global warming potential compared to the micron talc-based and fine-talc based hybrids, and separated graphene structure of upcycled graphene/talc hybrids. However, the global warming potential of separated graphene structure of upcycled graphene/Fe-fine talc hybrid was significantly lower than that of rGO, which indicates that a 'greener' graphene production could be supplied by upcycling from PS waste. This study can be regarded as a favorable guide to comprehend the dimension-controlled graphene formation on a mineral substrate from waste aromatic plastic source by upcycling in an environment-friendly, and economic way.

## **CHAPTER 4. UPCYCLING OF POLYSTYRENE WASTE INTO GRAPHENE GROWN ON ORGANICALLY MODIFIED MONTMORILLONITE AS A SUBSTRATE**

It is known that graphene formation is possible from waste plastics such as PP, and PS on talc substrate by upcycling. This chapter focuses on the approval of the graphene formation from waste PS by upcycling on OMMT surface rather than the talc surface. In order to explain the characteristics of the upcycled graphene on OMMT surface a systematic characterization was conducted. By this research, the influence of the substrate on the upcycled graphene formation is understood, and the characteristics properties of produced graphenes grown on different substrates can be compared.

### **4.1. INTRODUCTION**

The alternative way to upcycling the aromatic polymers is pyrolysing and carbonizing the aromatic polymer to synthesize carbon nanomaterials in the presence of organically modified montmorillonite (OMMT) as template and catalysis. MMT clay functions as a degrading catalytic template, enhancing the production of these light hydrocarbons and aromatics, to initiate their formation during the pyrolysis process [81]. This fact was supported by GC-MS analysis in earlier reports in the literature, where the addition of MMT clay increased the generation of hydrogen or methane by 2 to 2.5 times more while simultaneously increasing the aromatic content by 3 to 4 times [60]. In the study of Gong et al., mixed plastics consisting of PP, PE, PS, PET, and PVC were effectively transformed into carbon nanospheres (CNS) on organically modified montmorillonite (OMMT) [82]. Also, a simple method was developed to convert waste PP into graphene flakes with high yield on organically modified montmorillonite at 700°C by Gong et al.[60]. In this study, the conversion of waste PS into graphene structure on OMMT used as substrate and catalysis was achieved by upcycling. The impact of OMMT substrate on the formation of upcycled graphene was investigated in detail. Thus, within this study the compability between PS and OMMT was revealed.

### **4.2. EXPERIMENTAL**

#### **4.2.1 Materials**

The substrate, organically modified montmorillonite (OMMT)((Nano 1- 140)) was purchased from ESAN, Eczacıbaşı Company (Turkey). The carbon source of

polystyrene (PS) were supplied from Eurotech Company (Turkey) for upcycled graphene/OMMT hybrid additive fabrication from waste PS. To obtain separated graphene structures from hybrid additive, hydrofluoric acid (HF,  $\geq 37\%$ ), and nitric acid ( $\text{HNO}_3$ ,  $\geq 65\%$ ) were provided from Sigma-Aldrich.

#### **4.2.2. The formation of upcycled graphene/OMMT hybrid additive from polystyrene waste**

In order to fabricate the upcycled graphene/OMMT hybrid additive, firstly, the carbon source which was waste PS was mixed with OMMT in weight percentages of 80:20 via a high shear rate (3000 rpm) thermokinetic mixer (Dusatec) at the temperature of 180 °C. Then, waste PS/OMMT composite was heated up to 1000 °C and kept at 1000 °C for 5 min in an Argon atmosphere. By keeping the composite mixture at this temperature enabled the deposition of graphene structures on OMMT substrate. Furthermore, the graphene growth was ensured by the separation of upcycled graphene structure from OMMT substrate by acid treatments. For this purpose, the upcycled graphene/OMMT hybrid additive was treated with 20 wt % HF acid solution for 48 h at room temperature. Afterward, vacuum filtration, and subsequent drying at 50°C for 30 min was performed to collect the treated material. The dried samples were also treated with  $\text{HNO}_3$ : distilled water (1:2, v: v) mixture for 3 h at 110°C by refluxing. After 3 h, the reaction mixture was cooled down to room temperature and centrifuged at 7500 rpm for 15 min by washing with deionized water several times. Finally, the centrifuged separated graphene structures were dried at 80°C overnight.

#### **4.2.3. Characterization**

Neat OMMT, upcycled graphene/OMMT hybrid additive, and the separated graphene structure of upcycled graphene/OMMT hybrid were examined by various spectroscopic and microscopic characterization techniques. The surface functional groups of upcycled graphene/OMMT hybrid and OMMT were identified using the Fourier transform infrared spectroscopy (FT-IR, Thermo Scientific, Nicolet iS50 FTIR). Raman spectroscopy was conducted by using a Renishaw inVia Reflex Raman Microscope with 532 nm edge laser to examine the molecular arrangement and vibrational features of the prepared samples. X-Ray Diffraction (XRD) characterization technique was applied by a Bruker D2 Phaser diffractometer with a  $\text{CuK}\alpha$  radiation source to observe the characteristic graphene and talc peaks and crystal structure of the samples. X-Ray

Photoelectron Spectroscopy (XPS, Thermo Scientific, Waltham, Massachusetts, USA) characterization was performed for the elemental and chemical analysis of the samples. Surface morphology was investigated by Leo Supra 35VP Field Emission Scanning Electron Microscope (SEM, Carl Zeiss AG, Jena, Germany) and JEM-ARM200CFEG Ultra High Resolution Transmission Electron Microscopy (TEM, JEOL, Japan). Thermal characteristics of the samples were examined using a TGA instrument with Mettler Toledo TGA / DSC 3+ under a nitrogen environment between 25°C and 1000°C. Moreover, the environmental impact of the hybrid additives was analyzed by life cycle assessment (LCA) using SimaPro (release 9.3.0.2) software and ReCiPe 2016 v1.1 midpoint method, Hierarchist version.

### **4.3. RESULTS and DISCUSSION**

#### **4.3.1. Structural characteristics of the upcycled graphene/OMMT hybrid additive, and its separated graphene structure**

FTIR analysis was carried out to understand the structural features of the upcycled graphene/OMMT hybrid. FTIR spectra of neat OMMT and upcycled graphene/OMMT hybrid additive is given in Figure 17. The stretching vibration of hydroxyl (–OH) groups on the OMMT surface could be linked to the distinctive peaks seen at 3633  $\text{cm}^{-1}$  and 3435  $\text{cm}^{-1}$ . The bending vibration of –OH caused the formation of peaks at 1645  $\text{cm}^{-1}$  and 910  $\text{cm}^{-1}$ , while the stretching vibration of Si–O–Si generated absorptions at 1041  $\text{cm}^{-1}$  and 796  $\text{cm}^{-1}$ . By modifying MMT organically, characteristic absorption peaks of the vibration of saturated C–H bond were seen at 2929  $\text{cm}^{-1}$ , 2852  $\text{cm}^{-1}$ , and 1478  $\text{cm}^{-1}$ . These peaks revealed that the organic modifier had intercalated into the layers of MMT [56]. The strong peak nearly at 1070  $\text{cm}^{-1}$  could be correlated with the creation of Si-O-C bonding [83], which showed the carbon nanostructure formation on OMMT surface.

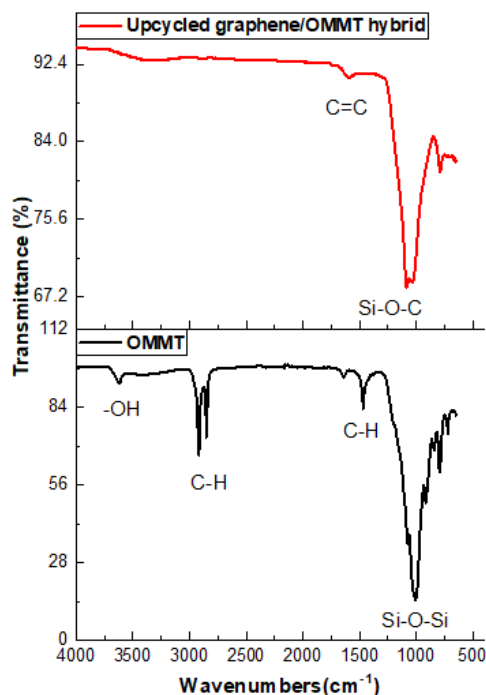


**Figure 17.** FTIR spectra of neat OMMT, and upcycled graphene/OMMT hybrid.

The structural features of OMMT, and upcycled graphene/OMMT hybrid were also determined by Raman spectroscopy and XRD analysis. Raman spectra and XRD patterns of upcycled graphene/OMMT hybrid additive and its separated graphene structure are given in Figure 18. In the Raman spectra of OMMT, the most prominent bands were observed at 2882 cm<sup>-1</sup> and 2847 cm<sup>-1</sup> assigned to the methylene antisymmetric and symmetric stretching modes [84]. As seen in Figure 18 (a), the G band at 1594 cm<sup>-1</sup> corresponded to an E<sub>2g</sub> mode of hexagonal graphite and was related to the vibration of sp<sup>2</sup> bonded carbon atoms in a graphite layer. On the other hand, the D band at 1343 cm<sup>-1</sup> belonged to the vibration of carbon atoms with dangling bonds in the plane terminations of disordered graphite. Moreover, the crystallinity of the upcycled graphene/OMMT hybrid was determined by the intensity ratio of the G and D bands. If I<sub>D</sub>/I<sub>G</sub> ratio decreases, a higher degree of structural organization is obtained [85]. A high I<sub>D</sub>/I<sub>G</sub> ratio was obtained for the separated graphene structure compared to the graphene/OMMT hybrid and this attributed to the relative high degree of graphitization of hybrid additive since graphene has started to grown on OMMT layer by layer [85]. A low amount of disordered carbons in the separated graphene structures after acid treatments was also supported by the XRD data, seen in Figure 18(b). In the XRD patterns, the basal (001), (003), (100), (110) and (300) planes of OMMT were observed

at  $2\theta=7.3^\circ$ ,  $19.8^\circ$ ,  $21.8^\circ$ ,  $35.8^\circ$  and  $61.7^\circ$ , respectively [86]. The (002) and (100) characteristic diffraction peaks of graphite occurred nearly at  $2\theta=26.3^\circ$ , and  $2\theta=43.8^\circ$ , respectively. After acid treatments, the intensity of the (002) peak increased substantially from 18.6 to 43.8 and the peak shifted to  $2\theta=24.3^\circ$ . Moreover, the average crystalline size of the separated graphene structures of upcycled graphene/OMMT hybrid was calculated as 1.29 nm using the Debye-Scherrer equation (mentioned in the chapter 3). Also, acid treated graphene/OMMT hybrid had a  $d_{002}$  spacing value of 0.366 nm which belonged to graphitic d spacing. The number of graphene layers in case of OMMT substrate presence was decided as 5.

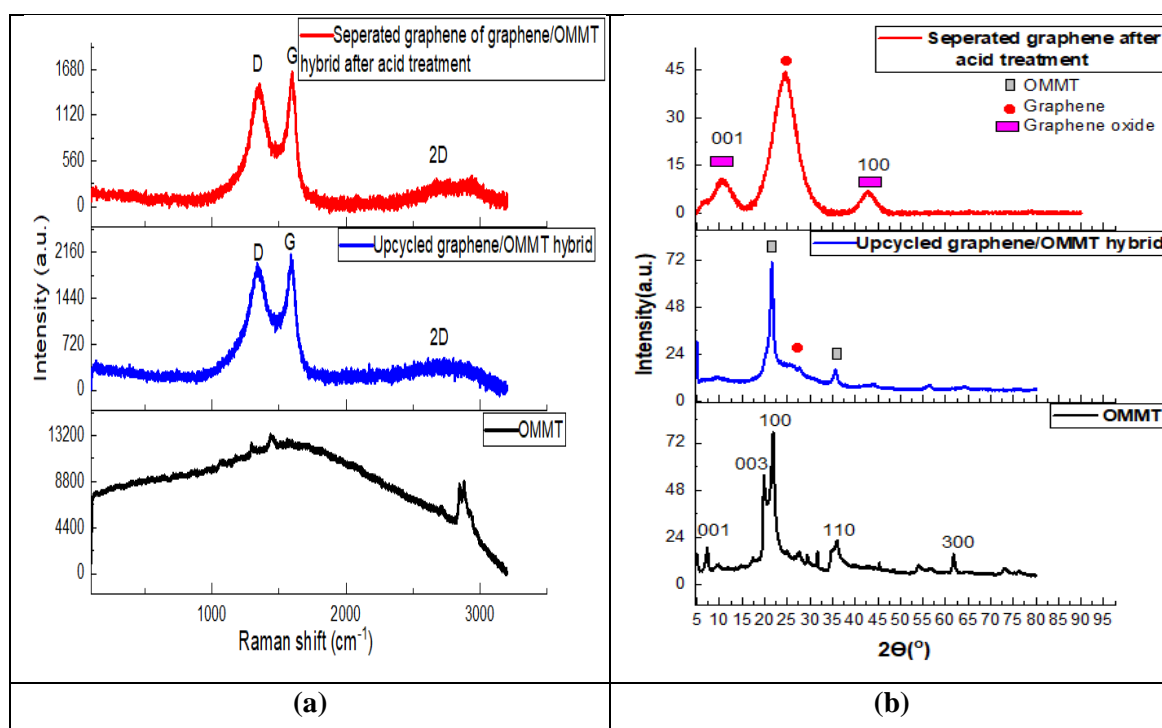


**Figure 18.** (a) Raman spectra, and (b) XRD patterns of OMMT, upcycled graphene grown on OMMT surface and its separated graphene structure after acid treatments.

#### 4.3.2. Chemical characteristics of the upcycled graphene/OMMT hybrid additive, and its separated graphene structure

The upcycled graphene/OMMT hybrid additive and its separated graphene structure were examined by XPS analysis to analyze the elemental composition, bonding, and surface groups of the hybrids and separated graphene structures. The elemental composition of the upcycled graphene/OMMT hybrid additive and its separated graphene structures are demonstrated in Table 7. The upcycled graphene/OMMT hybrid

consisted of 82.3 at % of C atom, and 17.7 at % of O atom, while its separated graphene structure included 84.4 at % of C, 15.4 at % of O, and 0.2 at % of Si.

**Table 7.** The elemental composition of the upcycled graphene/OMMT hybrid additive and its separated graphene structure after acid treatments.

Sample	C (at%)	O (at%)	Si (at%)
OMMT	50.2	33	16.21
Upcycled graphene/OMMT hybrid	82.3	17.7	-
Separated graphene of upcycled graphene/ OMMT hybrid after acid treatments	84.4	15.4	0.2

In addition, XPS survey scan of upcycled graphene/OMMT hybrid and its separated graphene structure was carried out and presented in Figure 19. The C=C  $sp^2$  bonding was observed at 284.5 eV in the XPS survey scan of both hybrid additive and its separated graphene structure, which underlined the carbon structure formation from PS waste. In addition, the hybrid additive and its separated graphene structure had O1s signals at 531.5 eV. However, the signal intensities of C1s and O1s peaks were higher in the XPS survey scan of separated graphene structure than that of upcycled graphene/OMMT hybrid additive.

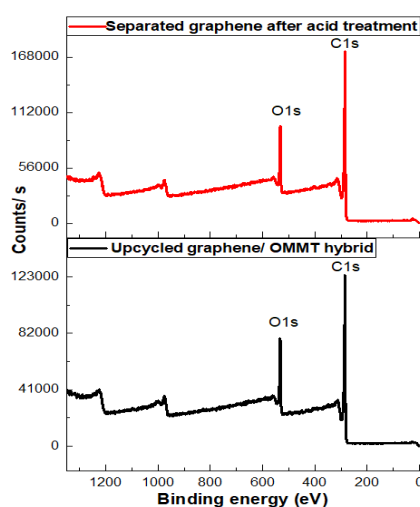


**Figure 19.** XPS survey scan of upcycled graphene/OMMT hybrid and its separated graphene structure after acid treatments.

### 4.3.3. Morphological properties of the upcycled graphene/OMMT hybrid additive, and its separated graphene structure

The surface morphology of the upcycled graphene/OMMT hybrid additive and its separated graphene structure after acid treatments was examined by SEM. SEM images of the upcycled graphene/OMMT hybrid, and its separated graphene structure are given in Figure 20. As seen in SEM image of Figure 20(b), graphene was grown on OMMT as a layered structure and it preserved 2D structure after acid treatment process.

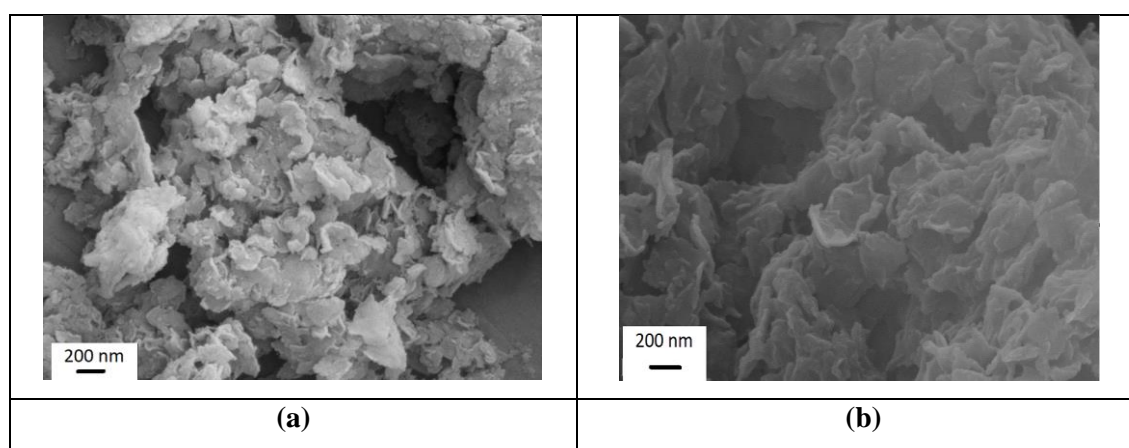


**Figure 20.** SEM images of (a) upcycled graphene/OMMT hybrid, and (b) its separated graphene structure after acid treatments.

### 4.3.4. Thermal properties of the upcycled graphene/OMMT hybrid additive, and its separated graphene structure

Thermal features of the upcycled graphene/OMMT hybrid additive, and its separated graphene structure was assessed by TGA thermograms. TGA thermograms of upcycled graphene/OMMT hybrid additive, and its separated graphene structure are depicted in Figure 21. The thermal degradation of OMMT occurred in four steps. The first one was attributed to absorbed water in the OMMT structure in the range of 25–90°C, followed by three additional steps in the range of 208–1000°C. Besides, the thermal degradation of upcycled graphene/OMMT hybrid additive below 200 °C was assigned to the elimination of absorbed water and functional groups that included oxygen on the graphitic nanomaterial surface. However, as the temperature rised over 300 °C, graphitic nanomaterial lost its weight slowly and steadily due to the thermal degradation of stable oxygen functions. In addition, the carbon material cannot be burned in an inert

state thus residual weight percentage of the hybrid continued to decrease [87]. Besides, under oxygen environment, PS/OMMT hybrid was started to oxidation at about 500°C as the other PS-derived hybrids.

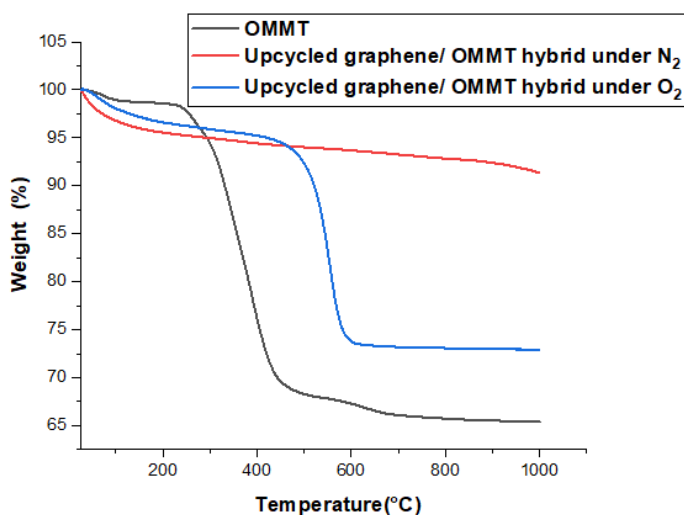


**Figure 21.** TGA thermogram of neat OMMT and upcycled graphene/OMMT hybrid.

Furthermore, the weight loss of neat OMMT, and upcycled graphene/OMMT hybrid at 250°C, 750°C and 1000°C are given in Table 8. Neat OMMT lost its 2.2 % of weight, while upcycled graphene/ OMMT hybrid lost its 4.8 of weight up to 250 °C. The dramatic weight loss of OMMT happened between 250°C and 750°C due to the oxygen groups on the MMT surface. This significant weight loss was eliminated in the hybrid structure because of the formation of graphitic structure on OMMT surface. At 1000 °C, the total weight loss of neat OMMT was determined as 34.6 %, while it was 8.6 % in the hybrid structure. In conclusion, the thermal stability of the upcycled graphene/OMMT hybrid additive was considerably higher than that of neat OMMT at 1000 °C.

**Table 8.** The weight loss of neat OMMT, and upcycled graphene/OMMT hybrid at 250°C, 750°C and 1000°C.

	Weight loss (%)		
	250°C	750°C	1000°C
Neat OMMT	2.2	34.1	34.6
Upcycled graphene/ OMMT hybrid (under N <sub>2</sub> )	4.8	7	8.6
Upcycled graphene/ OMMT hybrid (under O <sub>2</sub> )	3.7	26.8	27.1

#### **4.3.5. Life cycle assesment of the upcycled graphene/OMMT hybrid additive, and its separated graphene structure**

LCA analysis was conducted to understand the environmental impacts of PS-derived graphene/OMMT hybrid additive, and its separated graphene structure. The Ecoinvent 3- allocation cut off by classification, and Swiss input & output databases were used for the life cycle inventory (LCI). The waste scenario of the input materials was estimated as landfilled municipal solid waste for the rest of the world. The software system, SimaPro release 9.3.0.2, only considered the inputs with mass units in the evaluation of waste disposal scenario. The impact assessment comparison of the inputs was determined by the method, which includes the Intergovernmental Panels on Climate Change (IPCC) equivalence factors. Related to this, the environmental impacts of neat OMMT, graphene/OMMT hybrid additive, and its separated graphene structure are mentioned in Table 9. The most crucial environmental concern was global warming potential, which was mainly caused by the usage of hazardous materials, long production procedures, transformation, or waste scenario. In this research, the separation of graphene structures from OMMT substrate was the main process responsible for the high global warming potential with the value of 4.87 kg CO<sub>2</sub> eq (equivalent) due to the usage of acid treatments. On the other hand, as expected the lowest carbon release was generated by neat OMMT with 0.0765. Compared to the separated graphene structure, the graphene/OMMT hybrid additive had a less environmental concern since the hybrid production consumes less energy than the graphene separation. The global warming potential of neat OMMT, graphene/OMMT hybrid additive, and its its separated graphene structure was summarized and compared to the rGO, in Figure 22. The conventional rGO method had a dramatically high global warming potential compared to upcycled graphene structures.

**Table 9.** The environmental impacts of neat OMMT, graphene/OMMT hybrid additive, and its separated graphene structure.

	Unit	OMMT	Graphene/OMMT hybrid	Separated graphene from grapheneOMMT hybrid
<b>Global warming</b>	kg CO <sub>2</sub> eq	0.0765	0.659	4.87
<b>Stratospheric ozone depletion</b>	kg CFC11 eq	5.84E <sup>-9</sup>	1.01E <sup>-7</sup>	1.06E <sup>-5</sup>
<b>Ionizing radiation</b>	kBq Co-60 eq	0.000127	0.00236	0.0377
<b>Ozone formation. human health</b>	kg NO <sub>x</sub> eq	1.6E <sup>-5</sup>	0.00117	0.00996
<b>Ozone formation. terrestrial ecosystems</b>	kg NO <sub>x</sub> eq	1.63E <sup>-5</sup>	0.00121	0.0101
<b>Terrestrial acification</b>	kg SO <sub>2</sub> eq	1.37E <sup>-5</sup>	0.00212	0.0203
<b>Freshwater eutrophication</b>	kg P eq	1.65E <sup>-6</sup>	0.000317	0.00412
<b>Marine eutrophication</b>	kg N eq	8.23E <sup>-5</sup>	8.3E <sup>-5</sup>	0.000485
<b>Terrestrial ecotoxicity</b>	kg 1,4-DCB	0.00966	0.184	2.7
<b>Freshwater ecotoxicity</b>	kg 1,4-DCB	0.0432	0.036	0.284
<b>Marine ecotoxicity</b>	kg 1,4-DCB	0.0567	0.0487	0.377
<b>Human carcinogenic ecotoxicity</b>	kg 1,4-DCB	0.00167	0.026	0.285
<b>Human non-carcinogenic ecotoxicity</b>	kg 1,4-DCB	0.93	1.06	7.63
<b>Land use</b>	m <sup>2</sup> a crop eq	0.000329	0.00211	0.0274
<b>Mineral resource scarcity</b>	kg Cu eq	0.00105	0.000379	0.00356
<b>Fossil resource scarcity</b>	kg oil eq	0.000928	0.233	1.2
<b>Water consumption</b>	m <sup>3</sup>	3.29E <sup>-5</sup>	0.00662	0.0371

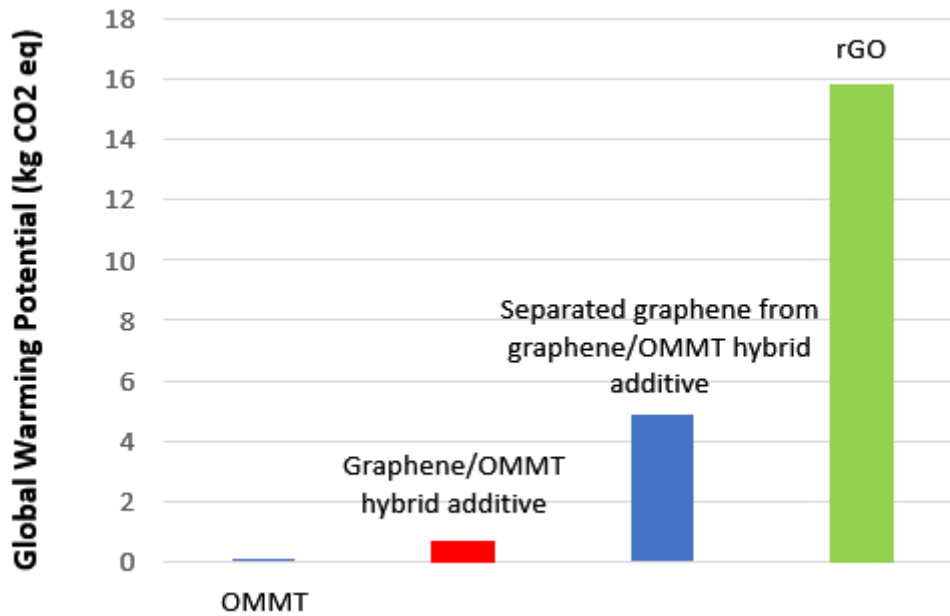


**Figure 22.** The comparison of global warming potential of neat OMMT, graphene/OMMT hybrid additives, its separated graphene structure, and rGO.

Moreover, the impact of production inputs on global warming potential during the hybrid and separated graphene structure formation is summarized in Table 10. It was observed that the highest impact on global warming potential was caused by the utilized energy especially during the collection of separated graphene structure from graphene/OMMT hybrid.

**Table 10.** The impact of production inputs of the upcycled graphene/OMMT hybrid additive and its separated graphene structure on global warming potential.

Process	Unit	OMMT	Graphene/OMMT hybrid additive	Separated graphene from graphene/OMMT hybrid additive
<b>Total of all processes</b>	kg CO <sub>2</sub> eq	0.0765	0.659	4.87
<b>Electricity</b>	kg CO <sub>2</sub> eq	-	0.324	4.2
<b>Hydrogen fluoride</b>	kg CO <sub>2</sub> eq	-	-	0.0553
<b>Nitric acid</b>	kg CO <sub>2</sub> eq	-	-	0.32
<b>PS</b>	kg CO <sub>2</sub> eq	-	0.308	0.0892

OMMT	kg CO <sub>2</sub> eq	0.000552	0.00011	3.2E <sup>-5</sup>
------	-----------------------	----------	---------	--------------------

#### 4.4. CONCLUSION

In this study, upcycled graphene growth on OMMT from PS waste was achieved and the effect of OMMT as template and catalyst to grow graphene was discussed. XRD, Raman and XPS analyses were demonstrated that graphitic structure growth on OMMT was obtained. Interlayer space was calculated as 0.366 and crystalline size was calculated as 1.27 nm using Debye-Sherrer equation. Raman results shows that less defected graphitic structure was obtained after the acid treatment of graphene/ OMMT hybrid with the value of I<sub>D</sub>/I<sub>G</sub> as 0.89. Upcycled graphene with the width of 200-300 nm calculated from the SEM images. Thus, OMMT helps the degradation of polystyrene waste by cleavage of bonds. Also, strong interphase bonding between the two phases was facilitated by the interfacial contacts between the benzene group of polystyrene and the amine groups of the coupling and intercalating agents grafted on MMT and this give rise to distribute polymer matrix uniformly.

## **CHAPTER 5. UPCYCLING OF POLYETHYLENE TEREPHTHALATE WASTE INTO GRAPHENE GROWN ON TALC AS SUBSTRATE**

In this chapter, the effect of aromaticity of PET source on the structural, morphologic, spectroscopic, and thermal characteristics of the resultant upcycled graphene grown on micron talc surface was discussed. In addition, the final features of the graphene grown on talc surface was comprehended in the presence of iron catalyst were determined and compared to that of upcycled graphene grown on non-treated micron talc surface.

### **5.1. INTRODUCTION**

PET is a long-chain polymer, and a member of the polyester family. Terephthalic acid (TPA) and ethylene glycol (EG), which are both generated from oil feedstock, are the intermediates used to create PET. PET is an amorphous glass-like substance in its most basic form [88]. By 2020, it is anticipated that the world's PET production would have increased from 42 million tonnes in 2014 to 72 million tonnes. In particular, the number of PET drinking bottles used climbed from 300 billion in 2000 to 480 billion in 2016, and by 2021, the number of bottles consumed will reach 583 billion [89]. PET is a key component of both single-use water bottles and the plastic packaging materials that are necessary for food safety in today's world. Since PET has aromatic ester connections, it is difficult to recycle PET effectively. The pollution/waste from this substance has also become increasingly evident in landfills and natural ecosystems all over the world as a result of the growth in global population and our changing lifestyles [90]. Incineration and chemical recycling are the two most popular solutions to PET disposal. Additionally, stronger legislation governing trash recovery is currently taking attention [91].

In this study, the conversion of waste PET into graphene structure on talc substrate was achieved by upcycling. The impact of aromatic structure of PET on the formation of upcycled graphene grown on talc surface was examined in detail. Moreover, the utilized micron talc surface was functionalized by iron treatment, and the effect of iron catalyst as well as the chemical structure of PET was discussed.

## **5.2 EXPERIMENTAL**

### **5.2.1. Materials**

Micron talc with the particle size of D50 = 12  $\mu\text{m}$  and fine talc with the particle size of D50 = 1.9  $\mu\text{m}$  were supplied from Micron'S company (Turkey) and Imerys company (France), respectively. The carbon sources in the form of polystyrene (PS) and polyethylene terephthalate (PET) were purchased from Eurotech Company (Turkey) for upcycled graphene/talc hybrid additive fabrication. To obtain separated graphene structures from hybrid additives, hydrofluoric acid (HF,  $\geq 37\%$ ), and nitric acid ( $\text{HNO}_3$ ,  $\geq 65\%$ ) were purchased from Sigma-Aldrich. To prepare the hybrid additive reinforced polypropylene (PP) composites, PP was acquired from Ravago Petrochemical Company (Turkey).

### **5.2.2. Converting of polyethylene terephthalate waste into upcycled graphene on talc surface**

The carbon source, waste PET, was blended with micron talc in the ratio of 80:20 (wt %) via a high shear (4500 rpm) thermokinetic mixer (Dusatec) at 250  $^{\circ}\text{C}$ . Then waste PET/ micron talc composite was heated to 1000  $^{\circ}\text{C}$  under Argon atmosphere, and kept at 1000  $^{\circ}\text{C}$  for 5 min for the formation of graphene structure on micron talc substrate. The same steps were also repeated with Fe-treated micron talc, whose iron treatment procedure was explained in the experimental section 3.2.

The formation of graphene on neat and Fe-treated talc surfaces was ensured by the separation of the upcycled graphene from micron talc surface, and Fe-treated micron talc substrates via HF and  $\text{HNO}_3$  acid treatments, as explained in the experimental section 3.2.

### **5.2.3. Characterization**

Talc samples (micron talc, Fe-micron talc), upcycled graphene/talc hybrid additives, and the separated graphene structures were analyzed detailly by several spectroscopic and microscopic characterization methods. The surface functional groups of upcycled graphene/micron talc hybrids obtained from PET waste and micron talc were identified using the Fourier transform infrared spectroscopy (FT-IR, Thermo Scientific, Nicolet iS50 FTIR). Raman spectroscopy was conducted by using a Renishaw inVia Reflex Raman Microscope with 532 nm edge laser to examine the molecular arrangement and

vibrational features of the prepared samples. X-Ray Diffraction (XRD) characterization technique was applied by a Bruker D2 Phaser diffractometer with a  $\text{CuK}\alpha$  radiation source to observe the characteristic graphene and talc peaks and crystal structure of the samples. X-Ray Photoelectron Spectroscopy (XPS, Thermo Scientific, Waltham, Massachusetts, USA) characterization was performed for the elemental and chemical analysis of the samples. Surface morphology was investigated by Leo Supra 35VP Field Emission Scanning Electron Microscope (SEM, Carl Zeiss AG, Jena, Germany) and JEM-ARM200CFEG Ultra High Resolution Transmission Electron Microscopy (TEM, JEOL, Japan). The thermal features of the samples were examined using a TGA instrument with Mettler Toledo TGA / DSC 3+ under a nitrogen environment between 25°C and 1000°C. The environmental consequences of the hybrid additives were analyzed by life cycle assessment (LCA) using SimaPro (release 9.3.0.2) software and ReCiPe 2016 v1.1 midpoint method, Hierarchist version

### **5.3. RESULTS and DISCUSSION**

#### **5.3.1. Structural characteristics of the upcycled graphene/talc hybrid additives, and their separated graphene structures**

The functional surface groups of directly, and catalytically grown graphene/micron talc hybrid additives from waste PET were determined by FTIR spectroscopy, and FTIR spectra of micron talc, directly grown graphene/micron talc hybrid, and catalytically grown graphene/Fe-micron talc hybrid are demonstrated in Figure 23. After both direct, and catalytic carbonization processes, C=O stretching occurred at about  $1720\text{ cm}^{-1}$ . Also, a strong C-O stretching at approximately  $1235\text{ cm}^{-1}$  was observed in the FTIR spectra of directly grown upcycled graphene/micron talc hybrid. However, after catalytic carbonization, these peak weakened due to the iron treatment of micron talc, which increased the polymer degradation ratio. After direct, and catalytic carbonization processes, the peak at  $720\text{ cm}^{-1}$  belonged to the C-H bending of benzene coming from PET source. Moreover, the formation of Si-O-C stretching underlined the chemical interaction of talc substrate and carbon source [92].

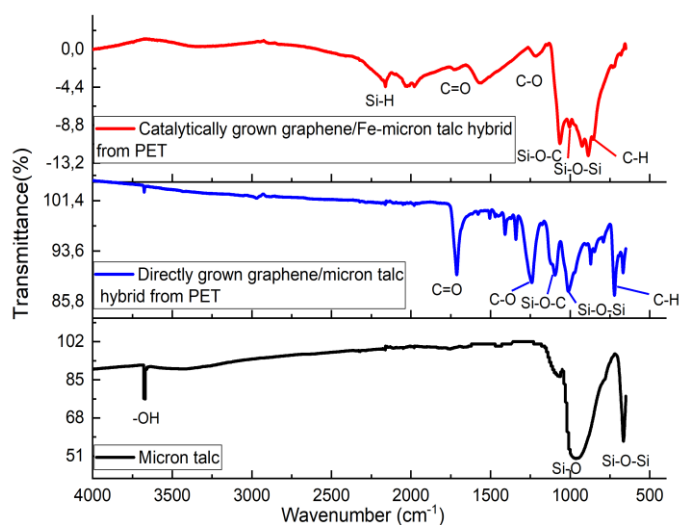


**Figure 23.** FTIR spectra of micron talc, directly grown graphene/micron talc hybrid, and catalytically grown graphene/Fe-micron talc hybrid.

On the other hand, Raman spectroscopy reveals information about carbon structures. Comparison Raman spectra of micron talc, Fe-micron talc, directly and catalytically grown graphene/micron talc hybrids, and their separated graphene structures are given in Figure 24. In the Raman spectra, D, and G peaks were observed at  $1344\text{ cm}^{-1}$  and  $1599\text{ cm}^{-1}$ , respectively. In addition, a large 2D band with a maxima located at about  $2685\text{ cm}^{-1}$  and  $2918\text{ cm}^{-1}$  for separated graphene/micron talc hybrids from directly and catalytically grown hybrid additives, respectively. rGO samples typically contain the 2D band, which can be utilized to determine the layered structure of graphene due to its high sensitivity to stacking of graphene layers [93]. Thus, it was obvious that the separated graphene structure contained some multilayer rGO based on the location and intensity of the 2D band. Additionally, the existence of highly organized carbon domains was understood in the structure of the hybrid additives, and separated graphene forms related to their low  $I_D/I_G$  value of 0.9 [93].

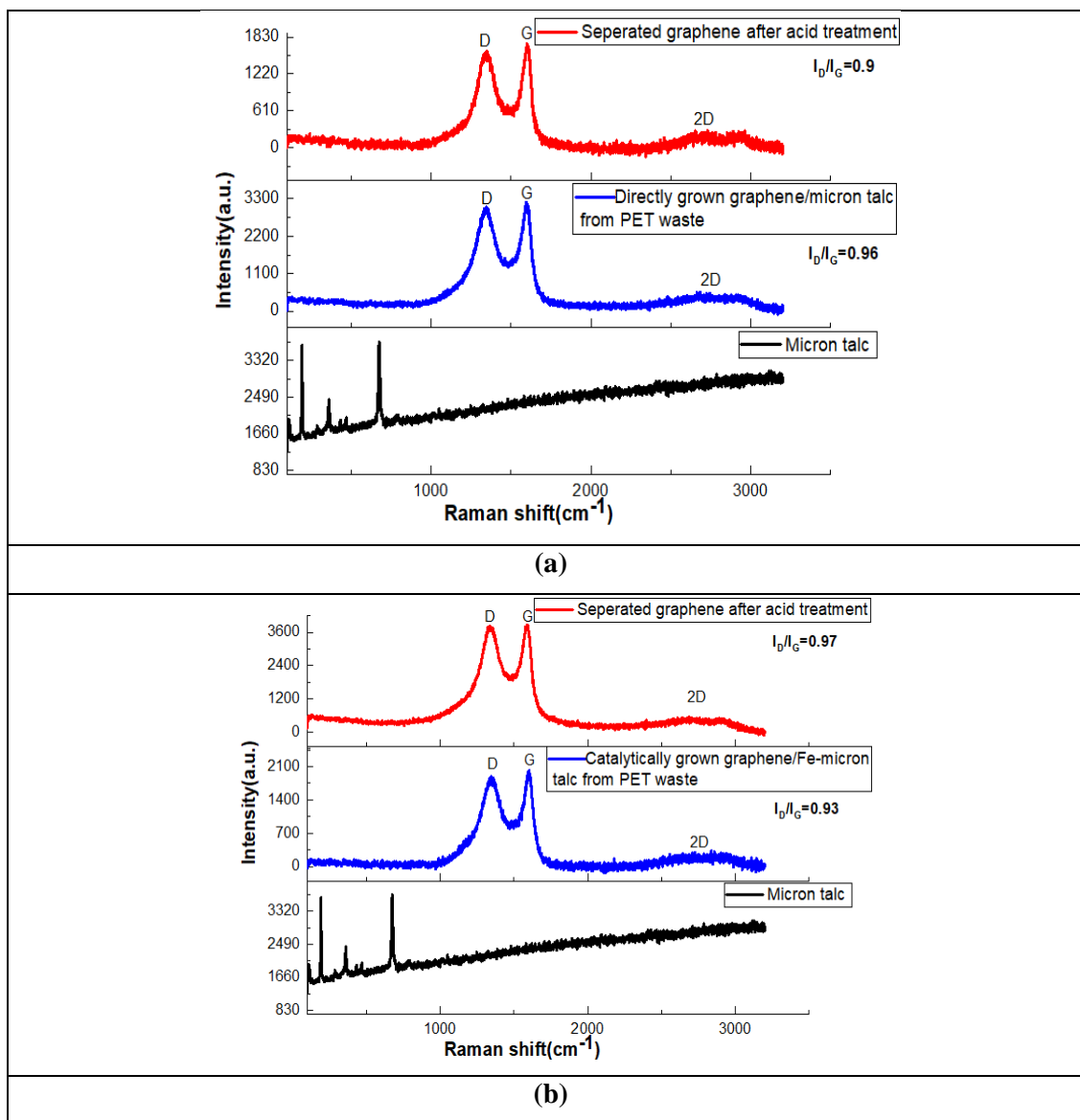


**Figure 24.** Comparison Raman spectra of micron talc, (a) directly, and (b) catalytically grown graphene/micron talc hybrid additives, and their separated graphene structures.

Moreover, comparison XRD patterns of micron talc, directly and catalytically grown graphene/micron talc hybrid additives, and their separated graphene structures are seen in Figure 25. After carbonization processes, two characteristic (002) and (100) diffraction peaks of graphite were observed at  $2\theta=26.4^\circ$  and  $2\theta=43^\circ$ , respectively [94]. Also, reflection plane of Fe-C bonds at  $2\theta=43.8^\circ$  occurred as a result of catalytic carbonization [95]. However, after catalytic carbonization, the intensity of these peaks decreased from 15.5 to 12 and from 7.9 to 2.2 for (002) and (100) diffraction planes, respectively. Thus, the direct carbonization allowed to grow a graphitic structure on micron talc surface more effectively than the catalytic carbonization. Moreover, after

acid treatments, the (002) peak intensity of catalytically grown graphene /Fe-micron talc hybrid from waste PET was determined as 35.6 and it was 32.6 for directly grown graphene/micron talc hybrid. Since these values were very close to each other, it was discovered that iron treatment of micron talc did not had a significant impact on the efficiency for the formation of a graphitic structure on micron talc surface.

The graphene structures separated from catalytically and directly grown graphene/micron talc hybrid additives had a d-spacing of 0.38 nm at  $2\theta \sim 23.4^\circ$ . The crystalline size of separated graphene structures from directly and catalytically grown graphene/micron talc hybrids was 1.06 nm and 1.04 nm, respectively. In connection with this, the number of separated graphene layers of both directly and catalytically grown graphene/micron talc hybrid additives were calculated as 4.

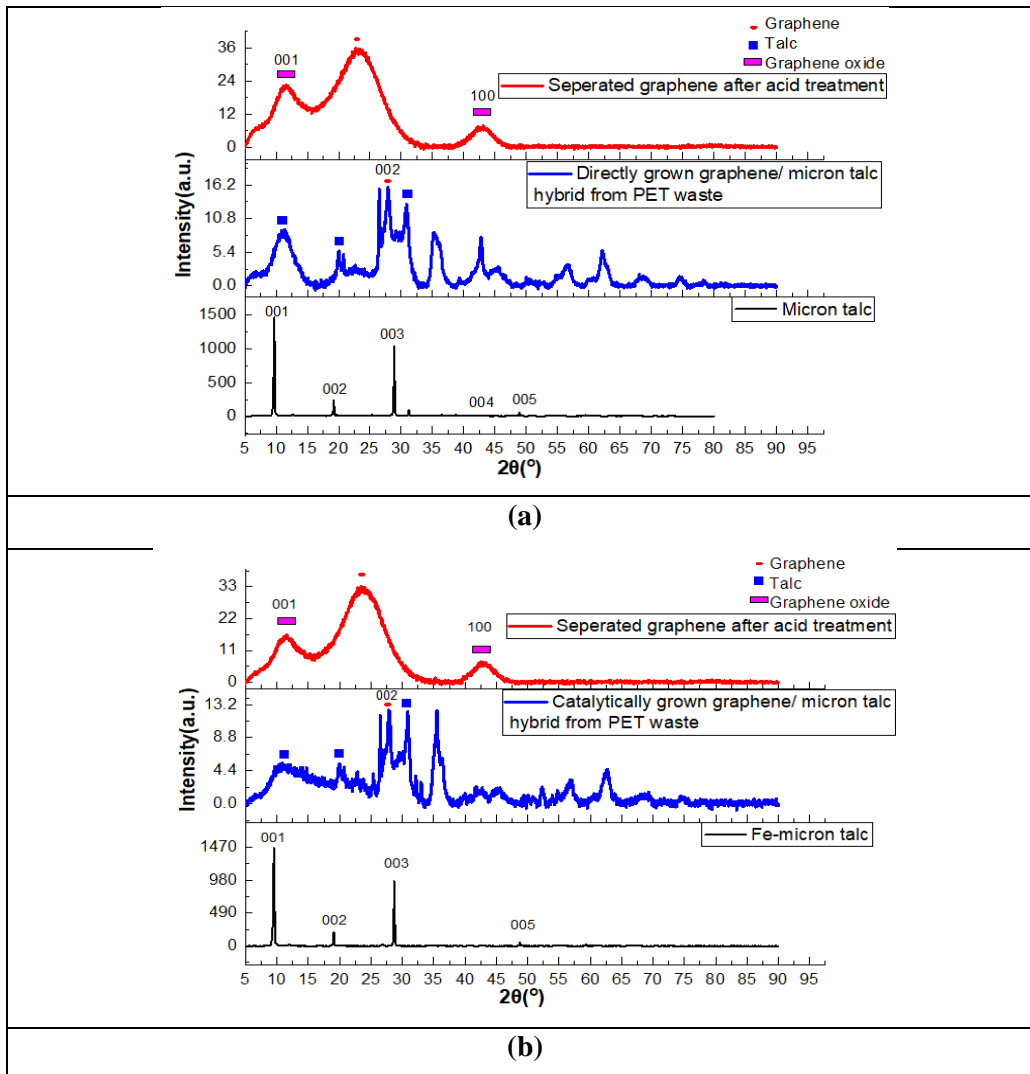


**Figure 25.** Comparison XRD patterns of micron talc, (a) directly, and (b) catalytically grown graphene/micron talc hybrid additives, and their separated graphene structures.

### 5.3.2. Chemical characteristics of the upcycled graphene/talc hybrid additives, and their separated graphene structures

In order to determine the elemental composition, of the directly and catalytically grown graphene/micron talc hybrids and their separated graphene structures, XPS characterization was carried out. Table 11 summarizes the elemental compositions of neat micron talc, directly and catalytically grown graphene/micron talc hybrid additives, and their separated graphene structures after acid treatments. Micron talc includes 52.72 at% of O, 21.66 at% of Si, 18.69 at% of Mg in its structure. After the direct carbonization process, the carbon content of directly grown graphene/micron talc hybrid increased to 46.93 at%, because of the carbon accumulation on micron talc from PET waste. The carbon content of catalytically grown graphene/Fe-micron talc hybrid was analyzed as 54.9 at%, the amounts of which was higher than the carbon content of its directly grown hybrid. Moreover, to confirm the creation of graphene, XPS characterization of separated hybrid additive graphene structures was performed. The carbon amount of separated graphene from directly grown graphene/micron talc hybrid was determined as 81.9 at% while graphene/Fe-micron talc hybrid from catalytic carbonization had 82.4 at% of C.

**Table 11.** XPS elemental analysis of neat micron talc, directly and catalytically grown graphene/micron talc hybrid additives, and their separated graphene structures after acid treatments.

<b>Sample</b>	<b>C (at%)</b>	<b>O (at%)</b>	<b>Si (at%)</b>	<b>Fe (at%)</b>	<b>Mg (at%)</b>	<b>Others (at%)</b>
Micron talc	-	52.7	21.7	-	18.5	6.9
Directly grown graphene /micron talc hybrid	46.9	36.7	12.2	-	4.2	-
Catalytically grown graphene /Fe-micron talc hybrid	54.9	33.1	9.5	-	2.5	-
Separated graphene of graphene/micron talc hybrid after acid treatments	81.9	17.3	-	-	1.4	0.8
Separated graphene of graphene/Fe-micron talc hybrid after acid treatments	82.4	16.7	-	-	-	0.9

### 5.3.3. Morphological characteristics of the upcycled graphene/talc hybrid additives, and their separated graphene structures

The surface characteristics of the obtained hybrid additives, and their separated graphene structures were analyzed by SEM, and SEM images of directly and catalytically grown graphene/micron talc hybrid additives, and their separated graphene structures are shown in Figures 26 and 27, respectively. Directly grown graphene/micron talc hybrid from waste PET had layered and condensed structure. However, after catalytic carbonization, fiber-like structures grown on the Fe-micron talc substrate were visible. The diameter of these fiber-like structures was between 50-150 nm. Thus, with the help of Fe catalyst, fiber-like structures could be formed from waste PET source.

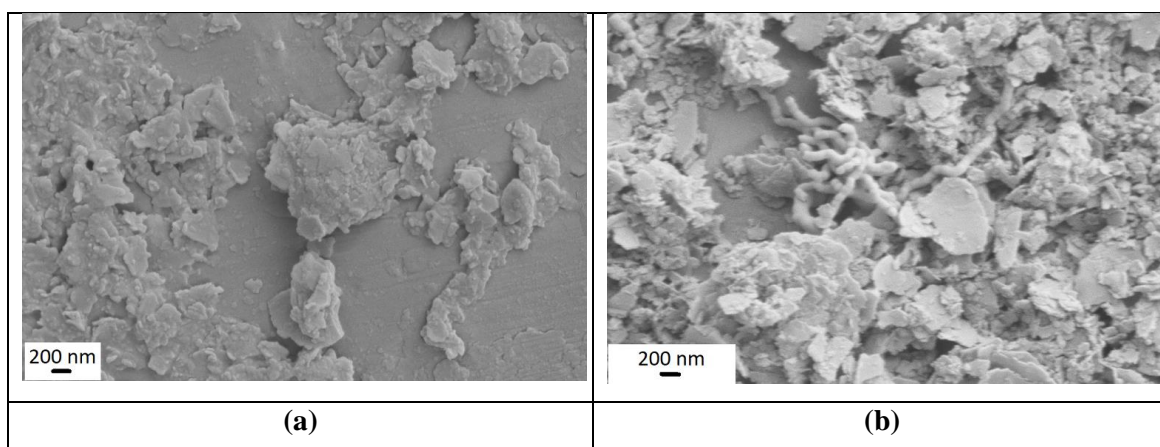


**Figure 26.** SEM images of (a) directly and (b) catalytically grown graphene /micron talc hybrid additives from waste PET.

After acid treatments, the layered structure of separated graphene of directly grown graphene/micron talc hybrid was more apparent. Also, fiber-like structures with the diameter of 50-150 nm were visible in the structure of separated graphene of catalytically grown graphene/Fe-micron talc hybrid.

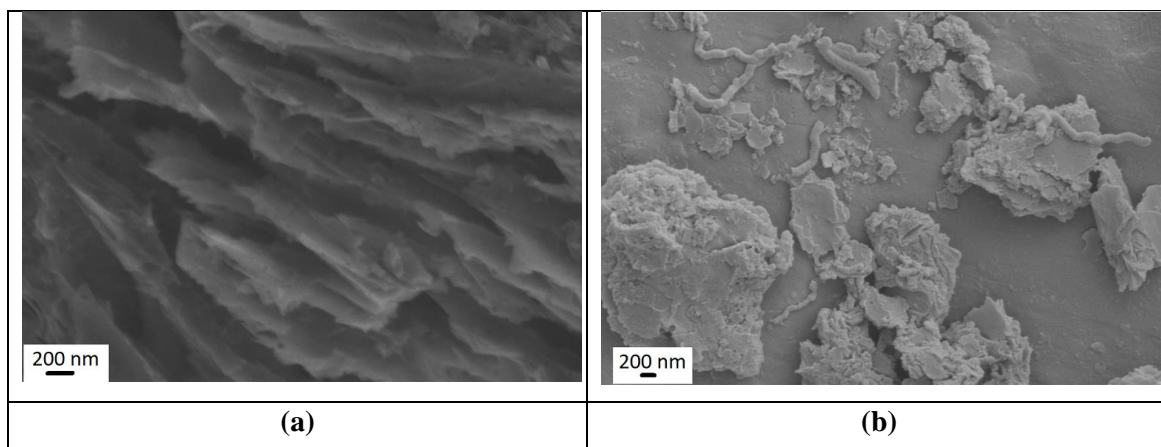


**Figure 27.** SEM images of separated graphene structures of (a) directly and (b) catalytically grown graphene /micron talc hybrid additives from waste PET.

#### **5.3.4. Thermal properties of characteristics of the upcycled graphene/talc hybrid additives, and their separated graphene structures**

TGA thermograms of micron talc, Fe-micron talc, directly and catalytically grown graphene /micron talc hybrid additives from waste PET under nitrogen and oxygen are given in Figure 28. The thermal degradation of directly and catalytically grown hybrid additives occurred in three steps: the first one was attributed to the loss of hydroxyl, epoxy functional groups, and water molecules in the range of 25–150°C. The weight loss for all PET-derived samples followed two additional steps in the range of 208–1000°C. The pyrolysis of the remaining oxygen-containing groups resulted in yet more weight loss at 450 and 600 °C [96]. After 600 °C, the weight loss belonged to the sublimation of the carbon framework and the conversion of thermotolerant O-species. For Figure 28(b), TGA analysis also confirmed that PET-derived hybrids hybrids started oxidation about 400°C because of carbonyl groups in the PET structure. Also, the thermal stability of directly and catalytically grown hybrid are nearly the same.

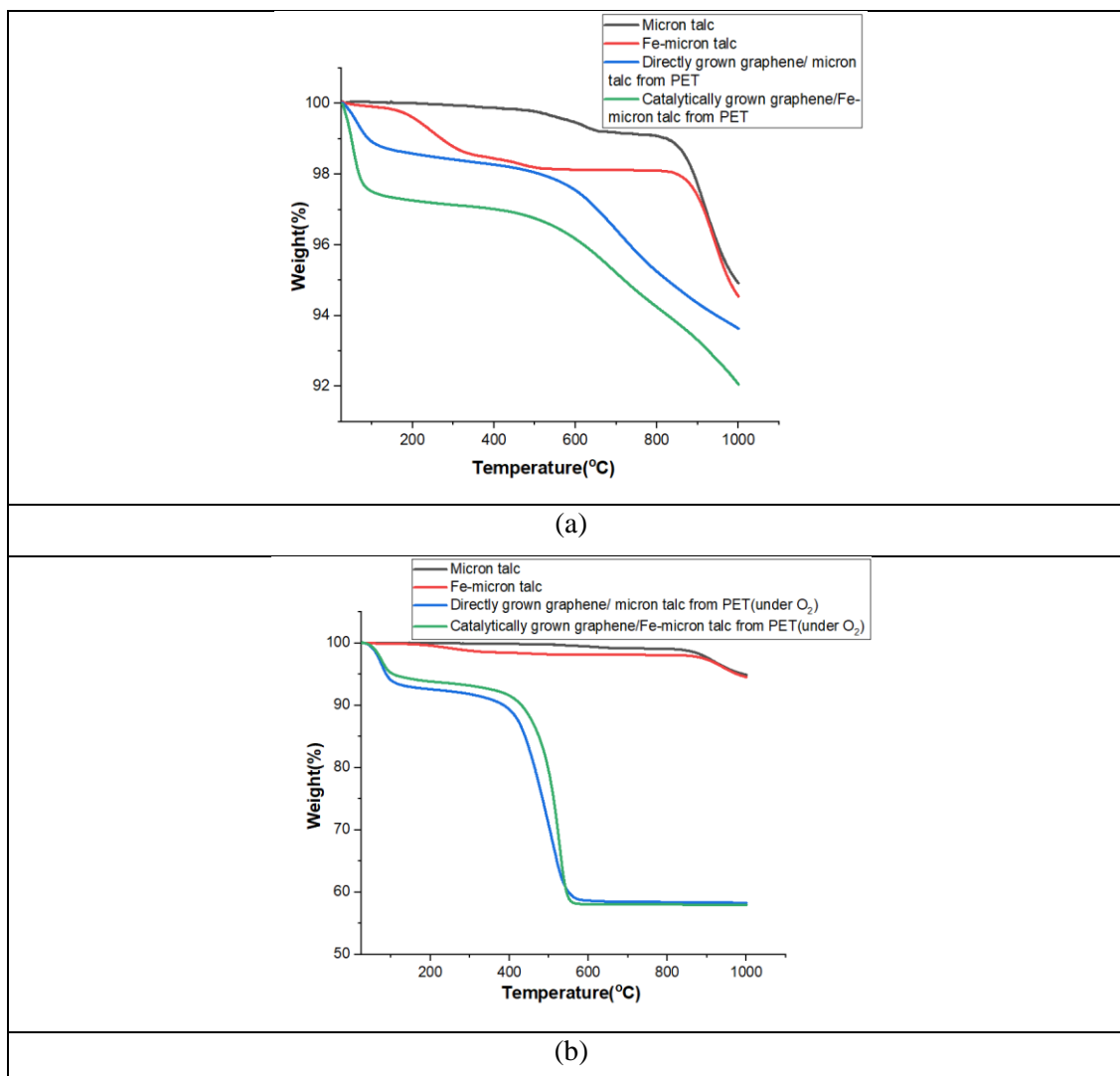


**Figure 28.** TGA thermograms of micron talc, Fe-micron talc, directly and catalytically grown graphene /micron talc hybrid additives from waste PET (a) under nitrogen and (b) oxygen.

Furthermore, the weight loss of neat micron, Fe-micron talc, directly and catalytically grown graphene/micron talc hybrid at 250°C, 750°C and 1000°C are given in Table 12. Neat micron talc did not lose its weight up to 250°C and it lost only 0.1% its weight until 750°C while Fe-micron talc lost its 1.9% of weight up to 750 °C. Because micron talc lost its weight between 315°C and 525°C due to intercalated ions in the talc layers [80]. Moreover, after carbonization, directly grown graphene/ micron talc hybrid lost 1.5% of its weight up to 250°C and lost 4.1% of its weight up to 750°C. However, catalytically grown graphene/ micron talc hybrid lost 2.8% of its weight up to 250°C and lost 5.2% of its weight up to 750°C. This difference between two hybrids comes from Fe intercalation on the talc surface. At 1000 °C, the total weight loss of directly

and catalytically grown graphene/ micron talc hybrid was determined as 6.4% and 8%, respectively. In conclusion, the thermal stability of the directly grown graphene/ micron talc hybrid was considerably higher than that of catalytically grown graphene/ micron talc at 1000 °C.

**Table 12.** The weight loss of micron talc, Fe-micron talc, directly and catalytically grown graphene/ micron talc hybrid at 250°C, 750°C and 1000°C.

	Weight loss (%)		
	250°C	750°C	1000°C
Micron talc	0	0.1	4.1
Fe-micron talc	0.8	1.9	5.5
Directly grown graphene/ micron talc hybrid (under nitrogen)	1.5	4.1	6.4
Catalytically grown graphene/ micron talc hybrid (under nitrogen)	2.8	5.2	8
Directly grown graphene/ micron talc hybrid (under oxygen)	7.7	41.5	41.7
Catalytically grown graphene/ micron talc hybrid (under oxygen)	6.5	42	42.1

### 5.3.5 Comparative life cycle assessment of PET-derived graphene/talc hybrid additives and their separated graphene structures

The aim of this LCA study is the assesment of the environmental impacts of the PS-derived hybrid additives and their separated graphene structures. Comparative research on the environmental impacts of directly and catalytically grown graphene/talc hybrid additives and their separated graphene structures from was PET was performed using a consequential life cycle assessment, and the results are presented in Table 13, considering only one batch of graphene growth. In addition, during the analysis, Ecoinvent 3- allocation cut off by classification, and Swiss input & output databases were used for the life cycle inventory (LCI). The waste scenario of the input materials was estimated as landfilled municipal solid waste for the rest of the world. The software system, SimaPro release 9.3.0.2, only considered the inputs with mass units in the evaluation of waste disposal scenario. The impact assessment comparison of the inputs was determined by the method, which includes the Intergovernmental Panels on Climate Change (IPCC) equivalence factors. Based on the analyses results in Table 13, the lowest global warming potential was determined as 0.33 kg CO<sub>2</sub> eq (equivalent) of

waste PET, and the highest global warming potential was calculated as 5.27 kg CO<sub>2</sub> eq belonging to the separated graphene from graphene/Fe-treated talc hybrid additive. The reason for the differences on the global warming potential of the materials depended on their production duration, and hazardous effects of the utilized chemicals. In addition, iron treatment of micron talc caused more carbon footprint compared to the non-treated counterpart.

Furthermore, the comparison histogram of the global warming potential of neat waste PET, directly and catalytically grown graphene/talc hybrid additives, their separated graphene structures, and reduced graphene oxide (rGO) are demonstrated in Figure 29. As consistent with the Table 13, Figure 29 showed that the highest carbon footprint was caused by the separated graphene of graphene/Fe-treated talc hybrid additive. However, the conventional method of the graphene production (rGO) still had significantly higher global warming potential than the separated graphene structures.

**Table 13.** The environmental impacts of directly and catalytically grown graphene/talc hybrid additives from waste PET

	Unit	PET waste	Graphene/talc hybrid additives	Graphene/Fe-treated talc hybrid additives	Separated graphene from graphene/talc hybrid additives	Separated graphene from graphene/Fe-treated talc hybrid additives
<b>Global warming</b>	kg CO <sub>2</sub> eq	0.33	0.586	2.04	4.85	5.27
<b>Stratospheric ozone depletion</b>	kg CFC11 eq	2E <sup>-6</sup>	1.69E <sup>-6</sup>	2.09E <sup>-6</sup>	1.1E <sup>-5</sup>	1.12E <sup>-5</sup>
<b>Ionizing radiation</b>	kBq Co-60 eq	0.0117	0.00918	0.0199	0.0397	0.0428
<b>Ozone formation. human health</b>	kg NO <sub>x</sub> eq	0.000689	0.00122	0.00391	0.00997	0.0108
<b>Ozone formation. terrestrial ecosystems</b>	kg NO <sub>x</sub> eq	0.000721	0.00125	0.00396	0.0101	0.0108
<b>Terrestrial acidification</b>	kg SO <sub>2</sub> eq	0.000894	0.00205	0.00731	0.0203	0.0218
<b>Freshwater eutrophication</b>	kg P eq	6.52E <sup>-5</sup>	0.00036	0.00156	0.00413	0.00448
<b>Marine eutrophication</b>	kg N eq	0.000199	0.000195	0.000506	0.000517	0.000607
<b>Terrestrial ecotoxicity</b>	kg 1,4-DCB	0.802	0.705	1.24	2.85	3.00
<b>Freshwater ecotoxicity</b>	kg 1,4-DCB	0.0205	0.0355	0.206	0.284	0.334
<b>Marine ecotoxicity</b>	kg 1,4-DCB	0.0277	0.0475	0.272	0.376	0.442
<b>Human carcinogenic ecotoxicity</b>	kg 1,4-DCB	0.0198	0.0356	0.122	0.288	0.313
<b>Human non-carcinogenic ecotoxicity</b>	kg 1,4-DCB	0.32	0.785	4.86	7.55	8.74
<b>Land use</b>	m <sup>2</sup> a crop eq	0.00493	0.00534	0.0138	0.0283	0.0308
<b>Mineral resource scarcity</b>	kg Cu eq	0.00109	0.00635	0.00601	0.00529	0.00519
<b>Fossil resource scarcity</b>	kg oil eq	0.16	0.209	0.536	1.19	1.29
<b>Water consumption</b>	m <sup>3</sup>	0.00389	0.00633	0.016	0.037	0.0398

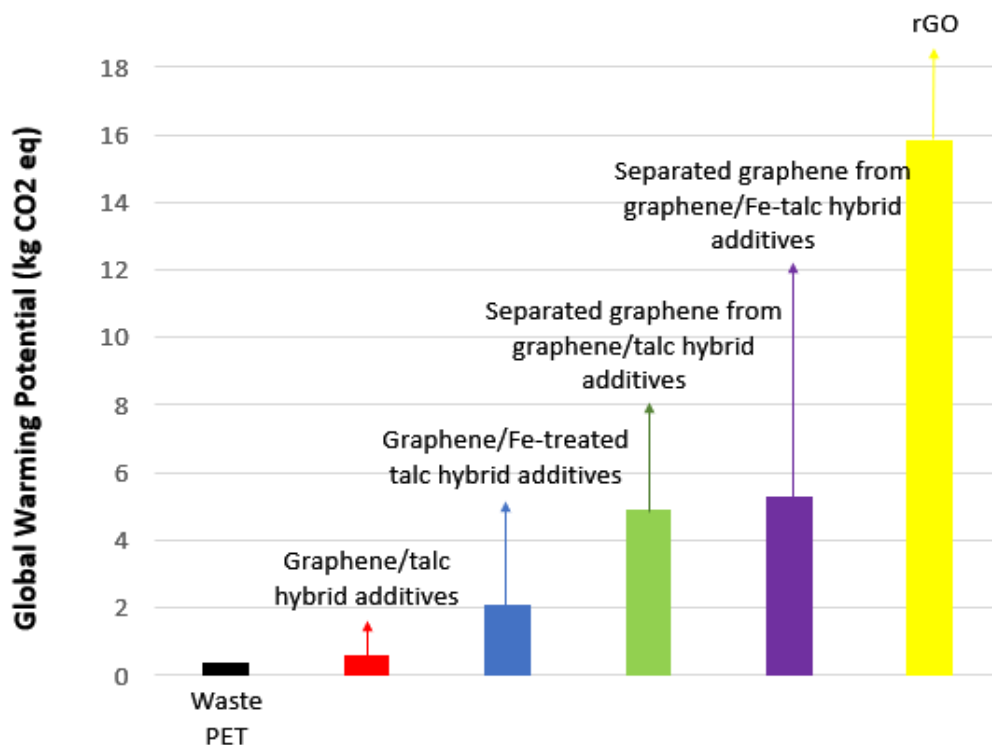


**Figure 29.** The comparison of global warming potential of neat waste PET, directly and catalytically grown graphene/talc hybrid additives, their separated graphene structures, and rGO.

The global warming potential of the production inputs of the hybrid additives and their separated graphene structures was given in Table 14. As seen in Table 14, the most influential parameter on the global warming potential was the electricity, with the other name ‘energy’. It was followed by the nitric acid, which has hazardous effects on the environment. On the other hand, the less global warming potential was supplied by the natural mineral, talc. In order to decrease the global warming potential of the products, less energy should be consumed as well as natural materials if possible.

**Table 14.** The impact of production inputs of the hybrid additives and their separated graphene structures on global warming potential.

Process	Unit	PET waste	Graphene/talc hybrid additives	Graphene/Fe-treated talc hybrid additives	Separated graphene from graphene/talc hybrid additives	Separated graphene from graphene/Fe-treated talc hybrid additives
<b>Total of all processes</b>	kg CO <sub>2</sub> eq	0.33	0.586	2.04	4.85	5.27
<b>Electricity</b>	kg CO <sub>2</sub> eq	-	0.324	1.54	4.2	4.56
<b>Hydrogen fluoride</b>	kg CO <sub>2</sub> eq	-	-	-	0.0553	0.0553
<b>Iron (III) chloride</b>	kg CO <sub>2</sub> eq	-	-	0.0178	-	0.00517
<b>Nitric acid</b>	kg CO <sub>2</sub> eq	-	-	-	0.32	0.32
<b>PET</b>	kg CO <sub>2</sub> eq	0.32	0.256	0.256	0.0743	0.0743
<b>Talc</b>	kg CO <sub>2</sub> eq	-	0.00696	0.00564	0.00202	0.00163

#### 5.4. CONCLUSION

This study provided a straightforward preparation method for upcycling PET plastic waste into carbon nanoparticles via catalytic and direct carbonization at 1000°C on micron talc as template. The effect of aromatic polymer type as carbon source on upcycled graphene growth was analyzed using PET waste. XRD, Raman and SEM analyses reveal that graphitic structure functionalized with oxygen groups was formed but the thermal decomposition of PET was not finished completely. The catalytic effect of Fe on the grown carbon nanomaterial structures on micron talc surface was investigated and fiber-like structures formation tendency was observed on Fe-micron talc with the diameter of 50-150 nm. Thus, changing parameters of carbonization, more dispersed and decomposed nanocarbon structures can be obtained.

## CHAPTER 6. CONCLUSIONS

The goal of this thesis was to use an upcycling approach to create graphene from aromatic plastic waste, PS and PET, on the surface of talc. Two types of talc, micron talc and fine talc, were provided in order to conduct an initial study on the impact of talc size on the creation of upcycled graphene using PS waste as carbon waste. The structures of the carbon nanoparticles that are produced on the talc surface can be adjusted depending on the talc size and catalyst existence. Rather than two-dimensional (2D) graphene plates, three-dimensional (3D) spherical nano-carbon structures can be created with the utilization of fine talc that is smaller than micron talc. However, sheet-like 2D graphene structures were obtained with micron talc. These mechanisms of graphene formation are given schematically in the Figure 30 and Figure 31.

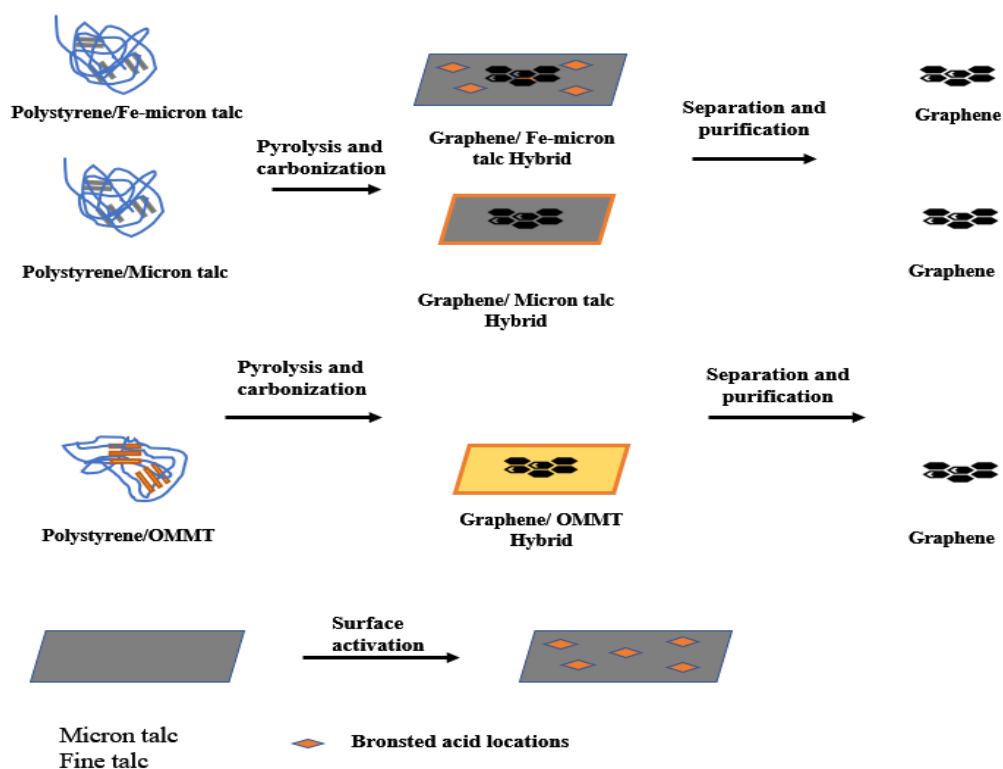


**Figure 30.** The concept for creating 2D sheet-like graphene structures from aromatic plastic waste on micron talc.

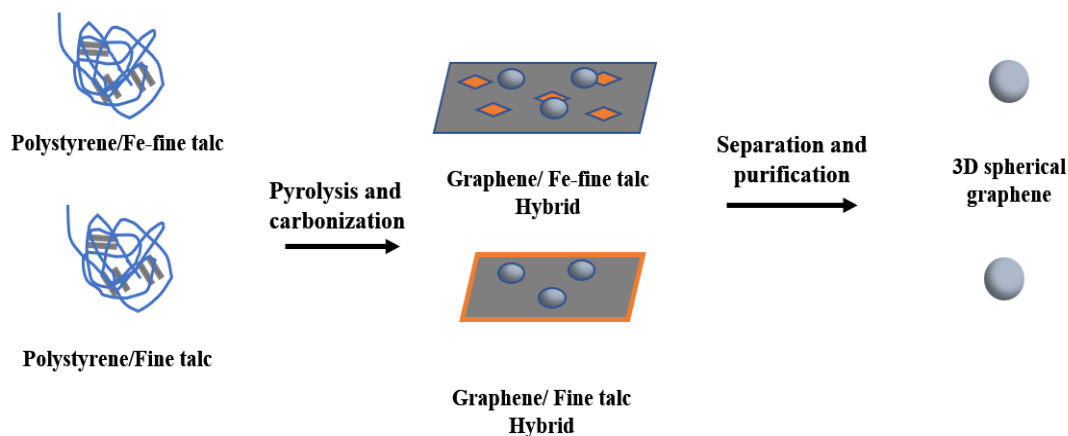


**Figure 31.** The concept for creating 3D spherical nano-carbon structures from aromatic plastic waste on fine talc.

The hydrophobic nature of talc makes it difficult to disperse it uniformly in polymer matrices.  $\text{FeCl}_3$  was used to modify the micron talc and fine talc surface to enhance the interaction between the talc/polymer. To evaluate the effects of surface modification on the generation of upcycled graphene, carbonization was performed on both neat micron talc and fine talc. In conclusion, in the initial studies, the size of the used talc and the surface modification of the talc were the main analyzed parameters for the creation of upcycled graphene.

The thermokinetic mixer was used to combine PS waste and Fe-treated talc/ neat talc in a ratio of 80:20 weight percent before carbonization. Then, in a chamber furnace in the argon environment, carbonization was carried out at  $1000^\circ\text{C}$  for 5 min to generate upcycled graphene. After obtaining graphene/talc hybrids, graphene was separated from the talc surface using HF and  $\text{HNO}_3$  acid treatment. The structure of the upcycled graphene and graphene/talc hybrids was studied using various microscopic, spectroscopic, and thermal characterizations. According to the findings of the characterization, it can be concluded that employing waste PS as a carbon source was successful in producing upcycled graphene on Fe-micron, Fe-fine, micron, and fine talc. It was realized that Fe catalyst helps to degrade the polymer to their monomers by breaking down their bonds.

In addition, upcycled graphene growth on OMMT from PS waste was obtained. XRD, Raman and XPS analyses were demonstrated that graphitic structure growth on OMMT was obtained. Interlayer space was calculated as 0.366 and crystalline size was

calculated as 1.27 nm using Debye-Sherrer equation. Upcycled graphene with the width of 200-300 nm calculated from the SEM images. Higher amount of smaller carbon nanomaterials grown on OMMT surface was obtained in contrast to the one that grown on neat micron talc surface. This is the indicator of OMMT behaves also like catalyst that helps to degrade polystyrene into light subunits and aromatics.

In addition, to analyze both aromatic polymer type effect used as carbon source and Fe catalyst effect, carbonization was performed with also PET waste as carbon source using neat micron talc and Fe-treated micron talc as substrate. In this study, carbon nanomaterials formation was achieved on surfaces of two different substrate, talc and montmorillonite, from waste PET and PS by a upcycling method. When PET and PS is compared, XRD reveals that PET give rise to higher interlayer space, 0.39, between the graphitic structures. Also PET- derived graphene has smaller crystalline domain size in contrast to PS-derived one. Also, SEM images reveal that PS- derived graphene has more clear layered structure than PET-derived one and PET degradation is not completely finished especially for grown on neat micron talc. Besides, thermal degradation showed that PS-derived graphene nanoplatelet/ talc hybrids are more thermally stable than PET- derived one because of higher amount of O group in the PET structure. Table 15 provides a summary of the findings of the thesis.

**Table 15.** Summary of graphene growth on the surface of OMMT, micron and fine talc.

Carbon source	Substrate	Surface activation	Graphene formation	Blending type	Details	Number of graphene layers obtained by Debye Scherer equations
Polystyrene	Micron talc D <sub>50</sub> =12 μm	FeCl <sub>3</sub>	✓	Thermokinetic mixing	The formation of few layered graphene sheets and confirmed by TEM	5
Polystyrene	Micron talc D <sub>50</sub> =12 micron	-	✓	Thermokinetic mixing	Graphene formation yield was lower than that grown-on Fe-micron talc regarding XRD and TEM characterization	4
Polystyrene	Micron talc D <sub>50</sub> =12 micron	-	✓	Twin-screw extrusion	More wrinkled and transparent graphene structure formation than thermokinetically mixed	4
Polystyrene	Fine talc D <sub>50</sub> =1.9 micron	FeCl <sub>3</sub>	✓	Thermokinetic mixing	Spherical 3D graphene fabrication was performed (proved by SEM)	7
Polystyrene	Fine talc D <sub>50</sub> =1.9 micron	-	✓	Thermokinetic mixing	The generation of spherical graphene was demonstrated and confirmed by TEM, but graphene yield was lower than grown on Fe-fine talc regarding XRD data	-
Polystyrene	Organically modified montmorillonite D <sub>50</sub> = <15 micron	-	✓	Thermokinetic mixing	Homogeneous distribution graphene structures and sheet like graphene formation (demonstrated by SEM)	5
Polyethylene terephthalate	Micron talc D <sub>50</sub> =12 micron	FeCl <sub>3</sub>	✓	Thermokinetic mixing	Sheet and fiber-like graphene structures were observed and confirmed by SEM	4
Polyethylene terephthalate	Micron talc D <sub>50</sub> =12 micron	-	✓	Thermokinetic mixing	Sheet-like graphene formation and confirmed by SEM	4

## REFERENCES

- [1] **Kong, S.C. Wong, T.L. Yang, M. Chow, C.F. and Tse, K.H.** (2017). Emerging practices in scholarship of learning and teaching in a digital era. *Emerging Practices in Scholarship of Learning and Teaching in a Digital Era*, 1–373, doi: 10.1007/978-981-10-3344-5.
- [2] **Zhuo, C. and Levendis, Y.A.** (2014). Upcycling waste plastics into carbon nanomaterials: A review. *J. Appl. Polym. Sci.* .
- [3] **Okan, M. Aydin, H.M. and Barsbay, M.** (2019). Current approaches to waste polymer utilization and minimization. *J Chem Technol Biotechnol*, 94,: 8–21.
- [4] **Yeung, C.W.S. Teo, J.Y.Q. Loh, X.J. and Lim, J.Y.C.** (2021). Polyolefins and Polystyrene as Chemical Resources for a Sustainable Future: Challenges, Advances, and Prospects. *ACS Materials Letters*, 3(12),: 1660–1676, doi: 10.1021/acsmaterialslett.1c00490.
- [5] **Amirov, R.K. Atamanuk, I.N. Vorobieva, N.A. Isakaev, E.H. Shavelkina, M.B. and Shkolnikov, E.I.** (2015). Synthesis of graphene-like materials by pyrolysis of hydrocarbons in thermal plasma and their properties. *Journal of Physics: Conference Series*, 653(1), doi: 10.1088/1742-6596/653/1/012161.
- [6] **Wong, S.L. Mong, G.R. Nyakuma, B.B. Ngadi, N. Wong, K.Y. Hernández, M.M. Armenise, S. and Chong, C.T.** (2022). Upcycling of plastic waste to carbon nanomaterials: a bibliometric analysis (2000–2019). *Clean Technologies and Environmental Policy*, 24(3),: 739–759, doi: 10.1007/s10098-021-02267-w.
- [7] **Jacquemin, L. Pontalier, P.Y. and Sablayrolles, C.** (2012). Life cycle assessment (LCA) applied to the process industry: A review. *International Journal of Life Cycle Assessment*, 17(8),: 1028–1041, doi: 10.1007/s11367-012-0432-9.
- [8] **Bohm, S. Ingle, A. Bohm, H.L.M. Fenech-Salerno, B. Wu, S. and Torrisi, F.** (2021). Graphene production by cracking. *Philosophical Transactions of the Royal Society A: Mathematical, Physical and Engineering Sciences*, 379(2203), doi: 10.1098/rsta.2020.0293.
- [9] **Kumar, N. Salehiyan, R. Chauke, V. Joseph Botlhoko, O. Setshedi, K. Scriba,**

- M. Masukume, M. and Sinha Ray, S.** (2021). Top-down synthesis of graphene: A comprehensive review. *FlatChem*, 27(November 2020),: 100224, doi: 10.1016/j.flatc.2021.100224.
- [10] **Chen, J. Yao, B. Li, C. and Shi, G.** (2013). An improved Hummers method for eco-friendly synthesis of graphene oxide. *Carbon*, 64(1),: 225–229, doi: 10.1016/j.carbon.2013.07.055.
- [11] **Phiri, J. Gane, P. and Maloney, T.C.** (2017). General overview of graphene: Production, properties and application in polymer composites. *Materials Science and Engineering B: Solid-State Materials for Advanced Technology*, 215,: 9–28, doi: 10.1016/j.mseb.2016.10.004.
- [12] **Kauling, A.P. Seefeldt, A.T. Pisoni, D.P. Pradeep, R.C. Bentini, R. Oliveira, R.V.B. Novoselov, K.S. and Castro Neto, A.H.** (2018). The Worldwide Graphene Flake Production. *Advanced Materials*, 30(44), doi: 10.1002/adma.201803784.
- [13] **Bhuyan, M.S.A. Uddin, M.N. Islam, M.M. Bipasha, F.A. and Hossain, S.S.** (2016). Synthesis of graphene. *International Nano Letters*, 6(2),: 65–83, doi: 10.1007/s40089-015-0176-1.
- [14] **Ruan, G. Sun, Z. Peng, Z. and Tour, J.M.** (2011). Growth of graphene from food, insects, and waste. *ACS Nano*, 5(9),: 7601–7607, doi: 10.1021/nn202625c.
- [15] **Raghavan, N. Thangavel, S. and Venugopal, G.** (2017). A short review on preparation of graphene from waste and bioprecursors. *Applied Materials Today*, 7,: 246–254, doi: 10.1016/j.apmt.2017.04.005.
- [16] **Kumar, R. Singh, R.K. and Singh, D.P.** (2016). Natural and waste hydrocarbon precursors for the synthesis of carbon based nanomaterials: Graphene and CNTs. *Renewable and Sustainable Energy Reviews*, 58,: 976–1006, doi: 10.1016/j.rser.2015.12.120.
- [17] **Ikram, R. Jan, B.M. and Ahmad, W.** (2020). Advances in synthesis of graphene derivatives using industrial wastes precursors; prospects and challenges. *Journal of Materials Research and Technology*, 9(6),: 15924–15951, doi: 10.1016/j.jmrt.2020.11.043.
- [18] **Akhavan, O. Bijanzad, K. and Mirsepah, A.** (2014). Synthesis of graphene from

- natural and industrial carbonaceous wastes. *RSC Advances*, 4(39),: 20441–20448, doi: 10.1039/c4ra01550a.
- [19] **Deng, J. You, Y. Sahajwalla, V. and Joshi, R.K.** (2016). Transforming waste into carbon-based nanomaterials. *Carbon*, 96,: 105–115, doi: 10.1016/j.carbon.2015.09.033.
- [20] **Zhang, F. Wang, F. Wei, X. Yang, Y. Xu, S. Deng, D. and Wang, Y.Z.** (2022). From trash to treasure: Chemical recycling and upcycling of commodity plastic waste to fuels, high-valued chemicals and advanced materials. *Journal of Energy Chemistry*, 69,: 369–388, doi: 10.1016/j.jechem.2021.12.052.
- [21] **Ma, C. Liu, X. Min, J. Li, J. Gong, J. Wen, X. Chen, X. Tang, T. and Mijowska, E.** (2020). Sustainable recycling of waste polystyrene into hierarchical porous carbon nanosheets with potential applications in supercapacitors. *Nanotechnology*, 31(3),: 035402, doi: 10.1088/1361-6528/ab475f.
- [22] **Hedayati, A. Barnett, C. Swan, G. and Orbaek White, A.** (2019). Chemical Recycling of Consumer-Grade Black Plastic into Electrically Conductive Carbon Nanotubes. *C*, 5(2),: 32, doi: 10.3390/c5020032.
- [23] **Wen, Y. Liu, J. Song, J. Gong, J. Chen, H. and Tang, T.** (2015). Conversion of polystyrene into porous carbon sheets and hollow carbon shells over different magnesium oxide templates for efficient removal of methylene blue. *RSC Advances*, 5(127),: 105047–105056, doi: 10.1039/c5ra18505j.
- [24] **de Paula, F.G.F. de Castro, M.C.M. Ortega, P.F.R. Blanco, C. Lavall, R.L. and Santamaría, R.** (2018). High value activated carbons from waste polystyrene foams. *Microporous and Mesoporous Materials*, 267(November 2017),: 181–184, doi: 10.1016/j.micromeso.2018.03.027.
- [25] **Roy, P.S. Garnier, G. Allais, F. and Saito, K.** (2021). Strategic Approach Towards Plastic Waste Valorization: Challenges and Promising Chemical Upcycling Possibilities. *ChemSusChem*, 14(19),: 4007–4027, doi: 10.1002/cssc.202100904.
- [26] **Fonseca, W.S. Meng, X. and Deng, D.** (2015). Trash to Treasure: Transforming Waste Polystyrene Cups into Negative Electrode Materials for Sodium Ion Batteries. *ACS Sustainable Chemistry and Engineering*, 3(9),: 2153–2159, doi:

10.1021/acssuschemeng.5b00403.

- [27] **Çit, I. Sinağ, A. Yumak, T. Uçar, S. Misirlioğlu, Z. and Canel, M.** (2010). Comparative pyrolysis of polyolefins (PP and LDPE) and PET. *Polymer Bulletin*, 64(8),: 817–834, doi: 10.1007/s00289-009-0225-x.
- [28] **Jehanno, C. Alty, J.W. Roosen, M. De Meester, S. Dove, A.P. Chen, E.Y.X. Leibfarth, F.A. and Sardon, H.** (2022). Critical advances and future opportunities in upcycling commodity polymers. *Nature*, 603(7903),: 803–814, doi: 10.1038/s41586-021-04350-0.
- [29] Macromolecular Rapid Communications - 2021 - Choi - Upcycling Plastic Waste into High Value-Added Carbonaceous Materials.pdf.
- [30] **Elessawy, N.A. El-Sayed, E.M. Ali, S. Elkady, M.F. Elnouby, M. and Hamad, H.A.** (2020). One-pot green synthesis of magnetic fullerene nanocomposite for adsorption characteristics. *Journal of Water Process Engineering*, 34(August 2019),: 101047, doi: 10.1016/j.jwpe.2019.101047.
- [31] **László, K. Bóta, A. and Dékány, I.** (2003). Effect of heat treatment on synthetic carbon precursors. *Carbon*, 41(6),: 1205–1214, doi: 10.1016/S0008-6223(03)00048-4.
- [32] **Zhang, B. Song, C. Liu, C. Min, J. Azadmanjiri, J. Ni, Y. Niu, R. Gong, J. Zhao, Q. and Tang, T.** (2019). Molten salts promoting the ‘controlled carbonization’ of waste polyesters into hierarchically porous carbon for high-performance solar steam evaporation. *Journal of Materials Chemistry A*, 7(40),: 22912–22923, doi: 10.1039/c9ta07663h.
- [33] **Hopewell, J. Dvorak, R. and Kosior, E.** (2009). Plastics recycling: Challenges and opportunities. *Philosophical Transactions of the Royal Society B: Biological Sciences*, 364(1526),: 2115–2126, doi: 10.1098/rstb.2008.0311.
- [34] **Khan, S. Anjum, R. Raza, S.T. Ahmed Bazai, N. and Ihtisham, M.** (2022). Technologies for municipal solid waste management: Current status, challenges, and future perspectives. *Chemosphere*, 288(P1),: 132403, doi: 10.1016/j.chemosphere.2021.132403.
- [35] **Patrício Silva, A.L. Prata, J.C. Walker, T.R. Duarte, A.C. Ouyang, W.**

- Barcelò, D. and Rocha-Santos, T.** (2021). Increased plastic pollution due to COVID-19 pandemic: Challenges and recommendations. *Chemical Engineering Journal*, 405(August 2020),: 126683, doi: 10.1016/j.cej.2020.126683.
- [36] **Maharana, T. Negi, Y.S. and Mohanty, B.** (2007). Review article: Recycling of polystyrene. *Polymer - Plastics Technology and Engineering*, 46(7),: 729–736, doi: 10.1080/03602550701273963.
- [37] **Thakur, S. Verma, A. Sharma, B. Chaudhary, J. Tamulevicius, S. and Thakur, V.K.** (2018). Recent developments in recycling of polystyrene based plastics. *Current Opinion in Green and Sustainable Chemistry*, 13,: 32–38, doi: 10.1016/j.cogsc.2018.03.011.
- [38] **Vanapalli, K.R. Sharma, H.B. Ranjan, V.P. Samal, B. Bhattacharya, J. Dubey, B.K. and Goel, S.** (2021). Challenges and strategies for effective plastic waste management during and post COVID-19 pandemic. *Science of the Total Environment*, 750,: 141514, doi: 10.1016/j.scitotenv.2020.141514.
- [39] **Zhao, X. Boruah, B. Foo Chin, K. Đokić, M. Modak, J.M. Sen Soo, H. Zhao, X. Boruah, B. Chin, K.F. Đokić, M. Soo, H.S. and Modak, J.M.** (2021). Upcycling to Sustainably Reuse Plastics. *Advanced Materials*, 2100843, doi: 10.1002/ADMA.202100843.
- [40] **Geim, A.K. and Novoselov, K.S.** (2007). The rise of graphene PROGRESS. *Nature Materials*, 6(3),: 183–191, 17330084.
- [41] **Yi, M. and Shen, Z.** (2015). A review on mechanical exfoliation for the scalable production of graphene. *Journal of Materials Chemistry A*, 3(22),: 11700–11715.
- [42] **Zhang, L. Li, X. Huang, Y. Ma, Y. Wan, X. and Chen, Y.** (2010). Controlled synthesis of few-layered graphene sheets on a large scale using chemical exfoliation. *Carbon*, 48(8),: 2367–2371, doi: 10.1016/J.CARBON.2010.02.035.
- [43] **Camara, N. Rius, G. Huntzinger, J.R. Tiberj, A. Mestres, N. Godignon, P. and Camassel, J.** (2008). Selective epitaxial growth of graphene on SiC. *Applied Physics Letters*, 93(12),: 123503, doi: 10.1063/1.2988645.
- [44] **Zhang, Y. Zhang, L. and Zhou, C.** (2013). Review of Chemical Vapor Deposition of Graphene and Related Applications. *Accounts of Chemical*

*Research*, 46(10),: 2329–2339, doi: 10.1021/AR300203N.

- [45] **Cao, N. and Zhang, Y.** (2015). Study of reduced graphene oxide preparation by hummers' method and related characterization. *Journal of Nanomaterials*, 2015, doi: 10.1155/2015/168125.
- [46] **Berktaş, I. Hezarkhani, M. Haghghi Poudeh, L. and Saner Okan, B.** (2020). Recent developments in the synthesis of graphene and graphene-like structures from waste sources by recycling and upcycling technologies: a review *Graphene Technol.* 5:59–73.
- [47] **Li, Z. Chen, K. Chen, Z. Li, W. Biney, B.W. Guo, A. and Liu, D.** (2021). Removal of malachite green dye from aqueous solution by adsorbents derived from polyurethane plastic waste. *Journal of Environmental Chemical Engineering*, 9(1),: 104704, doi: 10.1016/j.jece.2020.104704.
- [48] **Yuan, X. Cho, M.K. Lee, J.G. Choi, S.W. and Lee, K.B.** (2020). Upcycling of waste polyethylene terephthalate plastic bottles into porous carbon for CF<sub>4</sub> adsorption. *Environmental Pollution*, 265,: 114868, doi: 10.1016/J.ENVPOL.2020.114868.
- [49] **Ko, S. Kwon, Y.J. Lee, J.U. and Jeon, Y.P.** (2020). Preparation of synthetic graphite from waste PET plastic. *Journal of Industrial and Engineering Chemistry*, 83,: 449–458, doi: 10.1016/j.jiec.2019.12.018.
- [50] **Ezzat, M.N. and Ali, Z.T.A.** (2022). Green approach for fabrication of graphene from polyethylene terephthalate (PET) bottle waste as reactive material for dyes removal from aqueous solution: Batch and continuous study. *Sustainable Materials and Technologies*, 32(November 2021),: e00404, doi: 10.1016/j.susmat.2022.e00404.
- [51] **Mensah, K. Mahmoud, H. Fujii, M. and Shokry, H.** (2021). Upcycling of Polystyrene Waste Plastics to High Value Carbon by Thermal Decomposition. *Key Engineering Materials*, 897,: 103–108, doi: 10.4028/WWW.SCIENTIFIC.NET/KEM.897.103.
- [52] **Kango, S. Kalia, S. Celli, A. Njuguna, J. Habibi, Y. and Kumar, R.** (2013). Surface modification of inorganic nanoparticles for development of organic-inorganic nanocomposites - A review. *Progress in Polymer Science*, 38(8),: 1232–

1261, doi: 10.1016/j.progpolymsci.2013.02.003.

- [53] **Kocanali, A.** (2021). Upcycling to Sustainable Conversion of Polypropylene Waste to Graphene Grown Talc Hybrids as Additive for Efficient Thermoplastic Processing and its Systematic Life Cycle Assessment.
- [54] **Belgacem, K. Llewellyn, P. Nahdi, K. and Trabelsi-Ayadi, M.** (2008). Thermal behaviour study of the talc. *Optoelectronics and Advanced Materials, Rapid Communications*, 2(6),: 332–336.
- [55] **Kalantari, K. Ahmad, M. Bin. Shameli, K. and Khandanlou, R.** (2015). Size-controlled synthesis of Fe<sub>3</sub>O<sub>4</sub> magnetite nanoparticles on the exterior of talc layers. *Research on Chemical Intermediates*, 41(4),: 2139–2151, doi: 10.1007/s11164-013-1336-4.
- [56] **Zhang, Y. Liu, Y. Liu, J. Guo, P. and Heng, L.** (2017). Super water absorbency OMMT/PAA hydrogel materials with excellent mechanical properties. *RSC Advances*, 7(24),: 14504–14510, doi: 10.1039/c7ra00372b.
- [57] **Calizo, I. Bao, W. Miao, F. Lau, C.N. and Balandin, A.A.** (2007). The effect of substrates on the Raman spectrum of graphene: Graphene- on-sapphire and graphene-on-glass. *Applied Physics Letters*, 91(20),: 201904, doi: 10.1063/1.2805024.
- [58] **Nanda, S.S. Kim, M.J. Yeom, K.S. An, S.S.A. Ju, H. and Yi, D.K.** (2016). Raman spectrum of graphene with its versatile future perspectives. *TrAC Trends in Analytical Chemistry*, 80,: 125–131, doi: 10.1016/J.TRAC.2016.02.024.
- [59] **Ferrari, A.C. and Basko, D.M.** (2013). Raman spectroscopy as a versatile tool for studying the properties of graphene. *Nature Nanotechnology*, 8(4),: 235–246, doi: 10.1038/nnano.2013.46.
- [60] **Gong, J. Liu, J. Wen, X. Jiang, Z. Chen, X. Mijowska, E. and Tang, T.** (2014). Upcycling waste polypropylene into graphene flakes on organically modified montmorillonite. *Industrial and Engineering Chemistry Research*, 53(11),: 4173–4181, doi: 10.1021/ie4043246.
- [61] **Ni, Z.H. Wang, H.M. Ma, Y. Kasim, J. Wu, Y.H. and Shen, Z.X.** (2008). Tunable stress and controlled thickness modification in graphene by annealing.

- ACS Nano*, 2(5),: 1033–1039, doi: 10.1021/nn800031m.
- [62] **Wang, C. Han, H. Wu, Y. and Astruc, D.** (2022). Nanocatalyzed upcycling of the plastic wastes for a circular economy. *Coordination Chemistry Reviews*, 458,: 214422, doi: 10.1016/j.ccr.2022.214422.
- [63] **Gayathri, S. Jayabal, P. Kottaisamy, M. and Ramakrishnan, V.** (2014). Synthesis of few layer graphene by direct exfoliation of graphite and a Raman spectroscopic study. *AIP Advances*, 4(2), doi: 10.1063/1.4866595.
- [64] **Kakaei, K. Esrafil, M.D. and Ehsani, A.** (2019). Graphene Surfaces In: Interface Sci. Tehcnology. pp 1–445.
- [65] **Kogure, T. Kameda, J. Matsui, T. and Miyawaki, R.** (2006). Stacking structure in disordered talc: Interpretation of its X-ray diffraction pattern by using pattern simulation and high-resolution transmission electron microscopy. *American Mineralogist*, 91(8–9),: 1363–1370, doi: 10.2138/am.2006.2196.
- [66] **Ferrage, E. Martin, F. Petit, S.. Pejo-soucaille, S. Micoud, P. Fourty, G. Ferret, J.. Salvi, S. De Parseval, P. and Fortune, J.. P.** (2003). Evaluation of talc morphology using FTIR and H/D substitution. *Clay Minerals*, 38(2),: 141–150, doi: 10.1180/0009855033820084.
- [67] **Gao, Y. Hou, F. Hu, S. Wu, B. Wang, Y. Zhang, H. Jiang, B. and Fu, H.** (2018). Graphene Quantum-Dot-Modified Hexagonal Tubular Carbon Nitride for Visible-Light Photocatalytic Hydrogen Evolution. *ChemCatChem*, doi: 10.1002/cctc.201701823.
- [68] **Furlan, A. Jansson, U. Lu, J. Hultman, L. and Magnuson, M.** (2015). Structure and bonding in amorphous iron carbide thin films. *Journal of Physics Condensed Matter*, 27(4), doi: 10.1088/0953-8984/27/4/045002.
- [69] **Sharma, R. Chadha, N. and Saini, P.** (2017). Determination of defect density, crystallite size and number of graphene layers in graphene analogues using X-ray diffraction and Raman spectroscopy. *Indian Journal of Pure and Applied Physics*, 55(9),: 625–629.
- [70] **Saner, B. Okyay, F. and Yürüm, Y.** (2010). Utilization of multiple graphene layers in fuel cells. 1. An improved technique for the exfoliation of graphene-based

- nanosheets from graphite. *undefined*, 89(8),: 1903–1910, doi: 10.1016/J.FUEL.2010.03.036.
- [71] **Sheshmani, S. and Fashapoyeh, M.A.** (2013). Suitable chemical methods for preparation of graphene oxide, graphene and surface functionalized graphene nanosheets. *Acta Chimica Slovenica*, 60(4),: 813–825, 24362985.
- [72] **Kovtun, A. Jones, D. Dell’Elce, S. Treossi, E. Liscio, A. and Palermo, V.** (2019). Accurate chemical analysis of oxygenated graphene-based materials using X-ray photoelectron spectroscopy. *Carbon*, 143,: 268–275, doi: 10.1016/J.CARBON.2018.11.012.
- [73] **Sarac, E.C. Poudesh, L.H. Zanjani, J.S.M. Letofsky-Papst, I. Cebeci, F.Ç. Aydin, I. Menciloglu, Y. and Okan, B.S.** (2019). Performance Comparison of CVD Grown Carbon Nanofiber Based on Single- and Multi-Layer Graphene Oxides in Melt-Compounded PA6.6 Nanocomposites. *Open Journal of Composite Materials*, 09(02),: 99–123, doi: 10.4236/ojcm.2019.92005.
- [74] **Patel, B.R. Kalb, P.D. and Lageraen, P.R.** (1995). Review of potential processing technoques for the encapsulation of wastes in thermoplastic polymers. *Environmental & Waste Technology Center*, 4–5.
- [75] **Tang, B. Guoxin, H. and Gao, H.** (2010). Raman spectroscopic characterization of graphene. *Applied Spectroscopy Reviews*, 45(5),: 369–407, doi: 10.1080/05704928.2010.483886.
- [76] **Castillo, L.A. López, O. V. García, M.A. Barbosa, S.E. and Villar, M.A.** (2019). Crystalline morphology of thermoplastic starch/talc nanocomposites induced by thermal processing. *Heliyon*, 5(6), doi: 10.1016/j.heliyon.2019.e01877.
- [77] **Hang, B.T. and Anh, T.T.** (2021). Controlled synthesis of various Fe<sub>2</sub>O<sub>3</sub> morphologies as energy storage materials. *Scientific Reports*, 11(1),: 1–10, doi: 10.1038/s41598-021-84755-z.
- [78] **Kaniyoor, A. and Ramaprabhu, S.** (2012). A Raman spectroscopic investigation of graphite oxide derived graphene. *AIP Advances*, 2(3),: 0–13, doi: 10.1063/1.4756995.
- [79] **Geng, Y. Wang, S.J. and Kim, J.K.** (2009). Preparation of graphite nanoplatelets

- and graphene sheets. *Journal of Colloid and Interface Science*, 336(2),: 592–598, doi: 10.1016/j.jcis.2009.04.005.
- [80] **Fiorentino, B. Fulchiron, R. Bounor-Legaré, V. Majesté, J.C. Leblond, J.C. and Duchet-Rumeau, J.** (2015). Chemical modification routes of synthetic talc: Influence on its nucleating power and on its dispersion state. *Applied Clay Science*, 109–110,: 107–118, doi: 10.1016/j.clay.2015.02.026.
- [81] **Karakoti, M. Pandey, S. Tatrari, G. Dhapola, P.S. Jangra, R. Dhali, S. Pathak, M. Mahendia, S. and Sahoo, N.G.** (2022). A waste to energy approach for the effective conversion of solid waste plastics into graphene nanosheets using different catalysts for high performance supercapacitors: A comparative study. *Materials Advances*, 3(4),: 2146–2157, doi: 10.1039/d1ma01136g.
- [82] **Gong, J. Michalkiewicz, B. Chen, X. Mijowska, E. Liu, J. Jiang, Z. Wen, X. and Tang, T.** (2014). Sustainable conversion of mixed plastics into porous carbon nanosheets with high performances in uptake of carbon dioxide and storage of hydrogen. *ACS Sustainable Chemistry and Engineering*, 2(12),: 2837–2844, doi: 10.1021/sc500603h.
- [83] **Zakirov, A.S. Navamathavan, R. Jang, Y.J. Jung, A.S. Choi, C.K. and Lee, K.M.** (2007). Comparative study on the structural and electrical properties of low-k SiOC(-H) films deposited by using plasma enhanced chemical vapor deposition. *Journal of the Korean Physical Society*, doi: 10.3938/jkps.50.1809.
- [84] **He, H. Frost, R.L. Xi, Y. and Zhu, J.** (2004). Raman spectroscopic study of organo-montmorillonites. *Journal of Raman Spectroscopy*, 35(4),: 316–323, doi: 10.1002/jrs.1165.
- [85] **Gong, J. Liu, J. Chen, X. Wen, X. Jiang, Z. Mijowska, E. Wang, Y. and Tang, T.** (2013). Synthesis, characterization and growth mechanism of mesoporous hollow carbon nanospheres by catalytic carbonization of polystyrene. *Microporous and Mesoporous Materials*, 176,: 31–40, doi: 10.1016/j.micromeso.2013.03.039.
- [86] **Zhang, X. Yi, H. Bai, H. Zhao, Y. Min, F. and Song, S.** (2017). Correlation of montmorillonite exfoliation with interlayer cations in the preparation of two-dimensional nanosheets. *RSC Advances*, 7(66),: 41471–41478, doi: 10.1039/c7ra07816a.

- [87] **Wang, Y. He, Q. Qu, H. Zhang, X. Guo, J. Zhu, J. Zhao, G. Colorado, H.A. Yu, J. Sun, L. Bhana, S. Khan, M.A. Huang, X. Young, D.P. Wang, H. Wang, X. Wei, S. and Guo, Z.** (2014). Magnetic graphene oxide nanocomposites: Nanoparticles growth mechanism and property analysis. *Journal of Materials Chemistry C*, 2(44),: 9478–9488, doi: 10.1039/c4tc01351d.
- [88] **Sinha, V. Patel, M.R. and Patel, J. V.** (2010). Pet waste management by chemical recycling: A review. *Journal of Polymers and the Environment*, 18(1),: 8–25, doi: 10.1007/s10924-008-0106-7.
- [89] **Choudhary, K. Sangwan, K.S. and Goyal, D.** (2019). Environment and economic impacts assessment of PET waste recycling with conventional and renewable sources of energy. *Procedia CIRP*, 80,: 422–427, doi: 10.1016/j.procir.2019.01.096.
- [90] **O-Reilly, M. and Stubbe, J.A.** (2020). PET polymer recycling. *Biochemistry*, 59(25),: 2316–2318, doi: 10.1021/acs.biochem.0c00457.
- [91] **Parra, J.B. Ania, C.O. Arenillas, A. Rubiera, F. and Pis, J.J.** (2004). High value carbon materials from PET recycling. *Applied Surface Science*, 238(1-4 SPEC. ISS.),: 304–308, doi: 10.1016/j.apsusc.2004.05.229.
- [92] **Zhengcai Pu. Van Ooij, W.J. and Mark, J.E.** (1997). Hydrolysis kinetics and stability of bis(triethoxysilyl)ethane in water-ethanol solution by ftir spectroscopy. *Journal of Adhesion Science and Technology*, 11(1),: 29–47, doi: 10.1163/156856197X01001.
- [93] **Mirjalili, A. Dong, B. Pena, P. Ozkan, C.S. and Ozkan, M.** (2020). Upcycling of polyethylene terephthalate plastic waste to microporous carbon structure for energy storage. *Energy Storage*, 2(6),: 1–12, doi: 10.1002/est2.201.
- [94] **Ishimaru, K. Hata, T. Bronsveld, P. Nishizawa, T. and Imamura, Y.** (2007). Characterization of sp<sup>2</sup>- and sp<sup>3</sup>-bonded carbon in wood charcoal. *Journal of Wood Science*, 53(5),: 442–448, doi: 10.1007/s10086-007-0879-7.
- [95] **Jaiswal, A. Kumar, R. and Prakash, R.** (2021). Iron/Iron Carbide (Fe/Fe<sub>3</sub>C) Encapsulated in S, N Codoped Graphitic Carbon as a Robust HER Electrocatalyst. *Energy and Fuels*, 35(19),: 16046–16053, doi: 10.1021/acs.energyfuels.1c02125.

- [96] **Mohamed, H.H. Alsanea, A.A. Alomair, N.A. Akhtar, S. and Bahnemann, D.W.** (2019). ZnO@ porous graphite nanocomposite from waste for superior photocatalytic activity. *Environmental Science and Pollution Research*, 26(12),: 12288–12301, doi: 10.1007/s11356-019-04684-3.